Summer 8-16-2024

Investigation of Calcium and Calmodulin Signaling During JC Polyomavirus Infection

Avery Bond
avery.bond@maine.edu

INVESTIGATION OF CALCIUM AND CALMODULIN SIGNALING DURING JC POLYOMAVIRUS INFECTION

By

Avery Bond

B.S. The University of New England, 2019

A DISSERTATION

Submitted in Partial Fulfillment of the

Requirements for the Degree of

Doctor of Philosophy

(in Microbiology)

The Graduate School

The University of Maine

August 2024

Advisory Committee:

Melissa Maginnis, Associate Professor of Microbiology, Advisor

Julie Gosse, Associate Professor of Biochemistry

Melody Neely, Associate Professor and Chair of Molecular and Biomedical Sciences

Sally Molloy, Associate Professor of Genomics

Clarissa Henry, Professor of Biological Sciences

INVESTIGATION OF CALCIUM AND CALMODULIN SIGNALING DURING JC POLYOMAVIRUS INFECTION

By Avery Bond

Dissertation Advisor: Dr. Melissa Maginnis

An Abstract of the Dissertation Presented
In Partial Fulfillment of the Requirements for the
Degree of Doctor of Philosophy
(in Microbiology)
August 2024

JC polyomavirus (JCPyV) infects 50-80% of the human population. In healthy individuals, JCPyV establishes a persistent, asymptomatic infection in the kidneys. In severely immunocompromised individuals, JCPyV infection can result in a fatal brain infection called progressive multifocal leukoencephalopathy (PML). PML causes a lytic infection of myelin-producing glial cells in the brain and becomes progressively debilitating, sometimes resulting in death within one year of symptom onset. There are currently no targeted, approved treatments for PML, underscoring the importance of continued research on JCPyV and PML.

To identify potential antiviral therapeutics, the Maginnis laboratory performed a large-scale drug screen using the National Institutes of Health Clinical Collection (NIH-CC), which contains FDA-approved drugs and therapeutics in various stages of clinical trials. Results demonstrated that several FDA-approved drugs from different drug classes reduce JCPyV infection and that multiple “hits” identified were drugs that target cellular calcium signaling pathways. Calcium channel blockers and related calmodulin inhibitors were further characterized by viral infectivity assays with results supporting a role for calcium signaling during JCPyV infection. Calmodulin inhibitor, trifluoperazine (TFP), resulted in a significant

decrease in JCPyV infection in both transformed and primary kidney and brain cell types. Further, TFP also reduced infection of polyomaviruses BK and SV40 and the coronavirus SARS-CoV-2. Investigation into the impact of TFP on the JCPyV infectious cycle demonstrated the greatest reduction of JCPyV infection at the point of viral entry. Additional work showed that JCPyV stimulates increased intracellular calcium (Ca^{2+}) flux at times consistent with viral entry.

Exploring pre-approved drugs is a promising and demonstrated method for repurposing therapeutics to identify potential treatments for PML and other viral diseases, and findings that Ca^{2+} signaling is a key player in JCPyV infection could lead to the discovery of calcium-specific antiviral therapies to treat JCPyV infection and PML.

DEDICATION

To my parents and sister, with utmost gratitude, for all you have done to support me along the way.

To my big brother, I hope I've made you proud.

ACKNOWLEDGEMENTS

I would like to first extend a sincere thank you to all members of the Maginnis Lab over the past five years. Daily interactions with you all have been so enjoyable and you have all taught me so much in your own ways. Thank you to all of the undergraduates that I've had the opportunity to mentor; it has been so rewarding to see you grow in and out of the lab. Thank you to past graduate students, including Michael Wilczek and Colleen Mayberry for training me in my early days in the lab, Kashif Mehmood for all the laughs, Mason Crocker for getting me up to speed on his project that I would shortly take over, and Amanda Sandberg for a wonderful friendship in the lab and on the soccer field. Thank you to current graduate students Sophie Craig and Lucas Bennett for helping to foster a positive learning environment for all, and for all of the great memories we've shared together.

I'd like to thank the University of Maine and the graduate school for providing me with an opportunity to earn my doctoral degree. Within the department of Molecular and Biomedical Sciences, I want to thank all of the professors, graduate students, undergraduate students, and staff that I have interacted with. I am truly lucky to have met each and every one of you and feel fortunate to have belonged to this department. Thank you especially to each member of my committee for your feedback on my project, and most importantly, for dedicating your time to help me become a better scientist.

Thank you to my parents for your constant support while at UMaine, but also for your unwavering support throughout life. I would have never gotten to this point without you both and I could never thank you enough for all you've done for me. Thank you to my sister for helping to keep me sane throughout graduate school by making sure I get outdoors often.

Finally, I want to extend the biggest thank you to my mentor and advisor, Melissa Maginnis. You have established a fantastic laboratory environment which allows for deep learning, wonderful science, and lasting friendships alike. Thank you for helping to shape me into the scientist, and person, that I am today. You have been a listening ear when I need it and have provided me with incredible guidance both in and out of the lab. You have always encouraged me to reach for the next opportunity, and made sure I met my goals, even if it required an extra push. Thank you for ensuring my success in the lab and in graduate school, and thank you for allowing me to pursue a Ph.D. in your lab. I will forever feel fortunate to have spent these years under your guidance.

TABLE OF CONTENTS

LIST OF TABLES

LIST OF FIGURES

CHAPTER 1

INTRODUCTION

1.1. Viruses

Although viruses have existed for billions of years, it was only in the 19th century that virology, the study of viruses, emerged [4]. Since then, countless outstanding discoveries have been made in this field. There are now over 11,000 named virus species and these viruses range from harmless co-inhabitants of the human body to deadly pathogenic human viruses, all the way to viruses that infect bacteria and viruses that can be used to treat human cancers [5]. These tiny, non-living organisms are capable of a vast array of things, but perhaps they are best known for their ability to cause disease.

Viruses cause disease in plants, animals, and humans, and the impacts of these viral diseases can be moderate to severe. Common crop viruses include those that affect production of potatoes, wheat, bananas, tomatoes, cucumbers, and countless other plants [6]. The economic impact of these plant viruses can be devastating, with loss of revenue of over $1 billion annually in Africa due to impacts of cassava mosaic virus on cassava plants [7]. Human pathogenic viruses wreak havoc physically, emotionally, and financially, as evidenced by the recent COVID-19 pandemic caused by severe acute respiratory syndrome coronavirus 2 (SARS-CoV-2). COVID-19 has resulted in over 1 million recorded deaths in the United States and has become the 3rd leading cause of death globally [8, 9]. Examples of other major viral pandemics impacting human health include 1918 Spanish flu, HIV/AIDS, and 2009 swine flu [10, 11].

Pathogens encompass viruses, bacteria, fungi, and parasites and are generally defined as an organism that causes disease [12]. Viruses differ from other pathogens in the sense that they

are not considered to be a living organism. The composition of any particular virus is as follows: nucleic acid (the viral genetic material), proteins, and sometimes lipid and carbohydrate [13]. There are several types of viruses, including those with DNA or RNA genomes, single-stranded vs double-stranded genomes, and enveloped vs unenveloped virions.

In order to cause disease, a virus needs to invade host cells. Viruses are not living organisms and require host cell machinery to replicate. Although there are a few ways in which viruses can do this, a common route is through receptor-mediated endocytosis [14, 15]. Viruses may bind to a variety of cellular receptors which allows the virion to attach itself to the host cell. Once the virion is attached, it can enter the cell by fusion with the membrane (enveloped viruses) or cell-mediated uptake mechanisms (enveloped and nonenveloped viruses) [14]. Inside of the cell, the primary goal is to deliver the viral DNA or RNA so the viral genome may be replicated [16]. DNA viruses must deliver their genome to the nucleus of the cell, while RNA viruses generally complete replication in the cytosol [17]. After replication occurs, virions begin to assemble using the newly synthesized viral proteins to encapsidate the viral DNA or RNA [18]. Virions then traverse through the cell as they egress from the cell. Viral egress mechanisms include cellular apoptosis, lysis, and budding. Release of the newly synthesized virions from the cell allows for viral spread and invasion of neighboring cells [19].

As neighboring cells become infected and produce new viral progeny, the virus spreads throughout the host's body [20]. Viral loads become high in the host, and virus can then be spread to other potential victims by respiratory routes, fecal and urinary shedding, and through bodily secretions including blood, sweat, and semen [21]. The mechanism and route of spread differs from virus to virus, but most viruses gain access to a new host through interactions with

the epithelium, which consist of cells that line the outside surface and inner cavities of the body [22]. At this point, the viral infectious cycle begins again – the virus attaches to a host cell, becomes internalized, replicates its genome, assembles many new virions, and spreads to neighboring cells.

1.2. Polyomaviruses

Polyomavirus stands for multiple (*poly*) tumors (*oma*); this family of viruses received this name for the ability of the first isolated polyomavirus (murine polyomavirus) to induce multiple tumors when injected into animal models [23, 24]. To date, 80 polyomaviruses have been named with 14 of those being human polyomaviruses [25, 26]. Of these 14 human polyomaviruses, six are known to cause human disease [27]. Polyomaviruses often establish infection early in life, but are generally only associated with disease in immunocompromised individuals [28].

All polyomaviruses are nonenveloped and contain a double-stranded circular DNA (dsDNA) genome that is approximately 5000 bp in size [25]. Genomes encode at least two regulatory proteins, small tumor antigen (sTAg) and large tumor antigen (LTAg), and at least two structural proteins, viral protein 1 (VP1) and viral protein 2 (VP2), although some polyomaviruses have additional structural proteins viral protein 3 (VP3) and viral protein 4 (VP4) [29]. The tumor antigens (TAg) have been shown to interact with specific cellular proteins and may be involved in cell cycle regulation [30, 31]. VP1 and VP2 form the viral capsid, with VP1 serving as the outermost capsid protein [32].

1.3. Simian Virus 40 (SV40) Polyomavirus

SV40 was initially discovered in 1960 because of the contamination of inactivated and live attenuated forms of the polio vaccine [33]. The polio vaccine was prepared in rhesus monkey kidney cells, some of which came from monkeys naturally infected with SV40. Shortly after the initial discovery of SV40, it was shown to cause tumors in rodents and was able to transform several types of cells in culture [34-36]. Intensive research studies began to focus on SV40 because of the potential threat to human health, although ultimately did not prove a causal relationship between SV40 and human cancers, and it quickly became a useful laboratory model that was used in a variety of molecular biology studies [37].

1.4. Merkel Cell Polyomavirus (MCPyV)

MCPyV was discovered in 2008 and is estimated to persistently infect 80% of the global population, with initial infection occurring during childhood [38, 39]. Infection by MCPyV is asymptomatic for most, but upon immune suppression, advanced age, and/or ultraviolet exposure, MCPyV integrates into the host genome and results in Merkel cell carcinoma (MCC) [40, 41]. Although it is a rare neuroendocrine cutaneous malignancy, MCC has a case-fatality rate higher than that of melanoma and prevalence is only expected to increase [42, 43]. Despite early detection of MCC, nearly one third of MCC has metastasized prior to initial diagnosis, leading to high mortality and recurrence rates. Unfortunately, chemotherapy has shown limited efficacy [44, 45]. Recently there have been promising advances in immunotherapeutics, but there are currently no therapeutic agents specifically approved for the treatment of advanced MCC [46]. As MCC is frequently resistant to systemic treatments, treatment of MCC is often long-term to control disease burden, prevent flare-ups, and improve quality of life [46]. MCPyV

is the only polyomavirus known to cause cancer, underscoring the importance of this pathogen [47].

1.5. BK Polyomavirus (BKPyV)

BKPyV, like other polyomaviruses, is common in the human population and has been detected in over 80% of people [48]. Infection occurs early in life and the route of transmission is likely via the urinary or respiratory tract [49, 50]. Eventually BKPyV causes a persistent infection in the kidneys, where it infects renal tubules and cells of the transitional epithelium of the urinary tract [51]. The major concern with BKPyV infection is BK polyomavirus-associated nephropathy (BKPyVAN) [52]. BKPyVAN is an important cause of graft loss in kidney transplant recipients in up to 10% of patients; of those patients, up to 90% will lose their graft [53]. Infection occurs either by reactivation of latent infection or transmission of new infection from the donor kidney [54]. Guidelines for BKPyV-positive individuals receiving kidney transplants include modulation of immunosuppression to reduce the severity of immunosuppression by reducing the dose of a calcineurin inhibitor normally administered during transplants [55].

1.6. JC Polyomavirus (JCPyV)

The causative agent of the fatal demyelinating brain disease progressive multifocal leukoencephalopathy (PML), JCPyV, was one of the first human polyomaviruses to be discovered. In 1971, using extracts from the brain of a patient with Hodgkin's lymphoma who had recently died due to PML, replication of JCPyV in primary cell cultures of fetal glial cells was achieved, which established the first ex vivo system to study JCPyV [56]. Although seroprevalence of JCPyV is generally between 40 and 60%, JCPyV results in PML only in severely immunosuppressed patient populations [48, 57-60]. In otherwise healthy individuals, JCPyV is

contracted perorally and spreads to the kidney to establish a persistent infection, not unlike BKPyV [61]. However, unlike BKPyV, the primary concern with JCPyV is not kidney disease – the concern is with spread of JCPyV from the kidneys to the brain, where it infects oligodendrocytes and astrocytes to cause PML [56, 62].

1.7. Progressive Multifocal Leukoencephalopathy (PML)

PML is a disease of the central nervous system which results in demyelination due to destruction of oligodendrocytes by JCPyV [56, 63, 64]. Oligodendrocytes are the myelinating cells of the brain, and thus lysis of these cells results in deterioration of the myelin sheath on neurons, leading to interruptions in nerve impulses and causing neurological problems [65, 66]. Although it is not fully understood how JCPyV spreads from the kidneys to the brain, a few hypotheses exist. One theory is that JCPyV invades the bone marrow and enters B cells, using them as a reservoir and to cross the blood-brain barrier (BBB). Once across the BBB, JCPyV may escape from B cells, leading to infection in the central nervous system (CNS) [67, 68]. Another theory includes the potential that JCPyV may enter the brain via the choroid plexus, since primary choroid plexus epithelial cells express all receptors necessary for JCPyV infection, are susceptible to JCPyV infection in vitro, and are infected in patient tissue samples in vivo [69-71]. A final theory is that some individuals harbor a persistent JCPyV infection in the brain parenchyma or choroid plexus and this virus causes disease following the onset of immunosuppression [72].

Symptoms of PML are debilitating and include hemiparesis, gait and speech abnormalities, weakness, cognitive impairment, sensory symptoms, headache, visual changes,

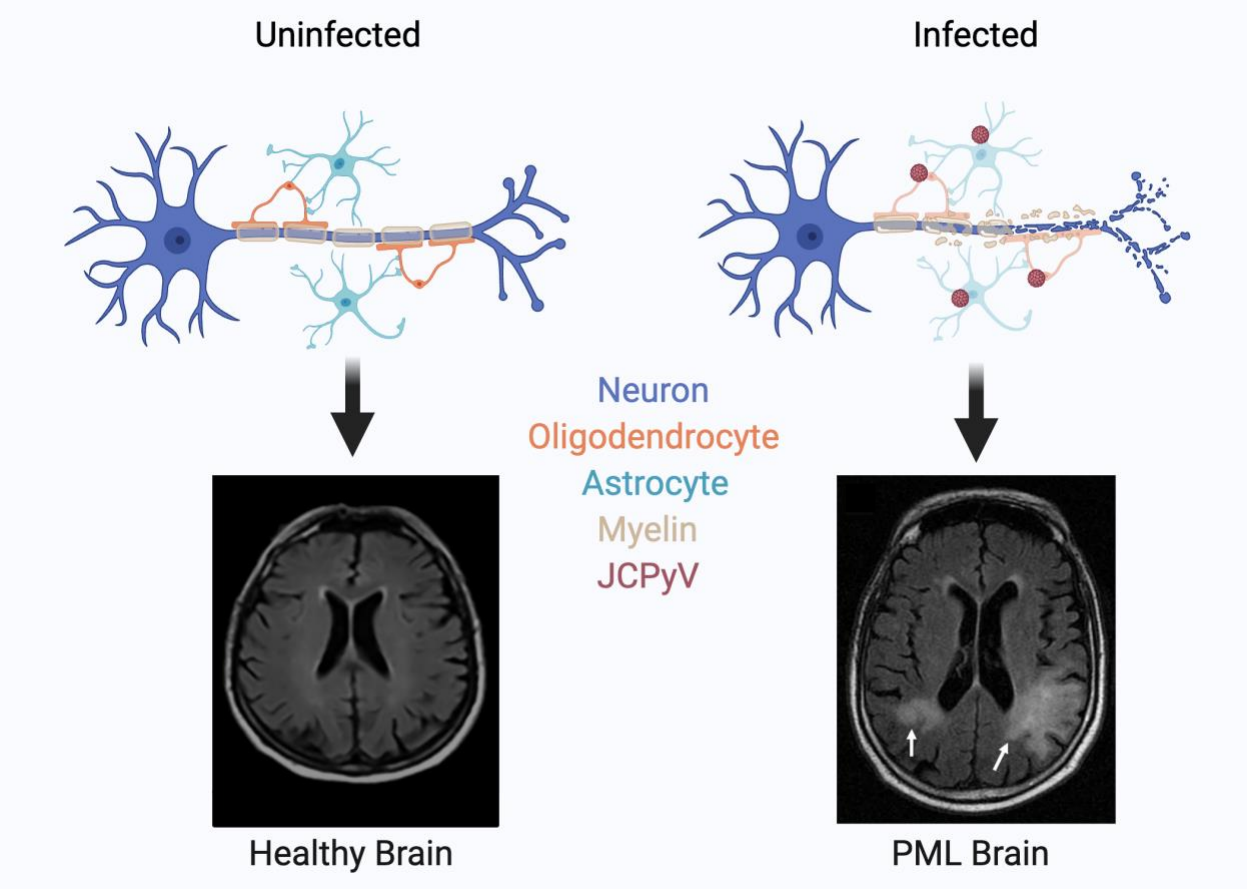

Figure 1.1. Progressive multifocal leukoencephalopathy. Uninfected glial cells (left) with intact neuronal myelin sheath result in healthy brain tissue as noted in the MRI free of white plaques. JCPyV-infected glial cells (right) result in glial cell death and demyelination of neuronal axons. JCPyV infection in the brain results in PML. White arrows denote areas of demyelination in the white matter of the PML brain. Healthy brain MRI adapted with permission from [1]. PML brain MRI adapted with permission from [2]. Figure created in BioRender.

and seizures [73-75]. PML is diagnosed through a combination of clinical, radiographic, and virologic evidence. The most accurate method for diagnosing PML is by brain biopsy, but it is rarely performed today. Commonly, diagnosis of PML is based on detection of JCPyV in the cerebrospinal fluid (CSF) by polymerase chain reaction (PCR), clinical presentation, and evidence of PML brain lesions by magnetic resonance imaging (MRI) [76].

As mentioned, immunocompromised individuals are most at-risk for development of PML, but especially those with HIV/AIDS and those undergoing immunosuppressive treatments

for diseases such as multiple sclerosis (MS), Crohn's disease, non-Hodgkin lymphoma, lupus, and rheumatoid arthritis [77-79]. Due to the AIDS pandemic in the 1980s, the incidence of PML increased up to 20 times in the 90s [80]. At this time, it was estimated that 85% of patients with PML were also seropositive for HIV-1 [81, 82]. Fortunately, highly active antiretroviral therapy (HAART) has resulted in a significant decrease in these numbers in the last 30 years [83]. More recently, a peak of PML incidence has arisen in populations receiving immune therapies. Natalizumab, an anti-$\alpha_4\beta_1$ and $\alpha_4\beta_7$ integrin used to treat MS and Crohn's disease, has been largely responsible for this peak in incidence [84]. Risk of developing PML is about 1:1000 in this patient population, which is still considered low [85, 86]. Before undergoing natalizumab treatment for MS, a risk stratification is carried out to weigh the associated benefits versus risks. Natalizumab was recently shown to be one of the most effective drugs for relapsing remitting MS, so this is an important decision to be made between patient and provider [87]. Unfortunately, there are no approved antiviral treatments for PML or prophylactic vaccines for JCPyV at this time [88].

1.8. Current Treatment Options

Current treatments for PML are aimed at immune reconstitution. In HIV+ patients receiving HAART, timely implementation of an effective drug regimen is key, as it can prevent the onset of acquired immune deficiency syndrome (AIDS) and therefore prevent PML [89]. For those receiving natalizumab, an immunosuppressant generally used to treat MS and Crohn's patients, removal of this therapeutic will restore immune function in these individuals, lessening the severity of PML in those patient populations. Immune reconstitution in those ending natalizumab treatment is achieved by plasma exchange to remove natalizumab from peripheral

circulation [90]. Both of these immune-modulating options can result in PML-immune reconstitution inflammatory syndrome (PML-IRIS) because of a vigorous response to JCPyV infection when immunosuppression is removed. PML-IRIS can actually worsen current PML symptoms or result in further neurological damage [91]. Due to the vigorous immune response to JCPyV upon immune reconstitution, corticosteroids are often administered to prevent excessive damage to infected tissues [92, 93]. Corticosteroids are usually given once an IRIS response is demonstrated so that the corticosteroids don't counteract the immune restoration [94].

For those patients whose immune systems cannot be reconstituted, such as those with hematological malignancies with depressed bone marrow or those treated with drugs that cause long term immune cell depletion even after treatment withdrawal, there is a need for direct anti-JCPyV therapies. These therapies can be categorized by antivirals, immune response modulators, and immunization strategies [89].

Antivirals can be further categorized by which step in the viral infectious cycle they target. One potential JCPyV attachment inhibitor, AY4, has been identified and demonstrated a reduction in JCPyV binding to SVGA cells in a dose-dependent manner. However, it is unknown whether AY4 can exert therapeutic activity within the CNS [95]. A few promising antivirals have been identified that interrupt JCPyV internalization with serotonin receptors: chlorpromazine, citalopram, risperidone, ziprasidone, and mirtazapine [96-102].

Retrograde transport of JCPyV to the endoplasmic reticulum (ER) has been inhibited by Retro-2 cycl, Retro-2.1, and brefeldin A [103-105]. Promising inhibitors of DNA replication include nucleoside analog cytarabine, nucleotide analogs cidofovir and brincidofovir [106-108].

Ganciclovir, topotecan, and leflunomide act at different stages of DNA replication and have been shown to reduce JCPyV infection in vitro [109-111]. Ganciclovir and leflunomide have resulted in successful treatment of PML in individual case reports [112, 113]. In BKPyV nephropathy, one study with leflunomide showed all subjects that maintained high enough blood levels of leflunomide had clearance of virus or progressive reductions in the viral load in blood and urine [114].

Immune modulation-based treatments are focused on restoring anti-JCPyV activity in those with PML. There was initial hope for type I interferons, but most data suggests they are unlikely to be an effective treatment option [115, 116]. Interleukin-2 (IL-2) and interleukin-7 (IL-7) have been used to restore depleted T-cell responses. IL-2 stimulates the growth of T-cells and other lymphocytes. PML patients treated with IL-2 showed steady improvement in neurological and cognitive functioning and in some cases near-complete resolution of symptoms and MRI abnormalities [117-120]. IL-7 aids in development, proliferation, survival, and homeostasis of all lymphocytes [121]. IL-7 treatment attempts for those with PML involve administration of IL-7 alone, with treatment of antivirals like mirtazapine or cidofivir, or as a component of a JCPyV vaccine [122-124]. Pembrolizumab, an immunotherapeutic which targets a protein on T cells called programmed cell death protein 1 (PD-1), has shown mixed results for treatment of PML [125].

Immunization for prophylaxis or treatment of PML has been attempted. Neurimmune Holding Ag, a biopharmaceutical company in Switzerland, is developing a recombinant JCPyV VP1-specific monoclonal antibody generated from memory B-cell pools from human donors, which includes donors recovered from PML and PML-IRIS. These antibodies are able to bind

both wild-type JCPyV VP1 and the most common PML-associated VP1 mutants [126]. Another report described a JCPyV-specific cytotoxic T lymphocyte (CTL) treatment in a patient with PML following stem cell transplantation and immunosuppression for graft-versus-host disease. JCPyV-specific CTLs were created from stem cell donor peripheral blood mononuclear cells which were stimulated with overlapping peptide pools for JCPyV VP1 and LTAg. Post-infusion, CTL activity against VP1 and LTAg was present and had not been before. JCPyV was also cleared from the CSF and the patient displayed clinical and MRI improvement [127]. Finally, many JCPyV vaccines are in various stages of drug development as prophylaxis for PML, including an oral JCPyV vaccine containing one or more JCPyV antigens, a vaccine with recombinant JCPyV VP1 CD4 T-cell epitope and recombinant human IL-7 to boost JCPyV-specific T-cell responses, and vaccines containing IL-7 and JCPyV VLPs [128-130]. In one case report of 2 PML patients, immunization with IL-7 and JCPyV VP1 resulted in an increase in neutralizing titer of antibodies against wild-type and PML mutants of JCPyV [131].

1.9. Polyomavirus Infectious Cycles

The first step of the JCPyV infectious cycle requires the engagement of JCPyV VP1 with α2,6-linked glycan lactoseries tetrasaccharide c (LSTc) [132, 133]. More recent findings indicate that JCPyV may also interact with adipocyte plasma membrane associated protein (APMAP) early on, as it appears to be important for productive JCPyV infection [134]. Though LSTc has been identified as the primary attachment receptor, non-sialylated glycosaminoglycans (GAGs) have also been identified as alternative attachment receptors for both wild-type and PML-mutant JCPyV strains [135]. A common feature between human polyomaviruses is the use of gangliosides as primary receptors. BKPyV attaches to gangliosides GD1b and GT1b, which serve

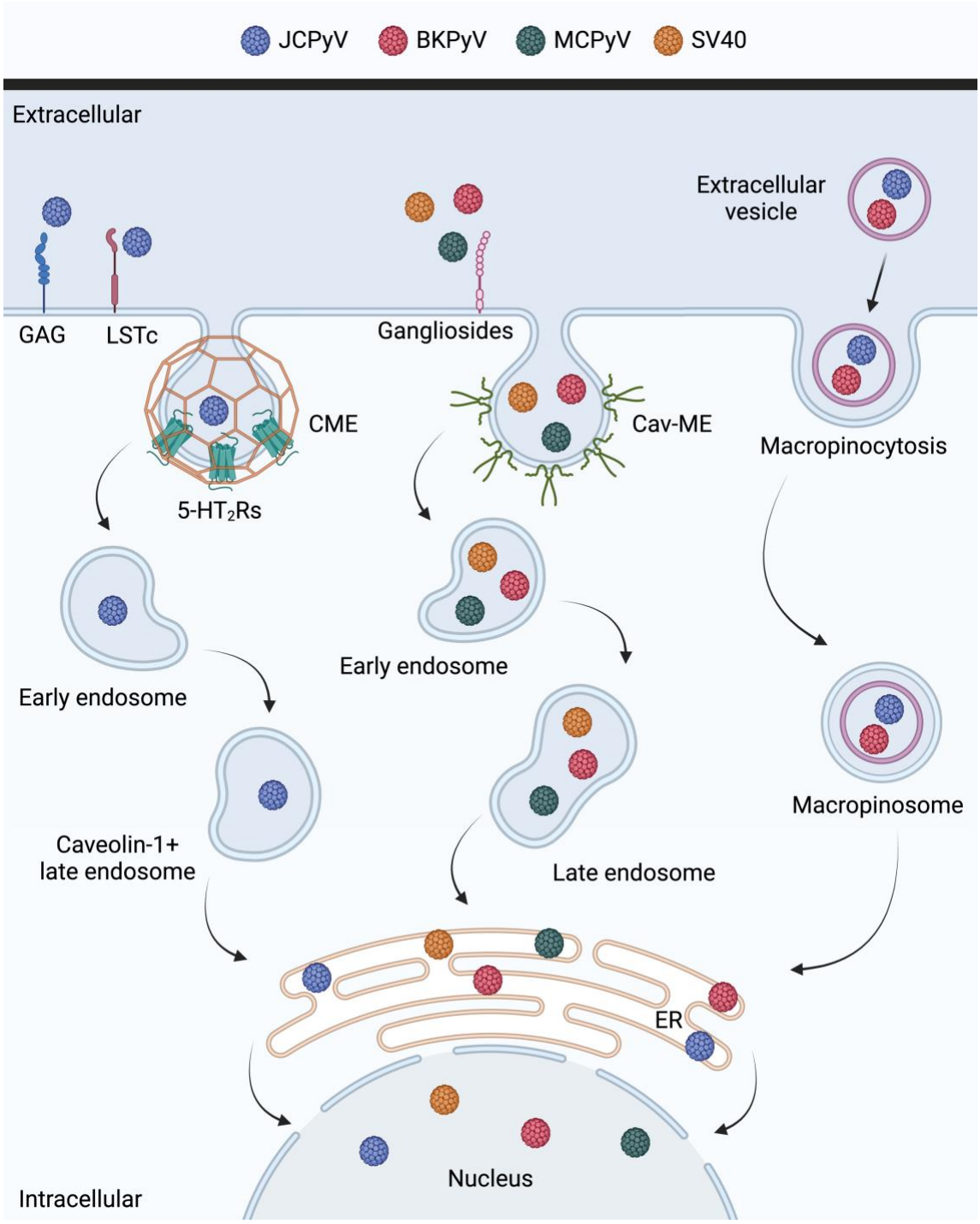

Figure 1.2. PyV infectious cycle. JCPyV enters host cells by attaching to LSTc and internalizing with 5-HT_2Rs via CME. JCPyV enters early endosomes, then is transferred to caveolin-1+ late endosomes, enters the ER, and finally is deposited in the nucleus. BKPyV, MCPyV, and SV40 enter host cells by attaching to gangliosides and internalizing via Cav-ME. These PyVs then enter early endosomes, transfer to late endosomes, enter the ER, and are deposited in the nucleus. Alternatively, JCPyV and BKPyV can utilize extracellular vesicles to enter host cells through micropinocytosis. JCPyV and BKPyV still deposit in the ER and make it to the nucleus in this mechanism of entry. Adapted from [3]. Figure created in BioRender.

as functional receptors, while JCPyV attaches to both and GD2 in addition [126, 136]. MCPyV

also binds to GT1b, with glycosaminoglycans serving as possible co-receptors [137]. In contrast, SV40 uses ganglioside GM1 as its primary attachment receptor, with major histocompatibility complex (MHC) class I serving as a co-receptor [138, 139].

Following attachment, JCPyV internalization occurs with serotonin receptors of the 5-HT_2 subtype through clathrin-mediated endocytosis (CME) [97, 99, 140-144]. For all other polyomaviruses that internalization has been investigated, caveolin-mediated endocytosis (Cav-ME) is utilized for entry [145-148]. Internalization by endocytosis results in deposition of SV40, MCPyV, JCPyV, and BKPyV in an early endosome (EE) [103, 148-151]. Interestingly, JCPyV and BKPyV have also been shown to utilize extracellular vesicles (EVs) as a means of receptor-independent internalization. Uptake of PyV-containing EVs by macropinocytosis may occur concurrently with CME and Cav-ME [152, 153].

After entering the cell, polyomaviruses (PyVs) are trafficked to the ER via the endolysosomal pathway with the help of microtubules and motor proteins dynein and kinesin [154-156]. Although JCPyV does enter EEs, the virus traffics in caveolin-1-dependent vesicles – a mechanism which is still poorly understood [151]. One theory is that these caveolae-derived vesicles could attach to EEs to release cargo into the EE in a pH-dependent, bidirectional manner [157]. PyVs are also known to accumulate within late endosomes, with most reliant on low pH, before arriving at the ER [148, 154, 155, 158]. As BKPyV and SV40 infections require syntaxin18, a soluble NSF attachment protein (SNAP) receptor located in the ER, it is thought that these viruses likely use syntaxin18 to enter the ER by vesicle fusion involving ER-resident protein ZW10 of the NRZ tethering complex and ER membrane protein complex subunits EMC4

and EMC7 [159, 160]. Once in the ER, PyV capsids are destabilized with the help of ER-resident redox proteins PDI, ERdj5, ERp57, ERp29, and/or ERp72 [161-163].

Capsid destabilization in the ER precedes PyV export into the cytoplasm to then access the nucleus for transcription and replication. This process is best understood for SV40, where ER-redox proteins lead to a destabilized hydrophobic viral capsid, which can then embed itself in the ER membrane and is eventually extracted into the cytosol with the assistance of ER associated degradation proteins, membrane chaperones, DNA J proteins, and cytosolic chaperones [161, 164-172].

To access the nucleus for viral transcription and replication, PyVs utilize nuclear transport machinery called importins [173]. Due to the degradation of the PyV capsid in the ER, nuclear localization sequences (NLS) of VP1, VP2, and VP3 are exposed, allowing for recognition by importins within the cytoplasm [174-178]. It has been proposed that VP2 and VP3 may also act as viroporins on the nuclear membrane to allow for nuclear entry of the viral genome [179, 180]. Nuclear transport of PyVs is not well characterized and there is a need for further exploration.

1.10. JCPyV Biology

JCPyV virions contain a dsDNA genome of approximately 5100 bp in size that is surrounded by the viral capsid [29]. The capsid contains three structural proteins – VP1, VP2, and VP3. VP1 serves as the major capsid protein with 72 pentamers forming the icosahedral capsid [181]. Each VP1 pentamer is bound to either a single VP2 or VP3 on the interior of the capsid [182]. The JCPyV genome is comprised of early genes and late genes that are separated by a non-coding control region (NCCR) which contains the origin of replication (ORI), the

promoter, and the enhancer elements [183]. The early genes encode for large T antigen (LTAg), small T antigen (sTAg), and three T antigen splice variants, whereas the late genes are located on the complementary strand and consist of VP1, VP2, VP3, agnoprotein, and two micro-RNAs [184, 185].

The NCCR is broken into blocks a, b, c, d, e, and f, and rearrangement of these blocks is associated with increased viral replication and more severe disease. In fact, several NCCR variants can even be found within a single infected person [29]. The archetype strain of JCPyV refers to the strain that is thought to be the transmitted form of the virus, since it is most often found in the urine of healthy or diseased individuals, but is rarely found in the brain of PML patients [185]. Archetype contains an NCCR with a-f blocks in alphabetical order [186]. In contrast, Mad-1 was the first JCPyV strain to be isolated from the brain of a PML patient and has a rearranged NCCR as such: a, c, e, a, c, e [187]. Another strain commonly found in PML patients, Mad-8, contains an NCCR comprised of a, b, c, e, b, c, e [188]. The virological

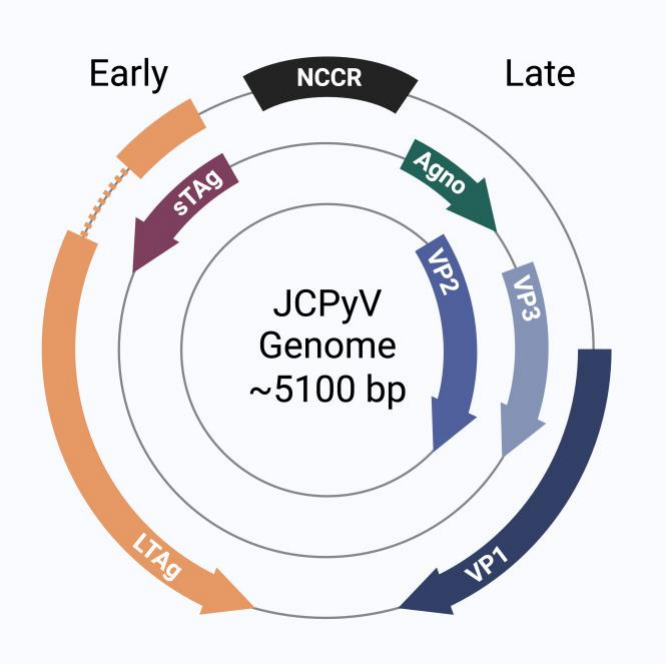

Figure 1.3. JCPyV genome. The JCPyV genome is ~5100 bp and is enclosed within a ~42 nm diameter capsid. JCPyV genome replication is bi-directional, with the origin of replication (ORI) located in the NCCR. Early genes sTAg and LTAg are expressed early on in the infectious cycle to aid with viral transcription and replication. Late genes VP1, VP2, VP3, and agnoprotein are expressed later on in the infectious cycle to aid in proper packaging of the viral genome. Figure created in BioRender.

advantage that such rearrangements have are that these duplications and deletions allow for more transcription factor binding sites, leading to advantages for JCPyV [181, 189].

VP1, the major capsid protein, is most known for its ability to facilitate viral attachment to host cells and for containing an NLS that mediates JCPyV entry into the nucleus [132, 190-193]. The minor capsid proteins, VP2 and VP3, are known for their roles in proper packaging of the genomic DNA and for their interactions with heat shock protein 70 which enhances viral DNA replication [194, 195]. Nonstructural protein, agnoprotein, is expressed during the late phase of the JCPyV infectious cycle [196]. Agnoprotein is found in and around the nucleus of infected cells and is known to be crucial for JCPyV transcription and replication [197-200]. Interestingly, agnoprotein also possesses viroporin activity and is involved in virus propagation and release [201-203]. Finally, LTAg, sTAg, and the three splice variants of TAg are responsible for many interactions with cellular proteins to favor viral transcription and replication. PyV genomes don't encode their own replication machinery so PyVs must induce S phase in host cells to utilize host cell replication machinery. LTAg is particularly well-known for its helicase activity, unwinding viral DNA during replication, and for its ability to bind p53 and the tumor suppressor retinoblastoma-associated protein, resulting in cell cycle arrest and aiding in DNA replication [204, 205]. These functions combined serve as powerful contributions to drive viral replication in the host.

1.11. Cell Signaling: MAPK and Calcium (Ca^{2+}) Signaling

Cellular signaling serves as a common mechanism for most physiological processes [206]. It is the way in which cells process extracellular and intracellular cues and communicate with one another. Signaling begins when cells receive an extracellular cue, stimulating receptors

on the cell surface [207]. This interaction triggers elaborate signaling networks within the cell, leading to the reprogramming of numerous biochemical, genetic, and structural processes [208]. The initial binding of a ligand can cause conformational changes of the receptor, which initiates well-controlled reactions carried out by secondary messengers or other signaling

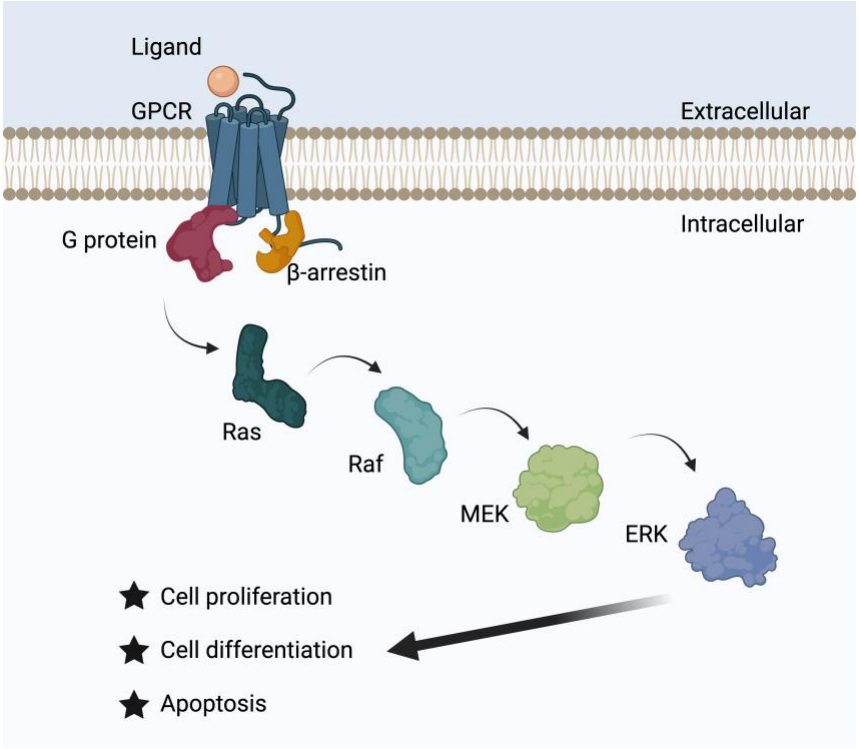

Figure 1.4. Simplified MAPK signaling pathway. Ligand binding to GPCRs activates the Ras-Raf-MEK-ERK signaling cascade. Ras activates Raf, which activates MEK, which phosphorylates ERK. Activation of this pathway stimulates cell proliferation, cell differentiation, and apoptosis responses. Figure created in BioRender.

intermediates and effectively transduces the message from receptor to final destination [209]. Cell signaling is used for countless biological processes, including development, cell growth and division, differentiation, migration, and apoptosis [210]. Some commonly studied signaling pathways include the mitogen-activated protein kinase (MAPK) cascades, Ca^{2+} signaling pathways, interferon cell signaling, integrin cell signaling, and the inflammatory response pathway.

The MAPK pathways are some of the most highly-studied signaling pathways due to their involvement in a wide variety of cellular processes, including proliferation, differentiation, apoptosis, and stress responses [211, 212]. They consist of three main kinases which activate and phosphorylate downstream proteins, namely MAPK kinase kinase, MAPK kinase, and MAPK. Within MAPK signaling, there are three distinct, well-known pathways in mammalian cells: the extracellular signal-regulated kinase (ERK) 1/2, the c-JUN N-terminal kinase 1, 2, and 3 (JNK1/2/3), and the p38 MAPK α, β, γ, and δ pathways [213]. The ERK1/2 pathway is generally activated in response to growth factors, hormones, and proinflammatory stimuli [214]. This pathway is activated upon ligand binding to a receptor tyrosine kinase at the plasma membrane, which then activates the small G-protein, Ras. Once activated, Ras then activates Raf, which activates MEK, which phosphorylates ERK1/2 [215]. Interestingly, many viruses have been shown to utilize the ERK1/2 pathway, including JCPyV [216, 217].

Another well-studied and biologically important signaling category is Ca^{2+} signaling. Ca^{2+} ions impact nearly all aspects of cellular life [218]. Ca^{2+} has a role in cell excitability, exocytosis, motility, apoptosis, and transcription [219]. One key principle of Ca^{2+} signaling is that a cellular response occurs upon change of intracellular Ca^{2+} concentration. There are both extrinsic and intrinsic cellular cues which can trigger Ca^{2+} signaling events; neurotransmitters, growth factors, antibodies, temperature, pH change, cytotoxic reagents, and microbial invasion can initiate spontaneous Ca^{2+} signals within specific cell types [220]. Stimulation of cells will normally lead to a temporary increase in cytosolic Ca^{2+} levels, which returns back to baseline at the end of stimulation [218]. Ca^{2+} signals can occur from two main sources of Ca^{2+}: influx of Ca^{2+} from the extracellular environment and Ca^{2+} release from intracellular stores. Intracellular stores of

calcium include the endoplasmic reticulum, mitochondria, Golgi, and lysosomes [221]. Located on the structures that contain intracellular Ca^{2+} stores are several Ca^{2+}-releasing channels – a few of the important channels are the inositol 1,4,5-triphosphate receptors (IP_3R), ryanodine receptors (RyR), two-pore channels (TPC), and transient receptor potential channels (TRPML) [222-225]. In addition to Ca^{2+}-releasing channels, cytosolic proteins such as calmodulin (CaM), Ca^{2+}/calmodulin-dependent kinase II, calcineurin, and IP_3 also serve as Ca^{2+} sensors and regulators, leading to a variety of biological outcomes [218].

1.12. Ca^{2+} Signaling in Viral Infection

Ca^{2+} signaling is a universal regulator of biological processes, and therefore is an attractive target for viruses, as they can alter the cellular environment to promote infection. Several viruses are known to rely on Ca^{2+}signaling for infection of host cells, and they are able to do so in part by regulating calcium flux from various intracellular and extracellular sources and by utilizing key Ca^{2+}-related proteins. Various Ca^{2+} channels and signaling proteins have been implicated in nearly all steps in the viral infectious cycle, including viral entry, trafficking, replication, virion assembly, maturation, and/or release [226, 227]. One category of well-studied calcium channels during viral infection are voltage gated Ca^{2+} channels (VGCC), which are located on the plasma membrane. Several FDA-approved inhibitors of VGCC exist, including verapamil and nifedipine, bolstering the rationale to study these channels [228]. VGCC blockers are capable of reducing infections by Epstein-Barr virus (EBV), Influenza A virus (IAV), human immunodeficiency virus (HIV), Japanese encephalitis virus (JEV), Zika virus (ZIKV), West Nile virus (WNV), Dengue virus (DENV), and New World arenavirus (NWA) [229-234]. Store operated

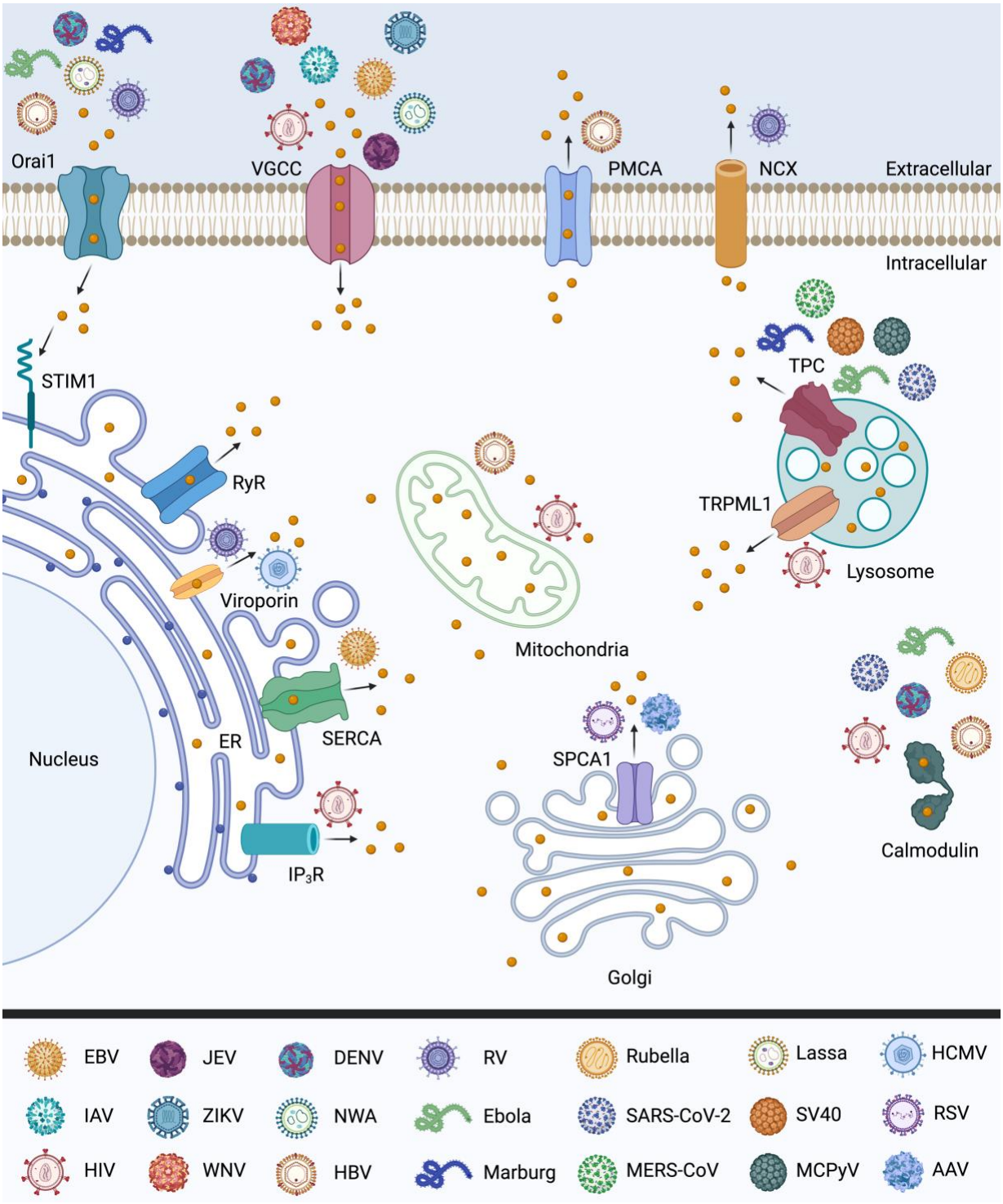

Figure 1.5. Viral interactions with Ca^{2+} channels, pumps, and cytosolic proteins. Many viruses utilize Ca^{2+}-related proteins to achieve successful infection of host cells. Commonly used Ca^{2+} influx channels include Orai1/STIM1 and several VGCCs. PMCA and NCX, Ca^{2+} efflux channels, are also utilized by some viruses. Intracellular Ca^{2+} stores such as the ER, mitochondria, Golgi, and lysosomes are targeted in a variety of ways, usually to promote Ca^{2+} release into the cytosol. Calmodulin, a cytosolic Ca^{2+} messenger protein, is also usurped by viruses to promote infection. Figure created in BioRender.

Ca^{2+} channels (SOCC) are channels stimulated by the loss of Ca^{2+} from the ER. These channels

include ORAI1 calcium release-activated calcium modulator 1 (Orai1) and stromal interaction molecule 1 (STIM1), which are located on the plasma membrane and ER, respectively [235]. Several viruses usurp these SOCC, including Hepatitis b virus (HBV), rotavirus (RV), DENV, Ebola, Marburg, and Lassa virus [236-239]. These viruses cause Ca^{2+} release from the ER by STIM1-Orai1 mediated store operated Ca^{2+} entry, leading to enhanced viral replication and budding [240]. As viruses can manipulate Ca^{2+} channels that allow for Ca^{2+} entry into a cell, they are also capable of regulating the activity of Ca^{2+}-extruding channels like the plasma membrane Ca^{2+} ATPase (PMCA) and sodium-calcium exchanger (NCX). This can be crucial for ensuring the cell maintains cytosolic Ca^{2+} homeostasis. HBV and RV have been implicated in modulation of PMCA and NCX, respectively [237, 241].

The ER is commonly exploited during viral infection and is used to support various steps in the viral infectious cycle. As such, ER Ca^{2+} stores are targeted by several viruses to drive replication and enhance viral infection. Some viruses utilize their own proteins as viroporins to disrupt the ER membrane and deplete ER Ca^{2+} stores, while others rely on host ER Ca^{2+} channels to promote release of Ca^{2+} into the cytosol. Examples of viroporins are RV nonstructural protein 4 (NSP4) and human cytomegalovirus (HCMV) US21 – both of which act as Ca^{2+} channels to mobilize Ca^{2+} into the cytosol [242, 243]. Alternatively, EBV modulates the expression and activity of SERCA3, a host ER Ca^{2+} pump [244]. Yet another example of viral modulation of ER Ca^{2+} stores is by HIV-1, where HIV-1 proteins activate IP_3R for efficient trafficking and viral release [245].

Mitochondrial Ca^{2+} signaling is disrupted by HBV, HCV, HIV, and Coxsackievirus B3 to support enhanced replication or to induce host cell apoptosis, aiding in viral egress [246-249].

Ca^{2+} stores in lysosomes are also targeted by several viruses. Normally, lysosomal Ca^{2+} stores drive important processes such as signal transduction, vesicular trafficking, autophagy, and exocytosis [228]. Due to this, lysosomal Ca^{2+} stores are yet another attractive target for viral manipulation. Two-pore Ca^{2+} channels (TPCs) are located on endo-lysosomal membranes and are hijacked by Ebola during entry into host cells [250]. In addition, Marburg virus, Middle East respiratory syndrome coronavirus (MERS-CoV), SARS-CoV-2, MCPyV, and SV40 infections are also inhibited by TPC blockers [251-253]. Another endolysosomal Ca^{2+} channel, transient receptor potential mucolipin 1 (TRPML1), is important for endolysosomal acidification, which is likely important for degradation of the HIV-1 protein, Tat [254]. Finally, the Golgi apparatus (GA) Ca^{2+} ATPase pump, secretory pathway calcium ATPase 1 (SPCA1), is usurped by viruses such as respiratory syncytial virus (RSV) and adeno-associated virus (AAVs) for viral glycoprotein maturation (RSV) and trafficking and transduction (AAVs) [255, 256].

The intracellular Ca^{2+} sensing protein, CaM, has also been implicated in viral infection and pathogenesis. CaM is ubiquitously expressed in eukaryotic cells and is capable of transducing the intracellular Ca^{2+} signal changes into divergent cellular events by binding to a variety of cellular proteins [227]. Two HIV proteins, Nef and gp160, are known to interact with CaM in a Ca^{2+}-dependent manner [257]. As Ca^{2+}/CaM-dependent signaling pathways have diverse roles, CaM is thought to play multiple roles during the HIV infectious cycle. HBV is a major cause of hepatocellular carcinoma – a highly aggressive cancer. HBV X protein physically interacts with CaM to regulate CaM-associated actin polymerization, leading to enhanced liver cancer cell migration [258]. Rubella virus nonstructural protease domain has been shown to contain a CaM-binding domain and the association of CaM with the CaM-binding domain is

necessary for nonstructural protease activity and infectivity [259]. Importantly, CaM antagonist W-7 inhibits DENV infection [260]. Both W-7 and another CaM antagonist trifluoperazine (TFP) also reduce Ebola virus-like particle (VLP) budding [261]. CaM has also been recently implicated in SARS-CoV-2 infection, as TFP significantly decreases SARS-CoV-2 infection [262].

1.13. Ca^{2+} Signaling and Polyomaviruses

Ca^{2+} signaling has been implicated in many viral infections as a major contributor to a successful viral infectious cycle. Although many studies have focused on the involvement of Ca^{2+} signaling and Ca^{2+} pumps in viral infection, very few have investigated the role of Ca^{2+} during polyomavirus infections. The first published study on Ca^{2+} and polyomaviruses demonstrated that Ca^{2+} is an integral part of the polyomavirus capsid and plays a major role in stabilizing the intact virion structure [263]. Several years later, it was discovered that mutations in the calcium-binding domain of VP1 affect capsid assembly. Transfections with mutated viral DNA still led to normal viral protein synthesis, but infective progeny were not produced [264]. It is thought that the dissociation of Ca^{2+} ions from the capsid of SV40 may be expedited by lower Ca^{2+} concentration in the cytosol than the ER [164, 265]. Additionally, uncoating of JCPyV could be dependent on Ca^{2+}, since thapsigargin, and inhibitor of the ER SERCA Ca^{2+} pump, reduces JCPyV infection [266].

Most recently, several Ca^{2+} channel inhibitors have been shown to impact MCPyV and SV40 infection [253]. Findings demonstrated that the broad spectrum Ca^{2+} channel inhibitor, verapamil, inhibited both MCPyV and SV40 infections. A T-type Ca^{2+} channel inhibitor, flunarizine, decreased MCPyV infection, but not SV40. Strikingly, a two-pore Ca^{2+} channel inhibitor, tetrandrine, significantly reduced both MCPyV and SV40 infections. Tetrandrine

prevents SV40 capsid disassembly and exposure of minor capsid proteins, VP2 and VP3, leading to the hypothesis that ER fusion may be impacted by treatment with tetrandrine.

Taken together, Ca^{2+} has been implicated in polyomavirus capsid stability and capsid assembly, and likely during viral uncoating and ER fusion steps. Involvement of Ca^{2+} and Ca^{2+} signaling during polyomavirus infection, especially JCPyV infection, remains poorly understood and further investigation was warranted.

1.14. Summary

JCPyV causes the fatal, demyelinating disease PML. No targeted antivirals have been approved to treat this disease. Further understanding JCPyV-host interactions will help lead to identification or development of treatments for PML. By performing a large-scale drug screen with over 700 drugs from the National Institutes of Health (NIH) Clinical Collection, our laboratory identified potential antivirals, with Ca^{2+} signaling-related inhibitors as a category of interest. Previous work by Dobson et al. revealed a role for Ca^{2+} channels during MCPyV and SV40 infections, but Ca^{2+} channels had not yet been implicated in JCPyV infection [253]. The work described herein reveals a novel target for JCPyV infection: host intracellular Ca^{2+} signaling. Characterization of these inhibitors led to exciting findings for inhibition of not only JCPyV infection, but also BKPyV, SV40, and SARS-CoV-2 infections. Although multiple FDA-approved inhibitors were identified as JCPyV inhibitors, and a calmodulin inhibitor, trifluoperazine, was characterized to determine the mechanism for inhibition of JCPyV infection. This work revealed a potential antiviral for the treatment of JCPyV infection and PML and continues to further detail the implications of Ca^{2+} signaling in JCPyV infection.

CHAPTER 2

HIGH-THROUGHPUT DRUG SCREEN IDENTIFIES CALCIUM AND CALMODULIN INHIBITORS THAT REDUCE JCPYV INFECTION

This chapter represents a modified form of the published work from: Bond ACS, Crocker MA, Wilczek MP, DuShane JK, Sandberg AL, Bennett LJ, Leclerc NR, Maginnis MS. 2024. High-throughput drug screen identifies calcium and calmodulin inhibitors that reduce JCPyV infection. *Antiviral Research*, 222: 105817.

2.1. Introduction

JC polyomavirus (JCPyV) infects 50–80% of the human population and is the etiological agent of the debilitating neurodegenerative disease progressive multifocal leukoencephalopathy (PML) [185]. Infection is thought to occur via fecal-oral route early in life, as JCPyV is shed in urine and can be found in untreated wastewater [267, 268]. Immunocompetent individuals harbor an asymptomatic, persistent infection in the kidneys, while severely immunosuppressed individuals are at risk for JCPyV spread to the brain, resulting in PML [269]. People with HIV/AIDS or those undergoing immunosuppressive therapies for diseases such as multiple sclerosis are at greatest risk for development of PML [88]. PML can be fatal within one year if the underlying immunosuppression is left untreated, as there are currently no approved targeted therapies for PML [185].

Though patients can live with PML for up to 10 years, symptoms of PML are debilitating and quality of life is poor [270]. Polyomaviridae are non-enveloped, double-stranded DNA viruses, and include JCPyV, simian virus 40 (SV40), BK polyomavirus (BKPyV), and Merkel cell polyomavirus (MCPyV), among others [183]. Polyomavirus (PyV) capsids consist of three

structural proteins, including the major capsid protein viral protein 1 (VP1), which mediates interactions with host cells [271]. PyV genomes also encode the T-antigen (TAg) protein, which is a major regulatory protein in replication and infection [272]. JCPyV enters cells via clathrin-mediated endocytosis and requires the G-protein coupled receptor (GPCR) 5-hydroxytryptamine 2 subfamily of receptors (5-HT_2Rs), while MCPyV, BKPyV, and SV40 enter by caveolin-mediated endocytosis [99, 144, 145, 148]. Once internalized, PyVs transit the endolysosomal route and are deposited into the endoplasmic reticulum (ER) and eventually into the nucleus for transcription and replication [273]. Though it is known that JCPyV uses multiple signaling pathways during infection, including phosphatidylinositol-3-kinase (PI3K) and mitogen-activated protein kinase (MAPK), the intracellular signaling pathways activated during JCPyV infection remain poorly understood [216, 274].

Interestingly, SV40 and MCPyV have recently been reported to require calcium channel activation during infection. Verapamil, a transient (T-type) and long lasting (L-type) Ca^{2+} channel inhibitor, reduces SV40 and MCPyV infection. Additionally, a two-pore Ca^{2+} channel (TPC) inhibitor, tetrandrine, drastically reduced SV40 and MCPyV infections, likely during the endolysosomal fusion step in the viral infectious cycles [253]. Many other viruses also rely on calcium channel activity and calcium signaling at various points during infection, including severe acute respiratory syndrome coronavirus 2 (SARS-CoV-2) during entry [275], human immunodeficiency virus (HIV) during trafficking [276], and influenza during viral replication [230]. PyVs require Ca^{2+} ions for capsid stability, but whether JCPyV relies on calcium pumps and calcium signaling during infection has yet to be studied [264].

This study reports the results of a large-scale drug screen to discover potential antivirals for JCPyV infection and PML that identified calcium-signaling related inhibitors that reduce JCPyV infection. Drug screens represent an effective method for antiviral discovery, and similar screens have been performed for numerous viruses, including Ebola, Zika, and SARS-CoV-2 [277-279]. The screen was conducted using the NIH Clinical Collection (NCC), and changes in viral infection were assessed using a high-throughput In-Cell Western (ICW) assay for JCPyV infection. Forty-two drugs that reduced JCPyV infection were identified, and 19% of these hits were calcium-related drugs. Hits were further characterized by ICW and validated by fluorescent focus unit (FFU) infectivity assays [280]. Calcium- and calmodulin-specific drugs significantly reduced infection, and a selected calmodulin inhibitor, TFP, was investigated for its specific role in the JCPyV infectious cycle. Interestingly, calmodulin inhibitors also significantly impacted BKPyV, SV40, and SARS-CoV-2 infections. Together, results demonstrate that calcium and calmodulin-related pathways are necessary for JCPyV infection and also for BKPyV, SV40, and SARS-CoV-2 infections. TFP is currently an FDA-approved drug, and therefore has potential to be repurposed for treatment of JCPyV infection and PML, and possibly as a broad-spectrum antiviral.

2.2. Materials and Methods

2.2.1. Cell lines and viruses

SVGA cells [281] were maintained in complete minimum essential medium (MEM) (Corning) containing 10% fetal bovine serum (FBS), 1% penicillin-streptomycin (P/S) (Mediatech, Inc.), and 0.2% Plasmocin (InvivoGen). Renal proximal tubule epithelial cells (RPTEC) were maintained in complete renal epithelial growth medium (REGM) containing a renal epithelial

cell growth kit (ATCC) and 1% P/S. Vero E6 and HeLa cells were cultured in complete Dulbecco's modified Eagle medium (DMEM) (Corning) containing 10% FBS, 1% P/S, and 0.2% Plasmocin. HEK293A cells stably expressing 5-HT_{2C}R [141] in fusion with YFP (HEK-2C) were maintained in DMEM with 10% FBS, 1% P/S, 0.2% Plasmocin, and 1% G418 (MP Biomedicals) to maintain receptor expression. Cell lines were propagated in a humidified incubator at 37°C with 5% CO2 and were passaged 2–3 times weekly. RPTEC and Vero E6 cells were obtained directly from ATCC, while SVGA, HeLa, and HEK-2C cells were generously provided by the Atwood Laboratory (Brown University).

JCPyV strain Mad-1/SVEΔ, SV40 strain 777, and BKPyV Dunlop strain (Atwood Laboratory, Brown University) were generated and propagated as described previously [170, 282]. Crude supernatant stock was used in all experiments except when labeled purified virus is indicated. Labeling of JCPyV with Alexa Fluor 647 was described previously [133]. JCPyV, SV40, and BKPyV stocks were titered by FFU infectivity assay in SVGA (JCPyV) and Vero E6 cells (SV40 and BKPyV). Reovirus strain T3D was a gift from Pranav Danthi, Indiana University.

SARS-CoV-2 procedures were performed under BSL-3 conditions at the Diagnostic Research Laboratory (University of Maine, Co-Operative Extension). SARS-Related Coronavirus 2, Isolate hCoV-19/USA/OR- OHSU-PHL00037/2021 (Lineage B.1.1.7; Alpha Variant), NR-55461 was obtained through BEI Resources. Propagation of SARS-CoV-2 was performed as described previously [283] with modifications recently reported [284]. Titration of SARS-CoV-2 was performed by TCID50 assay as previously described [285].

2.2.2. Antibodies, inhibitors, and plasmids

Antibodies used to detect infectivity by FFU and ICW assays include PAB962, a monoclonal antibody (mAb) derived from a hybridoma supernatant for detection of JCPyV large TAg graciously provided by the Tevethia Laboratory, Penn State University [140]; PAB597, a mAb obtained from a hybridoma and targeted against JCPyV, SV40, and BKPyV viral protein 1 (VP1), generously provided by Ed Harlow and Walter Atwood; reovirus antisera, generously provided by Pranav Danthi; a primary antibody against SARS-CoV-2 nucleocapsid (NP) (Sino Biological, 40143-MM05); a primary antibody against phosphorylated ERK (pERK) (Cell Signaling Technology, 9101); secondary polyclonal goat anti-mouse and goat anti-rabbit Alexa Fluor 488 or 594 antibodies (Thermo Fisher); and secondary LI-COR 800 anti-mouse or anti-rabbit antibodies (LI-COR). DAPI (Thermo Fisher) was used for FFU assays to stain cell nuclei, while CellTag 700 (LI-COR) was used as a cell count normalization stain for ICW assays.

The NIH Clinical Collection was generously provided by Dr. Bernardo Mainou (Emory University) with inhibitors suspended in DMSO at 10 mM. Chemical inhibitors used in validation experiments possessed a purity of at least 98% and include W-7 (SC-201501) (Santa Cruz Biotechnology), Trifluoperazine HCl (S3201) (Selleckchem), Tetrandrine (SML3048-10 MG) (Sigma-Aldrich), Flunarizine (SC-201473) (Santa Cruz Biotechnology), Nifedipine (N7634-1G) (Sigma-Aldrich), Nimodipine (66085-59-4) (Acros Organics), and Nitrendipine (Santa Cruz Biotechnology) (SC-201466). All inhibitors were resuspended in DMSO (Tocris Bioscience), which was used as a volume-specific vehicle control. Concentrations of each inhibitor are listed in figures or figure legends where applicable.

Plasmids used for transfection of the infectious clone, including pUC19 and JC pUC19, were generously provided by the Atwood Laboratory, Brown University. JC pUC19 was created using JCPyV strain JC12 DNA, a subclone of Mad1-SVEΔ, subcloned into pUC19 at a BamHI site [192].

2.2.3. Drug screen

SVGA cells were plated to 70% confluence in 96-well plates in complete MEM. Inhibitors from the NCC were diluted in MEM containing 10% FBS (10% MEM) to a final concentration of 10 µM. Cells were pre-treated with each inhibitor in respective wells and incubated at 37°C for 1 h. JCPyV (MOI = 0.5 FFU/cell) in 10% MEM was added directly into each well containing inhibitor and incubated for 1 h. Cells were then fed with 10% MEM and incubated for the duration of the 72 h infection. Plates were fixed with 4% paraformaldehyde (PFA), stained for VP1 (1:40), and analyzed via ICW (described below). Each experimental plate also contained the controls: 4 wells of mock-infected cells (no virus), 4 wells of vehicle control DMSO for the drugs in the screen, 4wells of PD98059 (50 µM) (positive control for viral inhibition), and 4 wells of vehicle control DMSO for the PD98059 control. Three independent replicates were performed. Z-scores were used to identify hits (described below).

2.2.4. Cell viability assays

Cell viability under specified inhibitor concentrations was tested by MTS assay (G3581) (Promega) for each cell type and corresponding infection duration according to manufacturer's instructions. Cells were plated to 70% confluence in 96-well plates in complete media (MEM or DMEM), and toxicity assays were performed to mimic the experimental design of infectivity assays. Cells were pre-treated with inhibitor or DMSO volume control at 37°C for 1 h, mock-

infected with media at 37°C for 1 h, then inhibitor or DMSO control was added back for the duration of the infectious cycle. MTS reagent was added, incubated at 37°C for 1–4 h, then absorbance measurements were taken at 490 nm using an Agilent BioTek Cytation 5 Imaging Reader. Experiments were performed in triplicate. Concentrations that did not induce significant toxicity and maintained >80% cell viability in comparison to the relevant DMSO control were considered useable concentrations.

2.2.5. JCPyV and SV40 FFU and ICW infections

SVGA, HEK-2C, RPTEC, or Vero E6 cells were seeded in 96-well plates in 10% MEM (SVGA), REGM (RPTEC), or DMEM (HEK-2C and Vero E6) to achieve 70% confluence at the time of infection. Inhibitors were diluted in 10% MEM, REGM, or DMEM to concentrations indicated in figures, added to triplicate wells, and incubated at 37°C for 1 h. Cells were infected with JCPyV or SV40 in 10% MEM, REGM, or DMEM (MOIs indicated in figure legends) in absence of inhibitor and incubated at 37°C for 1 h. Infections were fed with 100 µl/well of 10% MEM, REGM, or DMEM containing appropriate concentrations of inhibitors and incubated for 48 h. Cells were fixed in 4% PFA, stained for TAg (JCPyV) (1:5) or VP1 (SV40) (1:40), and analyzed by FFU or ICW assay. All infections were performed in triplicate for a minimum of 3 replicates.

2.2.6. pERK assays

SVGA or HEK-2C cells were plated to 70% confluence in 96-well plates. Nifedipine or tetrandrine were diluted in 10% MEM or DMEM to concentrations indicated in figures, added to triplicate wells, and incubated at 37°C for 24 h. Cells were fixed in 4% PFA, stained for pERK (1:750) and CellTag (1:500), and analyzed by ICW assay. All experiments were performed in triplicate for a minimum of 3 replicates.

2.2.7. ICW staining and protein quantification

After fixation, wells were washed 3x with PBS-T for 5 min. Cells were permeabilized with 1% TX-100 at RT for 15 min then incubated in TBS Odyssey Blocking Buffer (LI-COR) at RT for 1 h. PAB962 (1:5), PAB597 (1:40), or pERK (1:750) primary antibody in TBS Odyssey Blocking Buffer were incubated at 4°C overnight while rocking. Cells were washed with PBS-T 3x for 5 min, then LI-COR 800 secondary anti-mouse or anti-rabbit antibody (1:10,000) and CellTag 700 (1:500) were incubated at RT for 1 h. Wells were washed, and liquid was removed prior to scanning. Plates were scanned using a LI-COR Odyssey CLx Infrared Imaging system for detection of 700 and 800 nm channel intensities. Settings were as follows; 42 µm resolution, medium quality, and 3.0 mm focus offset [280]. Channels were aligned after scanning using Image Studio software with the ICW module. The ICW analysis grid was used to outline each well and intensity values for the 700 and 800 channels within the wells were recorded. Infection was quantified by dividing the 800 channel intensity value by the 700 channel intensity value times 100. Values were then normalized to the relevant volume control.

2.2.8. BKPyV and reovirus infections

Vero E6 cells or HeLa cells were plated in 96-well plates in 10% DMEM to achieve 70% confluence at time of infection. Inhibitors were diluted in 10% DMEM to concentrations indicated in figures, added to triplicate wells, and incubated at 37°C for 1 h. For BKPyV, Vero E6 cells were infected in 10% DMEM in absence of inhibitor at 37°C for 2 h, then fed with 100 µl/well of DMEM containing appropriate concentrations of inhibitors and incubated for 72 h. For reovirus, HeLa cells were infected in 10% DMEM in absence of inhibitor at RT for 1 h, then fed

with 100 µl/well of DMEM containing appropriate concentrations of inhibitors and incubated for 24 h. Cells were fixed in 4% PFA, stained for viral protein, and analyzed by FFU assay.

2.2.9. SARS-CoV-2 infection

Under BSL-3 conditions, Vero E6 cells were plated in 10% DMEM in 96-well plates to 70% confluence. Inhibitors were diluted in 10% DMEM, added to wells, and incubated for 1 h. Cells were infected with SARS-CoV-2 in serum-free DMEM at 0.025 TCID50/cell in absence of inhibitor and incubated at 37°C for 1 h, then fed with 100 µl/well of 10% DMEM containing inhibitor and incubated at 37°C for 24 h. Cells were fixed with 4% PFA, stained for SARS-CoV-2 NP (1:500), and analyzed by FFU assay. All SARS-CoV-2 infections were performed in triplicate for 3 replicates in a BSL-3 laboratory.

2.2.10. FFU infectivity assay staining and quantification

JCPyV, SV40, BKPyV, reovirus: Infection plates were fixed with 4% PFA and washed with 0.1% PBS-Tween (PBS-T) 3x for 5 min each. Cells were permeabilized with 1% Triton X-100 (TX-100) in PBS at RT for 15 min and blocked with 10% goat serum in PBS at RT for 1 h. Primary antibody against JCPyV TAg (PAB962, 1:5), SV40/BKPyV VP1 (PAB597, 1:40), or reovirus (reovirus antisera, 1:500) in PBS were added to wells at RT for 1 h. Wells were washed 3x with PBS-T for 5 min each, then incubated with secondary polyclonal goat anti-mouse (JCPyV, SV40, BKPyV) or goat anti-rabbit (reovirus) Alexa Fluor 594 or 488 antibody (1:1000) in PBS at RT for 1 h. Cells were again washed 3x with PBS-T for 5 min and DAPI (1:1000) in PBS was added at RT for 5 min for visualization of cell nuclei. Plates were washed with PBS-T and PBS was added for storage. Infected cells were visualized by Nikon Eclipse Ti epifluorescence microscope (Micro Video Instruments, Inc.) and percent infection was quantified by dividing the number of TAg- (JCPyV),

VP1- (SV40 and BKPyV), or reovirus-positive cells per 10X (reovirus) or 20X (JCPyV, SV40, BKPyV) visual field by the total number of DAPI-positive cells, then multiplying by 100. This was repeated for 5 fields of view (FOV) per well. TAg- or VP1-positive cells were counted manually, while DAPI-positive cells were counted using a binary algorithm in the Nikon NIS-Elements Basic Research software. Cells were separated in the binary algorithm by intensity, diameter, and circularity to achieve an accurate count of the total number of DAPI-positive cells in each FOV.

SARS-CoV-2: Cells were fixed with 4% PFA, washed with PBS-T, and permeabilized with 1% TX-100. Primary antibody against SARS-CoV-2 NP in PBS (1:500) was added at RT for 1 h. Cells were washed 3x with PBS-T for 5 min, then secondary polyclonal goat anti-mouse Alexa Fluor 488 antibody (1:1000) in PBS was added at RT for 1 h. Wells were washed with PBS-T, and DAPI (1:1000) in PBS was added at RT for 5 min. Plates were washed with PBS-T, PBS was added for storage, and infected cells were visualized using a Nikon Eclipse Ti epifluorescence microscope. Infection was quantified by dividing the number of NP-positive cells per 20X visual field by the total number of DAPI-positive cells for 5 FOV per well and multiplying by 100.

2.2.11. Inhibitor time of addition assay

HEK-2C cells were plated to 70% confluence in 96-well plates overnight. Cells were either pre-treated (− 1 h), treated at the time of infection (0 h), or added back with inhibitor post infection (4, 6, 12, and 24 hpi). For all treatments the inhibitor was diluted in 10% DMEM at 37°C and 100 µl/well was added or 10% DMEM alone was added. Unless indicated, infections were performed in the absence of inhibitor. At 48 hpi cells were fixed with 4% PFA, stained for JCPyV TAg (1:5), and analyzed by ICW assay.

2.2.12. Flow cytometry

HEK-2C cells were plated to 100% confluence in 12-well plates. Cells were treated with DMSO or TFP at 37°C for 1 h. Plates were washed with 1X PBS and incubated in Cellstripper (Corning) at 37°C for 15 min to remove cells from plate. Cells were pelleted at 2000 rpm at 4°C for 5 min and washed with 1X PBS. Alexa Fluor 647-labeled JCPyV (JCPyV-647) in DMEM (without phenol red) was added to cells on ice for 1 h with agitation every 15 min (100 µl total volume). Cells were pelleted by centrifugation and fixed in 4% PFA for 10 min on ice, then resuspended in 300 µl of 1X PBS. Analysis was performed by flow cytometry for viral attachment using a LSRII system (BD Biosciences) equipped with a 640 nm AP-C laser line for at least 10,000 events. Data analyses were performed using BD FACSDiva and FlowJo software. Gating was performed to exclude complex and dead cells using FlowJo software.

2.2.13. Infectious clone

JC pUC19 and pUC19 plasmids were extracted from glycerol stocks using a HiSpeed Plasmid Maxi Kit (Qiagen) and digested with BamHI-HF (New England Biolabs) at 37°C for 2 h. Successful linearization of plasmids was determined by agarose gel electrophoresis.

SVGA cells were plated to 50% confluence in 12-well plates, then pre-treated with TFP or DMSO for 1 h at 37°C. Cells were then transfected with 2 µg/well of DNA containing the linearized plasmids of either JC pUC19 or pUC19 using Fugene 6 at a ratio of 1.5 µl Fugene: 1 µg DNA and incubated at 37°C. After 6 h, media was replaced with 10% MEM and allowed to incubate for 3 or 7 days, when cells were fixed and stained for newly synthesized VP1 (1:40) via FFU infectivity assay.

2.2.14. Confocal microscopy and image analysis

HEK-2C cells were plated to 70% confluence in number 1.5 96-well glass bottom plates (CellVis). Cells were pre-treated with TFP or DMSO in 10% DMEM at 37°C for 1 h then shifted to 4°C for 45 min to pre-chill. JCPyV-647 (MOI = 4 FFU/cell) was added at 4°C for 1 h to allow for synchronized viral attachment, cells were fed with pre-warmed media containing TFP or DMSO, then plates were shifted to 37°C for 2 h for viral internalization. Cells were fixed with 4% PFA, washed with 1X PBS, and stained with DAPI (1:1000). PBS was added to wells for storage. A Leica SP8 microscope was utilized for sample visualization at 63× magnification (oil immersion) using LAS X software. Images were acquired using diode 405 and white light lasers and cross sections of individual cells were analyzed (at least 30 cells per sample). ImageJ software was used to define regions of interest (ROIs) by using the polygon selection tool and 5-HT_{2C}R channel, excluding the plasma membrane [286]. Relative internalized virus was measured by relative fluorescence units per cell for background-corrected samples. Each experiment was performed 3 times, with graphs representing 3 independent replicates (90 cells per treatment).

2.2.15. Statistical analyses

Drug screen: The drug screen was performed with three independent replicates. Statistical significance (z-score) of the effect of each drug on JCPyV infectivity was scored using $z = (x - \mu)/\sigma$, where x represents the inhibitory effect of a given drug, μ represents the average inhibitory effect of all drugs within a single cell culture plate, and σ represents the standard deviation of the negative control for that plate. Each z-score was compared to a “hit” threshold that required it be lower than the negative value of the number of drugs on the same plate

multiplied by the standard deviation of the inhibitory effect of those drugs. Z-scores were normalized to the z-score threshold for the plate containing any particular drug.

Student's t-test: Using Microsoft Excel, two-sample Student's t tests were performed to determine statistical significance, assuming unequal variance, by comparing mean values of triplicate samples.

Standard error of the mean (SEM): Using Microsoft Excel, SEM was calculated to determine variation in a given population and was done so by calculating standard deviation and dividing by the square root of the sample size.

2.3. Results

2.3.1. NCC drug screen

There are currently no approved targeted therapies for JCPyV infection and PML, and the cellular factors required for JCPyV infection remain poorly understood. In order to identify potential therapeutics, a large-scale drug screen was performed using the NCC. The NCC contains over 700 drugs that have been tested in clinical trials, with many of them FDA approved [287]. To perform the drug screen, SVGA cells were pre-treated with inhibitors for 1 h, infected with JCPyV (MOI = 0.5 FFU/cell), incubated for 72 h, then fixed and stained for VP1 expression and analyzed using a high-throughput ICW assay (Fig. 2.1.A) [280]. Results demonstrated that 42 drugs from various drug classes, including receptor agonists and antagonists (36%), calcium signaling-related drugs (19%), enzyme inhibitors (19%), steroids (7%), antifungals (5%), antibiotics (5%), xanthine derivatives (5%), lignans (2%), and flavonoids (2%) were capable of reducing JCPyV infection in SVGA cells (Fig. 2.1.B.) (Supplemental Table 1). The largest drug hit category represented was receptor agonists and antagonists, and the

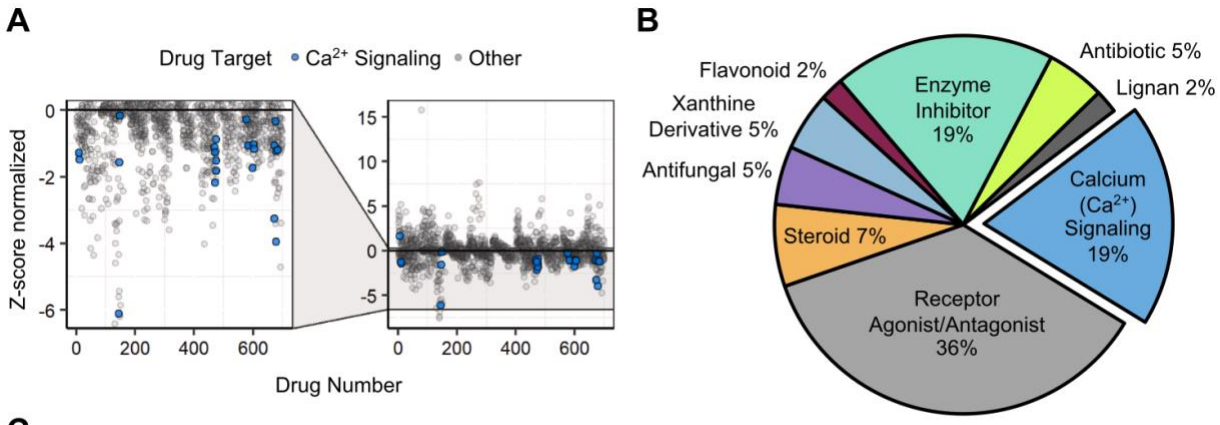

C

Drug Number	Drug Name	Drug Function
9	Nicardipine HCl	Ca^{2+} influx inhibitor
149	Dantrolene sodium	Sarcoendoplasmic reticulum Ca^{2+} inhibitor (RyR)
472	Topiramate	Ca^{2+} channel blocker (L-, R-type)
474	Nimodipine	Ca^{2+} influx inhibitor (L-type)
581	Isradipine	Ca^{2+} influx inhibitor (L-type)
603	Nicorandil	Ca^{2+} influx inhibitor via K^+ activation
676	Nifedipine	Ca^{2+} channel blocker
682	Trifluoperazine HCl (TFP)	Calmodulin (CaM) inhibitor

Figure 2.1. NIH-CC drug screen reveals several calcium-related drug hits.
(A) SVGA cells were pre-treated with each of >700 inhibitors [10 µM] from the NIH-CC, infected with JCPyV (MOI = 0.5 FFU/cell) at 37°C for 1 h, fed with MEM, then incubated at 37°C for 72 h. Cells were fixed and stained for VP1 and analyzed via ICW. Each drug replicate from the screen is represented by one dot, with calcium-related drugs shown in blue. The statistical significance (z-score) was calculated and normalized to the z-score threshold, represented by the black solid line. Drugs that reduced infection below this threshold were considered hits. (B) Hits from the screen were grouped into 9 categories. (C) Table displaying all calcium-related drug hits from the screen.

majority of the hits target GPCRs, which was of interest given the role of serotonin receptors in JCPyV entry and GPCR-related signaling in JCPyV infection [216, 288]. Calcium signaling-related drugs were the second largest category in the drug screen (Fig. 2.1.C.), revealing a novel area of inquiry for JCPyV research that also corroborated preliminary data gathered in our lab suggesting that a calmodulin inhibitor reduced JCPyV infection. Furthermore, a recent study had

demonstrated that SV40 and MCPyV infections are reliant on calcium channel activity [253], adding polyomaviruses to a large group of viruses that modulate calcium signaling during infection. Additionally, calcium is known to be required for PyV capsid stability [264], providing further rationale to explore calcium-related hits. Thus, subsequent validation studies focused on calcium-related drugs.

2.3.2. ICW screen of calcium-related drugs hits

To further validate hits from the drug screen, ICW assays were performed in triplicate for three replicates for selected drug hits nimodipine, nifedipine, and TFP and other related calcium and calmodulin inhibitors. Hits chosen represented the major inhibitor classes represented and were further explored in both glial (SVGA) and kidney (HEK-2C) cells, which are targets of JCPyV infection (Fig. 2.2.). Results showed that when SVGA and HEK-2C cells were treated with nimodipine, an L-type Ca^{2+} channel inhibitor, JCPyV infection was modestly reduced (Fig. 2.2.A.). A significant reduction in JCPyV infection was observed in HEK-2C cells when treated with nifedipine, another L-type Ca^{2+} channel inhibitor, but not in SVGA cells (Fig. 2.2.B.). Treatment of SVGA cells with tetrandrine, a NAADP-sensitive TPC inhibitor not included in the screen that blocks MCPyV and SV40 PyV infection [253], resulted in a slight, but not statistically significant, increase in JCPyV infection (Fig. 2.2.C.). However, a significant reduction in infection in HEK-2C cells was observed upon treatment with tetrandrine (Fig. 2.2.C.). No significant change in infection was found when SVGA or HEK-2C cells were treated with flunarizine, a T-type Ca^{2+} channel inhibitor not included in drug screen that blocks infection of MCPyV but not SV40 [253] (Fig. 2.2.D.). A significant reduction in JCPyV infection was observed when SVGA or HEK-2C cells were treated with trifluoperazine (TFP), a calmodulin inhibitor (Fig. 2.2.E.). A second calmodulin

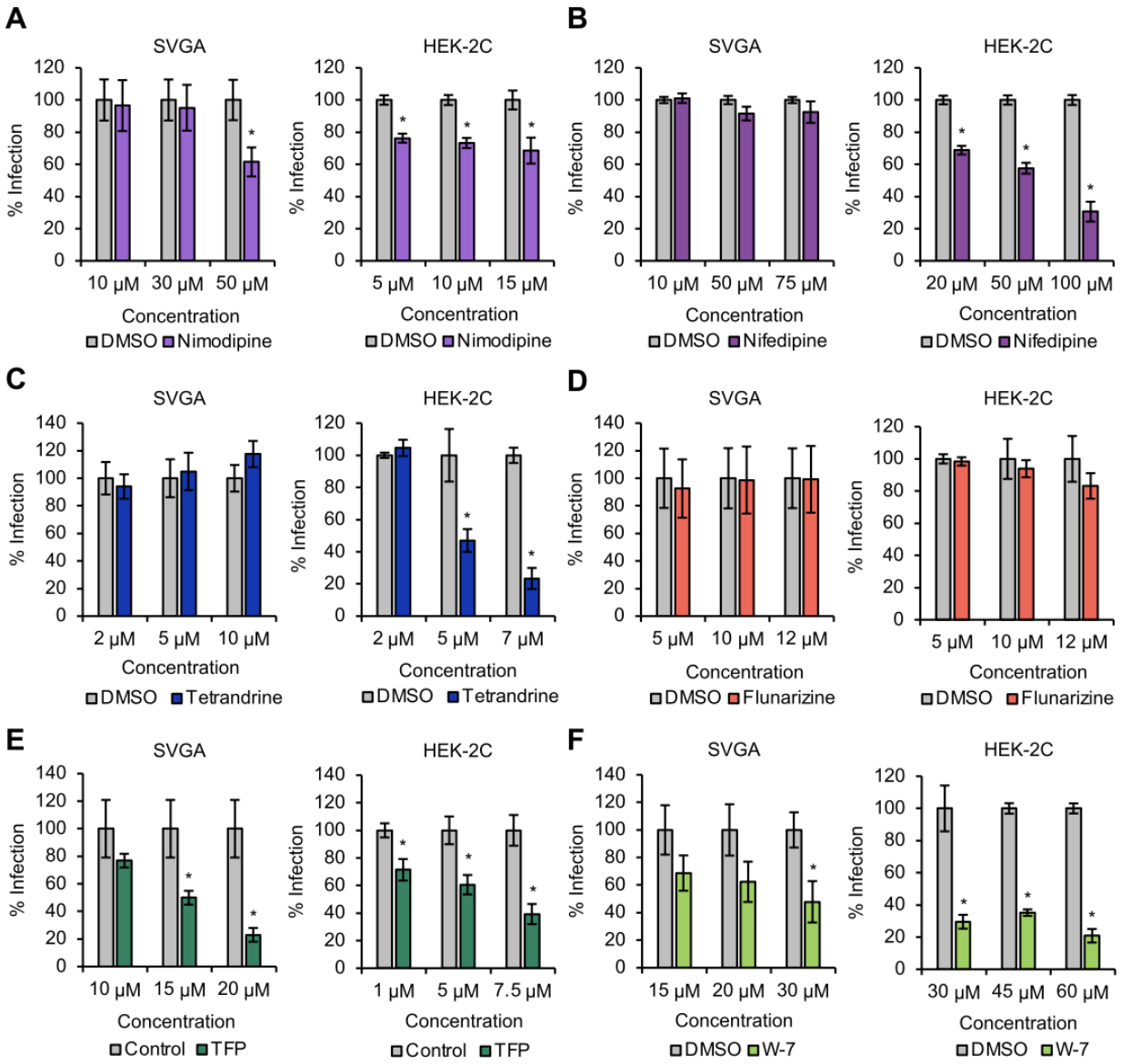

Figure 2.2. Calcium channel and signaling inhibitors reduce JCPyV infection in glial and kidney cell lines.

SVGA or HEK-2C cells were pre-treated at 37°C for 1 h with each drug at concentrations listed in figures. Cells were infected with JCPyV (MOI = 1 FFU/cell) at 37°C for 1 h in absence of inhibitor, then 100 µl/well of cell media containing inhibitor was added back and plates were incubated at 37°C. At 48 h, cells were fixed and stained for viral TAg and CellTag and analyzed by ICW using a LI-COR Odyssey CLx. Determination of % infection was calculated by subtracting background from the 800 nm channel (virus channel), then dividing the 800 nm signal from each well by its respective 700 nm signal (Cell Tag) and normalizing the control values to 100%. Graphs represent 3 replicates performed in triplicate. Error bars represent SEM. Student's t-test was used to determine statistical significance. *, $P < 0.05$.

inhibitor, W-7, that was not represented in the drug screen, was tested for the capacity to reduce JCPyV infection to further support a role for calmodulin during JCPyV infection.

Treatment with W-7 resulted in decreased JCPyV infection in both SVGA and HEK-2C cells (Fig. 2.2.F.). Other hits from the drug screen, dantrolene sodium and topiramate, did not significantly reduce infection (data not shown). Cytotoxicity profiles for drugs that significantly reduce infection (>50%) and were further characterized are shown in Table 2.1.

Table 2.1. Cell viability at various concentrations and timepoints post-inhibitor treatment. Concentrations that demonstrated <80% viability were not included in further validation studies.

		% Viability					
Inhibitor	Cell Type & Timepoint	≥100%	≥95%	≥90%	≥85%	≥80%	<80%
Tetrandrine	SVGA 48 h	10 μM	–	–	–	–	–
	HEK-2C 48 h	–	1 μM	7 μM	–	–	10 μM
Nifedipine	SVGA 48 h	–	–	–	75 μM	150 μM	200 μM
	HEK-2C 48 h	50 μM	100 μM	–	–	–	–
	Vero 48 h	20 μM	75 μM	–	100 μM	–	–
	RPTEC 48 h	–	–	–	50 μM	100 μM	–
W-7	SVGA 48 h	10 μM	–	15 μM	–	30 μM	50 μM
	HEK-2C 48 h	30 μM	–	–	60 μM	–	100 μM
	Vero 24 h	–	30 μM	–	60 μM	–	–
	Vero 48 h	45 μM	–	–	–	–	–
	Vero 72 h	45 μM	–	–	60 μM	–	–
TFP	SVGA 7 days	15 μM	–	–	–	–	–
	SVGA 48 h	–	–	20 μM	–	–	30 μM
	HEK-2C 48 h	7.5 μM	–	–	20 μM	–	30 μM
	Vero 24 h	10 μM	–	–	–	–	–
	Vero 48 h	20 μM	–	–	–	–	–
	Vero 72 h	15 μM	–	–	–	–	30 μM
	RPTEC 48 h	–	5 μM	7.5 μM	–	–	–
	HeLa 24 h	7.5 μM	–	–	–	10 μM	15 μM

2.3.3. FFU validation of ICW results

In order to verify hits that significantly reduced infection measured by ICW, focus-forming unit (FFU) assays were conducted. Infections were performed using the same experimental conditions as in ICW, but analyses differed in that cells were stained by indirect immunofluorescence and quantified by epifluorescence microscopy to identify characteristic markers of PyV infection. Results from FFU experiments demonstrated similar results observed in ICW experiments, further validating the ICW assay as an effective tool to quantify JCPyV infection (Fig. 2.3.) [280]. Nifedipine did not reduce JCPyV infection in SVGA cells, but significantly reduced JCPyV infection in HEK-2C cells (Fig. 2.3.A.). Additionally, nifedipine did not reduce SV40 infection (Fig. 2.3.B.). Similar trends were seen upon treatment with tetrandrine,

where JCPyV infection was not impacted in SVGA cells, but was significantly impaired in HEK-2C cells (Fig. 2.3.C.). Further, tetrandrine potently inhibited SV40 infection, confirming previous

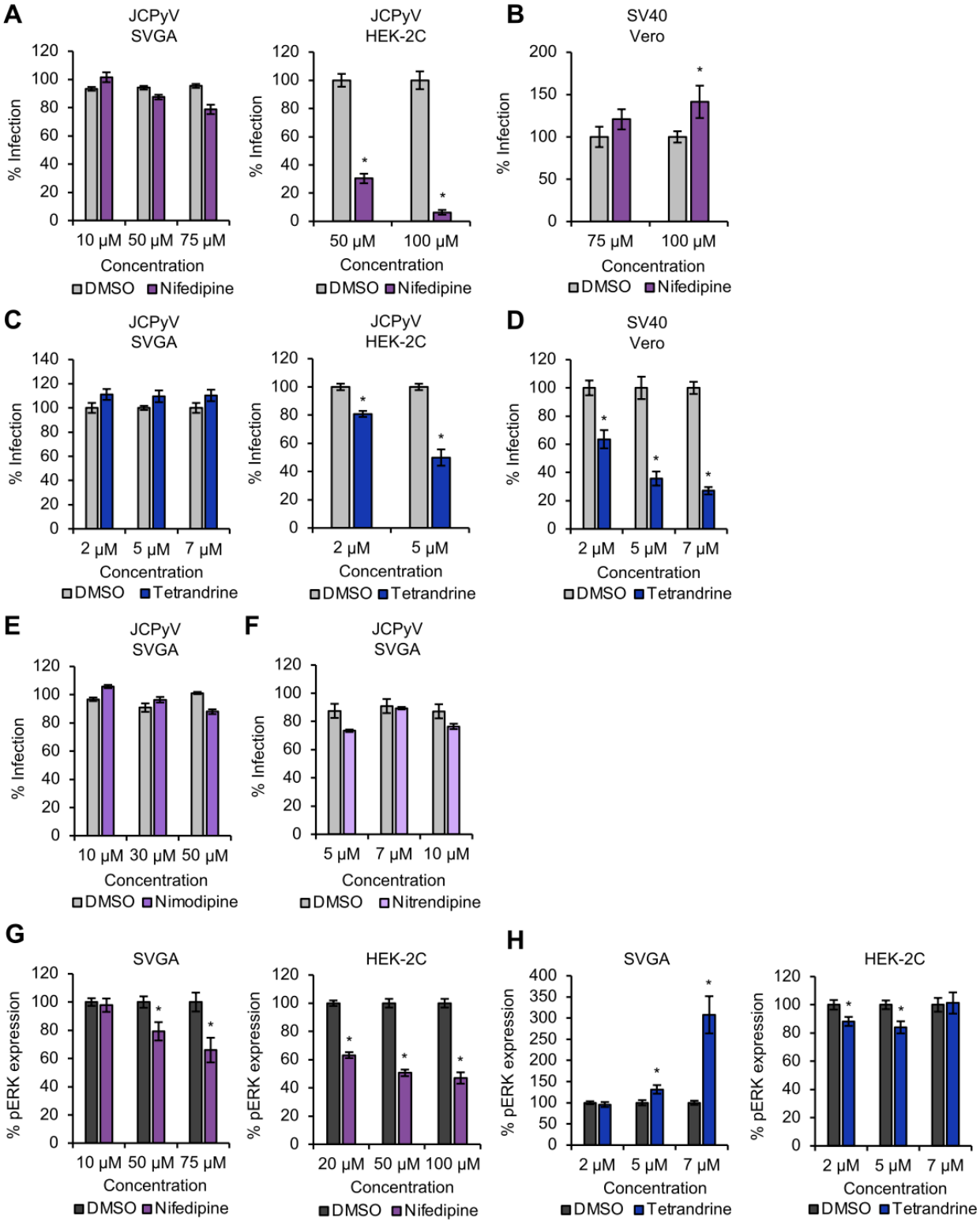

Figure 2.3. Tetrandrine and nifedipine exhibit cell type-dependent differences in JCPyV inhibition. SVGA, HEK-2C, or Vero cells were pre-treated with each inhibitor at 37°C for 1 h. JCPyV (A, C, E, F) (SVGA: MOI = 1 FFU/cell; HEK-2C: MOI = 0.5 FFU/cell) or SV40 (B and D) (MOI = 1 FFU/cell) were then added for a 1 h infection at 37°C in absence of inhibitor. Cells were fed with 100 µl/well of cell media containing inhibitor, then plates were incubated at 37°C for 48 h. PFA was added for fixation, then cells were stained for DAPI and (A, C, E, F) TAg or (B and D) VP1. Infections were quantified by FFU assay with 5 FOV/well counted. Determination of % infection was calculated by dividing the number of infected cells/the number of DAPI+ cells in each 20X visual field and normalizing to 100%. (G and H) SVGA or HEK-2C cells were treated with (G) nifedipine or (H) tetrandrine at 37°C for 24 h. Cells were fixed with PFA and stained for pERK and CellTag and analyzed by ICW using a LI-COR Odyssey CLx. Determination of % pERK expression was calculated by subtracting background from the 800 nm channel (pERK channel), then dividing the 800 nm signal from each well by its respective 700 nm signal (CellTag) and normalizing the control values to 100%. Graphs represent 3 replicates performed in triplicate. Error bars represent SEM. Student's t-test was used to determine statistical significance. *, $P < 0.05$.

findings [253] (Fig. 2.3.D.). Nimodipine and nitrendipine, both inhibitors of L-type Ca^{2+} channels, did not significantly reduce JCPyV infection in SVGA cells (Fig. 2.3.E and F). Interestingly, nifedipine and tetrandrine have been reported to alter MAPK signaling and ERK phosphorylation in a cell type-dependent manner [289-291]. Given the necessary role of MAPK activation and ERK phosphorylation in JCPyV infection [216], pERK levels were measured following cellular treatment with nifedipine and tetrandrine. SVGA and HEK-2C cells treated with nifedipine demonstrated a significant reduction in pERK levels, which correlates with reduced infection (Fig. 2.3.G.). Interestingly, while HEK-2C cells treated with tetrandrine also showed a reduction in pERK levels, SVGA cells treated with tetrandrine showed a dramatic increase in pERK (Fig. 2.3.H.), and these findings are consistent with outcomes of infection (Fig. 2.3.A–D.).

2.3.4. Calmodulin inhibitors reduce JCPyV infectivity

One hit from the drug screen included the calmodulin inhibitor trifluoperazine (TFP). In order to validate this hit from the screen, cells were treated with TFP, infected with JCPyV, and assessed for infection. In addition to TFP, another calmodulin inhibitor, W-7, was evaluated to test the role of calmodulin during JCPyV infection. TFP blocks calmodulin activity by binding

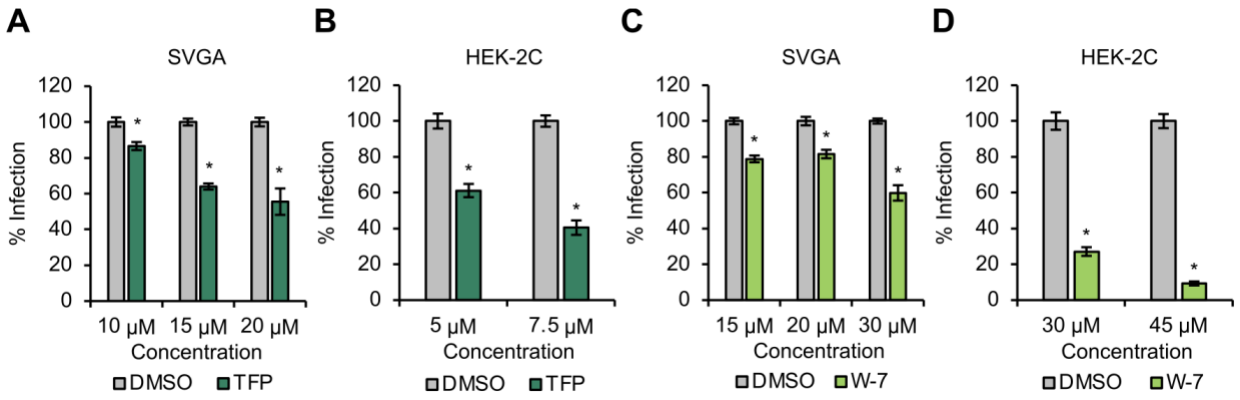

Figure 2.4. Calmodulin inhibitors decrease JCPyV infection.
TFP or W-7 were added to SVGA or HEK-2C cells at 37°C for 1 h for pre-treatment. Cells were then challenged with JCPyV (SVGA: MOI = 1 FFU/cell; HEK-2C: MOI = 0.5 FFU/cell) at 37°C for 1 h in absence of inhibitor. Infections were fed with 100 µl/well of cell media containing inhibitor, and plates were incubated at 37°C for 48 h. Cells were fixed in 4% PFA, then stained for JCPyV TAg and DAPI. Infections were quantified by FFU assay with 5 FOV/well counted. Determination of % infection was calculated by dividing the number of infected cells/the number of DAPI+ cells in each 20X visual field and normalizing to 100%. Graphs represent 3 replicates performed in triplicate. Error bars represent SEM. Student's t-test was used to determine statistical significance. *, $P < 0.05$.

directly to calmodulin and inducing a conformational change, while W-7 binds to each of two calmodulin domains to block CaM-dependent enzyme activity [292, 293]. Results showed that treatment of SVGA and HEK-2C cells with calmodulin inhibitors TFP and W-7 resulted in significant reduction of JCPyV infection, suggesting a role for calmodulin during JCPyV infection (Fig. 2.4.A–D.).

2.3.5. Calmodulin inhibitors reduce SV40, BKPyV, and SARS-CoV-2 infections

Due to the consistent reduction in JCPyV infection upon treatment with calmodulin inhibitors, it was questioned whether calmodulin may be a key factor during other polyomavirus infections and non-polyomavirus infections. Vero cells were treated with either TFP or W-7, challenged with either SV40 or BKPyV, and assessed for infection. Both SV40 and BKPyV infections were significantly reduced (Fig. 2.5.A–D.). These results suggest a potential role for calmodulin in the polyomavirus family of viruses. In addition to polyomaviruses, TFP and W-7 were also tested for their effects on the ssRNA virus SARS-CoV-2, as this is a prominent virus of

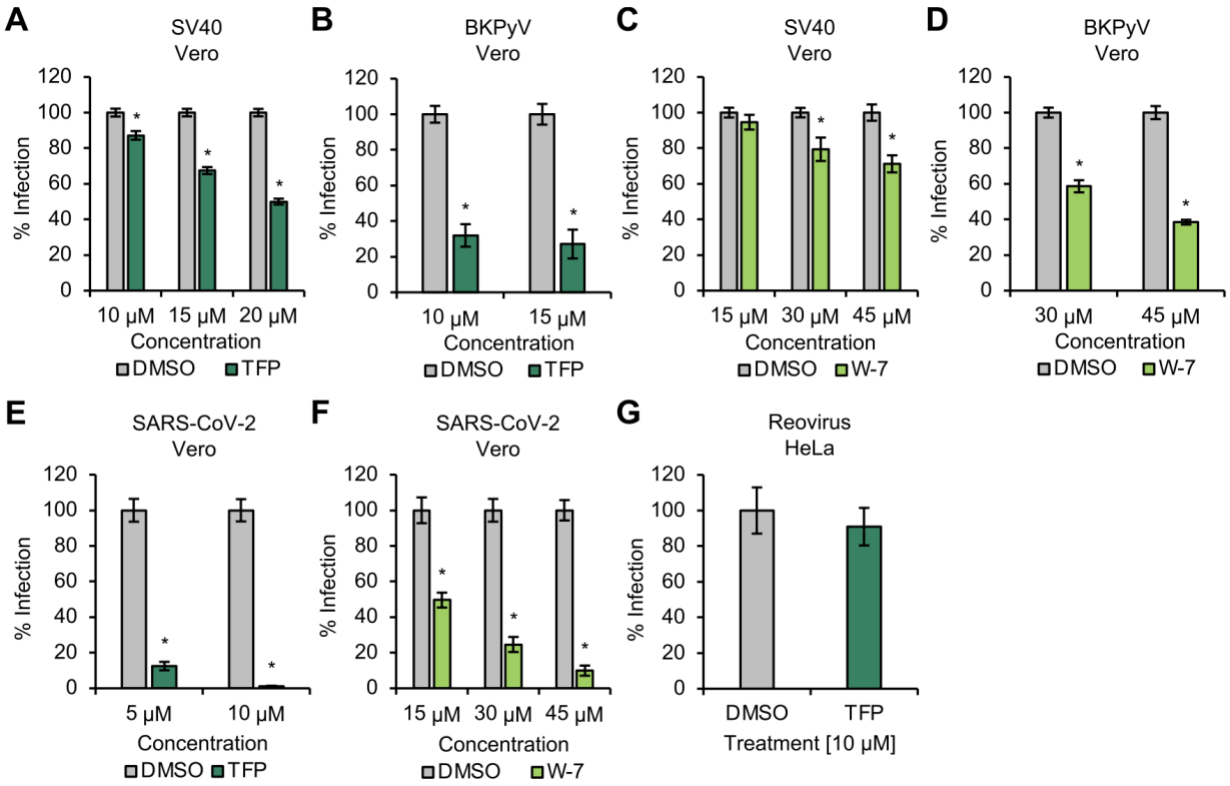

Figure 2.5. TFP and W-7 broadly reduce polyomavirus and coronavirus infections.
(A-F) Vero or (G) HeLa cells were pre-treated with (A and B, E and G) TFP or (C and D, F) W-7 at 37°C for 1 h. (A and C) Cells were infected with SV40 (MOI = 1 FFU/cell) at 37°C for 1 h, then fed with 100 µl/well of cell media containing inhibitor and plates were incubated at 37°C for 48 h. (B and D) Cells were infected with BKPyV (MOI = 4 FFU/cell) at 37°C for 2h, then fed with 100 µl/well of cell media containing inhibitor and plates were incubated at 37°C for 72 h. (E and F) Cells were infected with SARS-CoV-2 (TCID50 =0.025/cell) at 37°C for 1 h, then fed with 100 µl/well of cell media containing inhibitor and plates were incubated at 37°C for 24 h. (G) Cells were infected with reovirus (MOI = 300 FFU/cell) at RT for 1 h, then fed with 100 µl/well of cell media containing inhibitor and plates were incubated at 37°C for 24 h. Cells were fixed with 4% PFA and stained for viral protein, then quantified by FFU assay with 5 FOV/well counted. Determination of % infection was calculated by dividing the number of infected cells/the number of DAPI+ cells per visual field and normalizing to 100%. Samples were analyzed under the following magnifications: 10X (SV40, reovirus, and BKPyV); 20X (SARS-CoV-2). Graphs represent 3 replicates performed in triplicate. Error bars represent SEM. Student's t-test was used to determine statistical significance. *, $P < 0.05$.

concern and calmodulin is known to interact with the angiotensin-converting enzyme-2 (ACE2) receptor – the primary receptor involved in SARS-CoV-2 entry [294]. Since SARS-CoV-2 has been shown to be inhibited by TFP, it was hypothesized that TFP and W-7 would reduce SARS-CoV-2 infection [295]. Treatment with both TFP and W-7 resulted in dramatically impaired SARS-CoV-2

infection, indicating the importance of calmodulin during SARS-CoV-2 infection and suggesting TFP as a potential broad antiviral (Fig. 2.5.E and F). Importantly, it was previously reported that reovirus, a dsRNA virus, was not impacted by treatment with TFP [287]. As a negative control, HeLa cells were treated with TFP and infected with reovirus. Reovirus infection was not impacted by treatment with TFP, indicating that TFP and W7 demonstrate specificity for inhibition of certain viruses (Fig. 2.5.G.).

2.3.6. JCPyV infection of primary kidney cells

The lack of a tractable animal model for JCPyV infection reduces opportunities to test inhibitors, yet primary cell lines represent an innovative model that more accurately represents the cells in the human host. Renal proximal tubule cells (RPTECs), a primary kidney cell type,

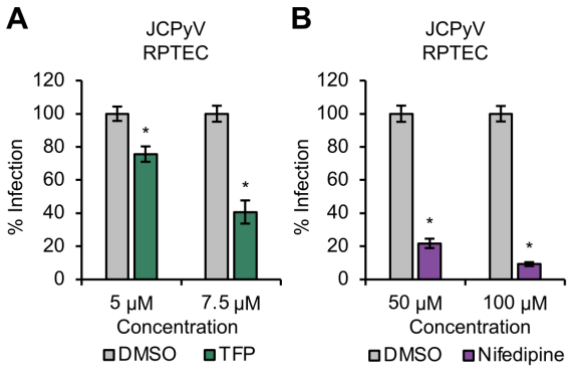

Figure 2.6. JCPyV infection is significantly impaired in primary RPTECs.
Cells were pre-treated with (A) TFP or (B) nifedipine at 37°C for 1 h. JCPyV (MOI = 2 FFU/cell) was added in absence of inhibitor at 37°C for 1 h, then cells were fed with 100 µl/well of cell media containing inhibitor. Plates were incubated at 37°C for 48 h, fixed with PFA, then stained for JCPyV TAg. Infected cells were quantified by FFU assay with 5 FOV/well counted. Determination of % infection was calculated by dividing the number of infected cells/the number of DAPI+ cells per 10X visual field and normalizing to 100%. Graphs represent 3 replicates performed in triplicate. Error bars represent SEM. Student's t-test was used to determine statistical significance. *, $P < 0.05$.

were treated with TFP or nifedipine and infected with JCPyV. TFP and nifedipine significantly reduced JCPyV infection in RPTECs (Fig. 2.6.A and B). Taken together, these results indicate that

the impacts of TFP and nifedipine on JCPyV infection in immortalized vs primary kidney cells are comparable.

2.3.7. Time of addition, attachment, entry, and trafficking of JCPyV during TFP treatment

To understand the step in the JCPyV infectious cycle that is inhibited by TFP, a time of addition assay was performed in HEK-2C cells. Results showed the most significant reduction in JCPyV infection when TFP was added at the time of virus addition, as well as up to 4 h-post infection (hpi), and no inhibition was observed at times after 6 hpi (Fig. 2.7.A.). These time points are consistent with viral attachment, entry, and trafficking, so these steps were further investigated [144, 170]. Flow cytometry was performed to determine whether TFP was impacting JCPyV attachment. HEK-2C cells were incubated with either DMSO (control) or TFP, then infected with JCPyV-647 in suspension. Results showed no significant difference in JCPyV attachment when cells were treated with TFP, indicating that TFP is not acting upon JCPyV infection during attachment (Fig. 2.7.B.). To determine whether TFP was affecting viral internalization or trafficking, confocal microscopy was performed to assess internalization of Alexa 647-labeled JCPyV in HEK-2C cells treated with TFP compared to the DMSO control. Viral internalization was significantly impaired in cells treated with TFP, suggesting that TFP is impacting JCPyV entry (Fig. 2.7.C.). To assess viral trafficking, cells were treated with TFP and transfected with the infectious clone of JCPyV, which bypasses viral entry and trafficking. Results showed that there was a modest reduction in JCPyV VP1+ cells, indicating a potential role for TFP in a post-entry step in JCPyV infection (Fig. 2.7.E.), yet the greatest reduction in infection was observed during viral entry.

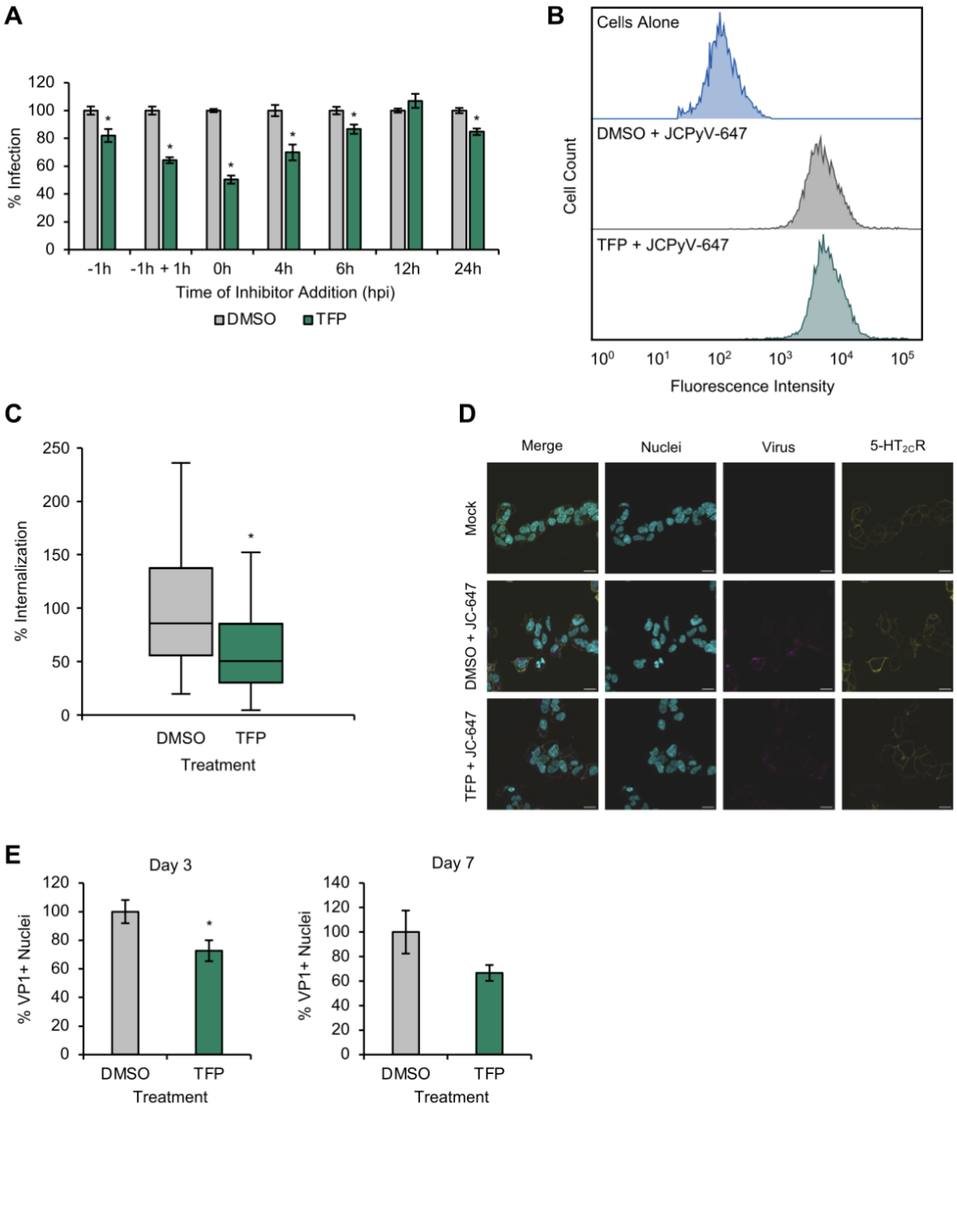
A
% Infection
120
100
80
60
40
20
0
-1h
-1h + 1h
0h
4h
6h
12h
24h
Time of Inhibitor Addition (hpi)
DMSO
TFP
B
Cells Alone
DMSO + JCPyV-647
TFP + JCPyV-647
Cell Count
10^0
10^1
10^2
10^3
10^4
10^5
Fluorescence Intensity
C
% Internalization
250
200
150
100
50
0
DMSO
TFP
Treatment
D
Merge
Nuclei
Virus
5-HT2cR
Mock
DMSO + JC-647
TFP + JC-647
E
Day 3
% VP1+ Nuclei
120
100
80
60
40
20
0
DMSO
TFP
Treatment
Day 7
% VP1+ Nuclei
140
120
100
80
60
40
20
0
DMSO
TFP
Treatment

Figure 2.7. TFP reduces JCPyV entry in kidney cells.
(A) TFP [7.5 µM] was added to HEK-2C cells 1 h prior to infection with JCPyV (MOI = 1 FFU/cell), simultaneously with JCPyV (t =0 h), or at times post-infection indicated in figure. At 48 h, cells were fixed and stained for JCPyV TAg and imaged on a LI-COR Odyssey CLx. Determination of % infection was calculated by subtracting background from the 800 nm channel (virus channel), then dividing the 800 nm signal from each well by its respective 700 nm signal (CellTag) and normalizing the control values to 100%. Graphs represent 3 replicates performed in triplicate. Error bars represent SEM. (B) HEK-2C cells were pre-treated with TFP at 37°C for 1 h, infected with JCPyV-647 on ice for 1 h, then fixed with PFA. Samples were analyzed by flow cytometry using a BD LSR II flow cytometer equipped with an APC laser line (640 nm). Data was analyzed using FACSDiva and FlowJo software, with gating performed to exclude complex or dead cells. Data is representative of 3 independent experiments with at least 5000 events per sample. (C) HEK-2C cells were pre-treated with TFP [7.5 µM] at 37°C for 1 h, pre-chilled to 4°C for 45 min, infected with JCPyV-647 at 4°C for 1h to allow for synchronized viral attachment, then shifted to 37°C for viral internalization. After 2 h, cells were fixed with PFA and stained with DAPI. Samples were imaged on a Leica SP8 confocal microscope at 63× magnification. ImageJ software was used to draw ROIs around the perimeter of each cell, excluding the plasma membrane, to collect mean intensity values for internalized virus. Graph represents 3 replicates with at least 30 cells analyzed per sample per replicate. (D) Representative images from internalization assay with nuclei (cyan), JCPyV-647 (magenta), and 5-HT_{2C}R (yellow). Scale bars = 20 µm. (E) SVGA cells were pre-treated with TFP [15 µM] at 37°C for 1 h, transfected with the JCPyV infectious clone in the presence of TFP, then media was replaced after 6 h. At day 3 or day 7, cells were fixed and stained for JCPyV VP1 and analyzed for % VP1+ nuclei. VP1+ nuclei were quantified by FFU assay with 5 FOV/well counted at 10× magnification. Determination of % VP1+ nuclei was calculated by dividing the number of VP1+ cells/the number of DAPI+ cells per visual field and normalizing to 100%. Graphs represent duplicate experiments where each duplicate contained three individual plasmid digestions and transfections per treatment condition. Samples were normalized to the average of control-treated samples (100%). Error bars represent SEM. Student's t-test was used to determine statistical significance. *, $P < 0.05$.

2.4. Discussion

In this report, we reveal findings from a large-scale drug screen performed in an attempt to discover potential antivirals for JCPyV infection and describe further characterization of calcium-related drug hits. Results from the drug screen identified 42 hits, with the most substantial drug categories being receptor agonists/antagonists, enzyme inhibitors, and calcium-related drugs. This study focused on the calcium-related drugs and found that TFP, W-7, nifedipine, and tetrandrine are capable of decreasing JCPyV infectivity. Nifedipine and tetrandrine, both calcium channel blockers, exhibited cell type-dependent inhibition of infection, which was partially explained by changes in pERK upon treatment of cells with the

inhibitors. Interestingly, TFP, an inhibitor of calmodulin and currently FDA-approved treatment for schizophrenia, may serve as a broad antiviral treatment for polyomavirus infections as well as coronavirus infections. Upon further investigation using time course experiments and targeted analysis of the infectious cycle, it was determined that TFP was impeding viral entry. Taken together, calcium-related drugs inhibited JCPyV infection, with calmodulin inhibitors broadly impacting polyomavirus and coronavirus infections.

Performing a high-throughput NCC drug screen to identify potential antivirals for JCPyV infection led to the discovery that calcium signaling-related inhibitors are capable of reducing JCPyV infectivity. Findings reported by Dobson et al. [253] that implicated host-cell calcium signaling during MCPyV and SV40 infections further contributed to the rationale to pursue these hits. Dobson et al. demonstrated that tetrandrine, an inhibitor of NAADP-sensitive TPCs, drastically reduced both MCPyV and SV40 infections, and the inhibition specifically impacted endosomal fusion with the endoplasmic reticulum. Although tetrandrine is an inhibitor of TPCs, tetrandrine has also been shown to inhibit calmodulin and act broadly as a calcium channel inhibitor [296]. Our findings showed that flunarizine, a T-type Ca^{2+} channel blocker, did not reduce JCPyV infection, yet, interestingly, Dobson et al. found that flunarizine significantly impaired MCPyV, but not SV40 infection. Nifedipine, an inhibitor of L-type Ca^{2+} channels, reduced JCPyV infection in HEK-2C cells but not SVGA cells. Because nifedipine also reduced pERK, this suggests either an off-target effect or possibly that reducing calcium signaling through L-type Ca^{2+} channels is impacting the MAPK pathway and therefore reducing JCPyV infection.

Treatment of cells with tetrandrine, the NAADP-sensitive TPC inhibitor, resulted in a cell-type dependent difference in outcomes for JCPyV infection. In SVGA cells, an immortalized glial cell line, tetrandrine slightly increased JCPyV infection. However, in HEK-2C cells, an immortalized kidney cell line, tetrandrine significantly reduced JCPyV infectivity. Interestingly, tetrandrine also reduced SV40 infection in Vero cells, an immortalized African green monkey kidney cell line, indicating a potential tissue-specific mechanism of reduction of polyomavirus infection by tetrandrine in kidney cell types. One possible explanation for this cell-type dependent difference in infection during tetrandrine treatment is a difference in signaling pathway regulation during infection. To delve deeper into this interesting finding, both cell types were treated with tetrandrine in the absence of JCPyV and levels of pERK were measured. After 24 h of treatment with tetrandrine, levels of pERK were significantly increased in SVGA cells, but significantly reduced in HEK-2C cells (Fig. 2.3.H.). This difference in relative levels of pERK, a key signaling protein known to be important for JCPyV infection, could help explain the cell-type dependent differences in infection. Of note, HEK-2C cells overexpress the 5-HT_2Rs, which contain calmodulin-binding domains [297, 298]. An additional explanation for these cell-type dependent differences in JCPyV infection may be due to differences in permissivity of SVGAs and HEK-2Cs. SVGAs are transformed with SV40 TAg, rendering them more permissive for JCPyV infection [281]. HEK-2Cs are poorly permissive for JCPyV infection prior to overexpressing the 5-HT_{2C} receptor [141]. Therefore, greater inhibition may be observed in the HEK-2C cell model due to reduced permissivity in this cell type. Although Ca^{2+} signaling and channel inhibitors seem promising, not all Ca^{2+} inhibitors proved effective in reducing viral infection. Flunarizine, a T-type Ca^{2+} channel blocker, did not reduce JCPyV infection, suggesting that JCPyV infection is

independent of T-type Ca^{2+} channel activity. L-type Ca^{2+} channel inhibitors nimodipine and nitrendipine did not have a major impact on JCPyV infection, but nifedipine significantly reduced JCPyV infection in HEK-2C cells. These results combined with the pERK nifedipine experiments (Fig. 2.3.G.) indicate that L-type Ca^{2+} channels may not be essential for JCPyV infection but rather impact ERK activation. Analysis of other drugs used in this study for pERK activation did not demonstrate a significant difference in pERK levels compared to controls (data not shown).

Inhibitors of calmodulin, TFP and W-7, showed a consistent decrease in JCPyV infection, indicating that calmodulin may play a key role during JCPyV infection. TFP also significantly reduced SV40, BKPyV, and SARS-CoV-2 infections, but not reovirus infection. To define how TFP was impacting the JCPyV infectious cycle, the inhibitor was added over a time course and found to reduce infection the most at 0–4 h, times consistent with viral attachment, entry, and trafficking (Fig. 2.7.A.). Further analysis of viral entry by confocal microscopy revealed that TFP significantly reduced viral internalization (Fig. 2.7.C.). To confirm our finding that viral entry (and not earlier events) is affected by TFP, viral attachment was assessed by flow cytometry and data showed that attachment was unaffected (Fig. 2.7.B.). Points post-entry were also investigated using the viral infectious clone, which bypasses entry and trafficking, and a modest reduction in VP1+ cells was observed. These data suggest that in addition to blocking viral internalization, TFP could also impact post-entry steps such as viral transcription (Fig. 2.7.E.). For instance, TFP could impact other components of calcium-signaling pathways such as calcineurin, which is activated by Ca^{2+} and calmodulin binding and then induces activation of NFAT4, a transcription factor required for JCPyV infection [299]. However, the time course experiments demonstrate

that while TFP induces a slight decrease at later times in the infectious cycle (6, 12, and 24 hpi), the greatest impact is consistent with the timing of viral entry or trafficking to proper cellular compartments (Fig. 2.7.A.). Only the JCPyV infectious cycle was analyzed, and thus TFP could be blocking other steps during BKPyV, SV40, and SARS-CoV-2 infections. Some commonalities between polyomaviruses and coronaviruses during infection include the requirement to enter cells by clathrin-mediated endocytosis and trafficking in the endosomal pathway [300], yet the later steps in the viral life cycle differ significantly for the dsDNA polyomaviruses compared to the ssRNA coronaviruses. Thus, the mechanisms of inhibition for other viruses explored in this study require more investigation. RPTECs, a primary kidney cell line, were used to better recapitulate JCPyV infection in human cells in absence of potentially altered signaling pathways due to immortalization of cells. TFP, an inhibitor of calmodulin, showed great potential to reduce JCPyV, SV40, BKPyV, and SARS-CoV-2 infections in immortalized cell lines. When RPTECs were treated with TFP and challenged with JCPyV, a significant reduction in infection was observed (Fig. 2.6.A.). Because nifedipine also showed a significant reduction in JCPyV infection in HEK-2C cells, nifedipine was also tested for the capacity to reduce JCPyV infection in primary RPTECs. A significant decrease in JCPyV infection upon treatment with nifedipine was also noted (Fig. 2.6.B.). These findings are important as the kidney is a major target of JCPyV infection. TFP is already an FDA-approved drug and is capable of crossing the blood-brain barrier, so there is a potential for repurposing TFP for treatment of JCPyV infection for PML [301]. Although primary cells are more similar to in vivo human infection than immortalized cells, they cannot fully recapitulate the in vivo environment. For this reason, in vivo studies should be performed to test efficacy of TFP on polyomavirus infections in a whole-body system. TFP may serve as one

potential treatment for polyomavirus infections, but other possible inhibitors remain to be discovered. TFP is currently an FDA-approved drug, and thus repurposing TFP as an antiviral would be an efficient means of drug discovery. This method of repurposing FDA-approved drugs is a well-demonstrated tactic and was utilized for the discovery of remdesivir for treatment of SARS-CoV-2 [302-304]. Additionally, large-scale screens such as the NCC have led to the identification of other potential anti-coronavirus drugs [305]. Given that TFP was demonstrated to inhibit polyomavirus and coronavirus infections and that TFP has previously been shown to inhibit dengue, Zika, hepatitis C virus, influenza, measles, Epstein-Barr, arenaviruses, and coronavirus infections, it may serve as a broad-spectrum inhibitor [306-312]. However, infection with reovirus, a dsRNA virus, was not impacted by treatment with TFP, hinting at a possible shared mechanism between multiple virus families, excluding Reoviridae. Many viruses are known to utilize calcium signaling pathways during infection, including HIV, influenza, and SARS-CoV-2, demonstrating a commonality between several virus families. Although polyomaviruses have been shown to rely on host cell calcium signaling for successful infection, the specific roles of calcium signaling during polyomavirus infection are still not well-understood and warrant further exploration.

2.5. Conclusions

A screen for inhibitors of JCPyV infection using the NCC led to the identification of 42 hits with antiviral activity against JCPyV. Calcium signaling-related inhibitors comprised a large portion of the hits from the screen. Upon further characterization, various calcium inhibitors reduced JCPyV infection in immortalized brain and immortalized and primary kidney cells. Of these, calmodulin inhibitors showed the greatest capacity to impact infection of JCPyV as well as

SV40, BKPyV, and SARS-CoV-2, suggesting that calmodulin inhibitors may serve as broad-spectrum antiviral therapeutics. Further analysis of the JCPyV infectious cycle showed that calmodulin inhibitor TFP disrupted infection at the point of viral internalization. Taken together, this work highlights the utility of repurposing drugs as antivirals and demonstrates that drug screens can effectively identify broad-spectrum antiviral treatments due to conservation in viral interactions with cellular targets.

CHAPTER 3

INFECTION BY JCPYV STIMULATES INTRACELLULAR CALCIUM FLUX IN GLIAL CELLS

3.1. Introduction

DNA viruses, like JCPyV, aren't usually equipped with their own machinery, and therefore must rely almost entirely on host cell components and functions to carry out the infectious cycle. The JCPyV infectious cycle involves initial attachment to host cells via interactions of VP1 with α2,6-linked sialic acid on LSTc [132, 133]. Serotonin receptors, 5-HT_2Rs, are GPCRs and facilitate internalization of JCPyV through CME [97, 99, 140-144]. JCPyV then traffics through early endosomes and caveolin-1+ late endosomes to reach the ER, where the capsid partially uncoats [151, 170]. Eventually, JCPyV translocates into the cytosol, then enters the nucleus where host DNA replication machinery is hijacked by the virus for transcription and replication of the JCPyV genome [177]. Additionally, viruses activate signaling pathways to gain control of the cell to carry out the infectious cycle. JCPyV infection activates several signaling pathways, including the MAPK/ERK and PI3K/AKT pathways to reprogram the cell and support viral infection [216, 217, 274, 313]. However, little is known about other cellular signaling pathways activated by JCPyV.

Cellular signaling regulates many essential biological processes, including cell growth and division, migration, division, and apoptosis [210]. One particular signaling system, the Ca^{2+} signaling pathway, is responsible for control of cell motility, excitability, transcription, exocytosis, and apoptosis [219]. Ca^{2+} signaling is essential in cell biology, with Ca^{2+} ions impacting nearly all aspects of cellular life [218]. Signaling in the Ca^{2+} pathways can begin with Ca^{2+} influx from the extracellular environment, or when Ca^{2+} is released from intracellular stores, including the ER,

mitochondria, Golgi, and lysosomes [221]. Several Ca^{2+} channels and pumps are present on the plasma membrane, as well as the membranes of intracellular Ca^{2+} stores to facilitate Ca^{2+} influx and efflux [222-224]. Additionally, several Ca^{2+}-sensing cytosolic proteins aid in the transduction of various Ca^{2+} signals by acting as messengers to relay information to target molecules in the cell [218].

Viruses are obligate intracellular parasites, meaning they rely on host cell machinery to carry out successful infections [314]. Ca^{2+} signaling is a common target for a variety of viruses, as it is involved in a wide variety of cellular functions and can be manipulated to strengthen the cellular environment to support viral infection. Ca^{2+} signaling has been implicated in viral entry, trafficking, replication, virion assembly, maturation, and/or release of a broad range of viruses [226, 227]. One of the larger intracellular Ca^{2+} stores is the ER, which is manipulated by viruses including RV, HCMV, EBV, and HIV-1 [242-245]. The ER contains a few Ca^{2+} channels that aid in Ca^{2+} release into the cytosol including: RyR, SERCA, and IP_3R [315]. IP_3R is the main Ca^{2+}-release channel in the ER and is involved in a pathway which begins at the plasma membrane when receptors are activated, causing phospholipase C (PLC) to cleave phosphatidylinositol 4,5-bisphosphate (PIP2) into IP_3 and DAG [316]. IP_3 then binds to the IP_3R, stimulating Ca^{2+} release from the ER [317].

Inhibition of MCPyV, SV40, and more recently, JCPyV, by various Ca^{2+}-related inhibitors has sparked interest in understanding how Ca^{2+} may be involved in polyomavirus infections [253, 318]. JCPyV infection was reduced by chemical inhibition of two-pore Ca^{2+} channels (TPCs), L-type Ca^{2+} channels, and calmodulin. Therefore, the objective of this study was to further delineate the necessity for and mechanism of Ca^{2+} involvement during JCPyV infection.

Given that JCPyV utilizes 5-HT_2Rs, a type of GPCR, during viral internalization, and GPCR stimulation can lead to activation of IP_3R-mediated Ca^{2+} release from the ER, exploration of ER Ca^{2+} stores during JCPyV infection was investigated using cell-based, molecular and genetic approaches.

3.2. Materials and Methods

3.2.1. Cells and viruses

SVGA cells [281] were maintained in complete minimum essential medium (MEM) (Corning) containing 10% fetal bovine serum (FBS), 1% penicillin-streptomycin (P/S) (Mediatech, Inc.), and 0.2% Plasmocin (InvivoGen). Cell lines were propagated in a humidified incubator at 37°C with 5% CO_2 and were passaged 2-3 times weekly. SVGA cells were generously provided by the Atwood Laboratory (Brown University).

JCPyV strain Mad-1/SVEΔ (Atwood Laboratory, Brown University) was generated and propagated as described previously [170, 282]. Crude supernatant stock was used in all experiments except when purified virus is indicated. JCPyV stocks were titered by FFU infectivity assay in SVGA cells.

3.2.2. Antibodies, dyes, siRNAs, and inhibitors

A monoclonal antibody (mAb) used to detect infectivity by FFU and ICW assays, PAB597, was obtained from a hybridoma and targeted against JCPyV viral protein 1 (VP1), generously provided by Ed Harlow and Walter Atwood. Secondary polyclonal goat anti-mouse Alexa Fluor 488 antibody (Thermo Fisher) was used for FFU assays, while secondary LI-COR 800 anti-mouse antibody (LI-COR) was used for ICW assays. DAPI (Thermo Fisher) was used for FFU assays to stain cell nuclei, and CellTag 700 (LI-COR) was used as a cell count normalization stain for ICW

assays. Antibodies used to detect proteins on Western blots include primary mAb against IP_3R2 (Santa Cruz Biotechnology), primary mAb against housekeeping protein GAPDH (Cell Signaling Technology), and secondary LI-COR 700 or 800 anti-mouse or anti-rabbit antibodies (LI-COR). Chameleon Duo Pre-Stained Protein Ladder (LI-COR) was used for protein size comparison on Western blots. Fluo-4 AM is a cell permeable dye used to detect intracellular Ca^{2+} flux (Thermo Fisher). IP_3R2 siRNA was used to silence the ITPR2 gene (Invitrogen) (Catalog # AM51331; siRNA ID # 106736)(Target sequence: GGACAGUGGAACAGCUUGUtt).

Chemical inhibitors and activators include 2-APB (Sigma-Aldrich), BAPTA-AM (Abcam), and Ionomycin (Thermo Fisher). All inhibitors and activators were resuspended in DMSO (Tocris Bioscience), which was used as a volume-specific vehicle control. Concentrations of inhibitors and activators are listed in figures or figure legends where applicable.

3.2.3. Ionomycin Fluo-4 AM plate reader assay

SVGA cells were plated to 70% confluence in 96-well clear bottom, black wall plates in phenol-free MEM containing 10% FBS (10% MEM). Fluo-4 AM was used according to manufacturer's instructions. First, it was diluted to a concentration of 4 µM in phenol-free MEM with no additives (Incomplete MEM). Cells were loaded with Fluo-4 AM at 37°C for 30 min, washed with incomplete MEM to remove excess dye, then incubated at 37°C for another 30 min for de-esterification of the AM ester. Cells were then pre-treated with BAPTA-AM (2.5 µM) in 10% MEM for 1 h. After pre-treatment, ionomycin (5 µM), ionomycin + BAPTA-AM, DMSO x1 (volume control for ionomycin), or DMSO x2 (volume control for ionomycin + BAPTA-AM) were added and fluorescence was immediately measured on an Agilent BioTek Cytation 5 Imaging Reader.

Fluorescence read settings include: excitation/emission 494/516 with bandwidth of 9 for both, read height 5.0 mm, normal read speed, read once/min for 3 h duration, at 37°C with 5% CO_2.

3.2.4. JCPyV Fluo-4 AM plate reader assay

SVGA cells were plated to 70% confluence in 96-well clear bottom, black wall plates in phenol-free MEM containing 10% FBS (10% MEM). Fluo-4 AM was used according to manufacturer's instructions. Fluo-4 AM was diluted to a concentration of 4 µM in phenol-free MEM with no additives (Incomplete MEM). Cells were loaded with Fluo-4 AM at 37°C for 30 min, washed with incomplete MEM to remove excess dye, then incubated at 37°C for another 30 min for de-esterification of the AM ester. Cells were then infected with pure JCPyV (MOI = 5 FFU/cell) or mock-infected (volume control using mock virus prep) in 10% MEM at 37°C for 1 h. After 1 h infection, fluorescence was measured on an Agilent BioTek Cytation 5 Imaging Reader. Fluorescence read settings are the same as in the ionomycin plate reader assay.

3.2.5. Cell viability assay

Cell viability under specified inhibitor concentrations was tested by MTS assay (Promega) for corresponding infection duration according to manufacturer's instructions. Cells were plated to 70% confluence in 96-well plates in 10% MEM and toxicity assays were performed to mimic the experimental design of infectivity assays. Cells were pre-treated with 2-APB or DMSO volume control at 37°C for 2 h, mock-infected with 10% MEM at 37°C for 1 h, then 100 µl of 10% MEM was added back for 72 h. MTS reagent was added, incubated at 37°C for 1–4 h, then absorbance measurements were taken at 490 nm using an Agilent BioTek Cytation 5 Imaging Reader. Experiments were performed in triplicate. Concentrations that did not induce

significant toxicity and maintained >80% cell viability in comparison to the relevant DMSO control were considered useable concentrations.

3.2.6. In-Cell Western (ICW) infections, staining, and protein quantification

SVGA cells were seeded in 96-well plates in 10% MEM to achieve 70% confluence at time of infection. 2-APB was diluted in 10% MEM to concentrations indicated in figure, added to triplicate wells, and incubated at 37°C for 2 h. Cells were infected with JCPyV (MOI = 2 FFU/cell) in 10% MEM in absence of inhibitor and incubated at 37°C for 1 h. Infections were fed with 100 µl/well of 10% MEM and incubated for 72 h. Cells were fixed in 4% PFA, stained for VP1 (1:40), and analyzed by ICW assay. Infections were performed in triplicate for a minimum of 3 replicates.

After fixation, cells were washed 3x with 0.1% PBS-Tween (PBS-T) for 5 min. Cells were permeabilized with 1% Triton X-100 (TX-100) in PBS at RT for 15 min then incubated in TBS Odyssey Blocking Buffer (LI-COR) at RT for 1 h while rocking. PAB597 (1:40) primary antibody in TBS Odyssey Blocking Buffer was added at 4°C overnight while rocking. Cells were washed with PBS-T 3x for 5 min, then LI-COR 800 secondary anti-mouse antibody (1:8,000) and CellTag 700 (1:500) were incubated at RT for 1 h while rocking. Wells were washed 2x with PBS-T, then 2x with PBS, and liquid was removed prior to scanning.

Plates were scanned using a LI-COR Odyssey CLx Infrared Imaging system for detection of 700 and 800 nm channel intensities. Settings were as follows; 42 µm resolution, medium quality, and 3.0 mm focus offset [280]. Channels were aligned after scanning using Image Studio software with the ICW module. The ICW analysis grid was used to outline each well and intensity values for the 700 and 800 channels within the wells were recorded. Infection was

quantified by dividing the 800 channel intensity value by the 700 channel intensity value times 100. Values were then normalized to the DMSO volume control.

3.2.7. siRNA knockdown of IP_3R2

SVGA cells were plated to 50% confluence in 12-well plates with 10% MEM. Media was replaced with 1 mL of fresh 10% MEM without antibiotics prior to adding siRNA. Transfections were performed using IP_3R2 siRNA (100 pmol/well) and RNAiMAX transfection reagent (Thermo Fisher) (3 µl/well) or nontargeting Silencer Negative Control #1 siRNA (Thermo Fisher) (100 pmol/well) and RNAiMAX (3 µl/well). RNAiMAX and each respective siRNA were combined and incubated together at RT for 10 min prior to transfection. RNAiMAX/siRNA was added dropwise to each well and incubated at 37°C for 72 h to allow for protein knockdown. Following transfection, cells were processed to determine knockdown by Western blot or were infected for FFU assay with JCPyV (MOI = 1 FFU/cell).

3.2.8. SDS PAGE and Western blotting

Wells from siRNA transfection plates were washed with PBS, and cells were removed using a cell scraper, then pelleted by centrifugation at 414 x g at 4°C for 5 min. Cell pellets were resuspended in 75 µl (3 wells) of RIPA lysis buffer (Thermo) containing protease (1:10, Sigma-Aldrich) and phosphatase inhibitors (1:100, Sigma-Aldrich) and incubated on ice for 20 min, pipetting to combine every 5 min. Samples were sonicated at 30% amplitude for a total of 9 seconds, with 3 seconds on and 5 seconds off between each round. Insoluble cellular material was then pelleted at 21,130 x g at 4°C for 10 min. Sample supernatant was transferred to a new tube and solids were discarded. Lysates were combined 1:1 with Laemmli Sample Buffer (BioRad) and heated at 70°C for 90 seconds. Samples were then loaded into a precast 4-15%

Mini TGX gel (BioRad) and proteins were resolved by SDS-PAGE at 12 mA current. Proteins were transferred to nitrocellulose membranes by wet transfer at 4°C with 300 mA for 2 h. Membranes were conditioned in TBS for 10 min prior to blocking with TBS Odyssey Blocking Buffer (LI-COR) at RT for 1 h while rocking. Block buffer was removed, and membranes were incubated with primary antibodies for IP_3R2 and GAPDH (housekeeping protein) in TBS Odyssey Blocking Buffer at 4°C overnight while rocking. Membranes were washed 3x with TBS-T at RT while rocking, then were incubated with secondary antibodies (LI-COR; 1:10,000) in TBS Odyssey Blocking Buffer at RT for 1 h while rocking. Before imaging on a LI-COR Odyssey CLx, membranes were washed 3x with TBS-T, then 3x with TBS. Membranes were imaged with the following settings: 84 µm resolution, high quality, and 0.0 mm focus offset. Reduction in protein expression was calculated by outlining the relative fluorescence of IP_3R2 bands and GAPDH bands in each lane with LI-COR ImageStudio Western blot analysis software (version 5.2), using background reduction selection criteria of average, border width 1, and top/bottom. IP_3R2 bands were normalized to GAPDH and protein reduction was calculated in comparison to the negative control siRNA band.

3.2.9. FFU infectivity assay, staining, and quantification

After a 72-h siRNA transfection, media was removed, and cells were infected were infected with JCPyV (MOI = 1 FFU/cell) at 37°C for 1 h. After 1 h infection, cells were fed with 1 mL/well of 10% MEM and incubated at 37°C for 72 h. Cells were fixed in 4% PFA, stained for VP1 (1:40), and analyzed by FFU assay. Infections were performed in triplicate for a minimum of 3 replicates.

Infection plates were fixed with 4% PFA and washed with PBS-T 3x for 5 min each. Cells were permeabilized with 1% TX-100 at RT for 15 min and blocked with 10% goat serum in PBS at RT for 1 h while rocking. Primary antibody against JCPyV VP1 (PAB597, 1:40) in PBS was added to wells at RT for 1 h while rocking. Wells were washed 3x with PBS-T for 5 min each, then incubated with secondary polyclonal goat anti-mouse Alexa Fluor 488 antibody (1:1000) in PBS at RT for 1 h while rocking. Cells were again washed 3x with PBS-T for 5 min, and DAPI (1:1000) in PBS was added at RT for 5 min for visualization of cell nuclei. Plates were washed with PBS-T and PBS was added for storage.

Infected cells were visualized by Nikon Eclipse Ti epifluorescence microscope (Micro Video Instruments, Inc.) and percent infection was quantified by dividing the number of VP1-positive cells per 20X visual field by the total number of DAPI-positive cells, then multiplying by 100. This was repeated for 5 fields of view (FOV) per well. VP1-positive cells were counted manually, while DAPI-positive cells were counted using a binary algorithm in the Nikon NIS-Elements Basic Research software. Cells were separated in the binary algorithm by intensity, diameter, and circularity to achieve an accurate count of the total number of DAPI-positive cells in each FOV.

3.2.10. Statistical analyses

Student's t-test: Using Microsoft Excel, two-sample Student's *t* tests were performed to determine statistical significance, assuming unequal variance, by comparing mean values of triplicate samples.

Standard error of the mean (SEM): Using Microsoft Excel, SEM was calculated to determine variation in a given population and was done so by calculating standard deviation and dividing by the square root of the sample size.

3.3. Results

3.3.1. JCPyV stimulation of intracellular Ca^{2+} by Fluo-4 AM detection

Although my thesis research showed that JCPyV infection is decreased upon treatment with various Ca^{2+} and Ca^{2+} signaling inhibitors, such as those that target calmodulin and L-type Ca^{2+} channels, details of the involvement of Ca^{2+} during JCPyV infection remain to be characterized [318]. To investigate Ca^{2+} flux during JCPyV infection, microplate reader assays were optimized for our cell culture system. Fluo-4 AM, a cell-permeable, fluorescent Ca^{2+} indicator dye, was used as a tool to detect changes in intracellular Ca^{2+} flux [319]. SVGA cells were loaded with Fluo-4 AM dye for 1 h, pre-treated with BAPTA-AM for 1 h, treated with ionomycin, then immediately placed in the microplate reader for fluorescence reads over the next 3 hours. Ionomycin, an ionophore and known activator of Ca^{2+} flux, was employed as a positive control [320, 321]. BAPTA-AM, a Ca^{2+} chelator, was used in combination with ionomycin to hinder the extent of the expected spike in Ca^{2+} upon ionomycin treatment [322]. Results demonstrated an initial Ca^{2+} spike upon treatment with ionomycin and a sustained overall increase in fluorescence over 3 hours compared to the DMSO volume control. Additionally, results showed that when ionomycin and BAPTA-AM were combined, a smaller and slightly delayed Ca^{2+} spike occurred in comparison to the ionomycin treatment alone (Fig. 3.1.A). After optimization of the Fluo-4 AM plate reader assay, this assay was used to assess Ca^{2+} flux during JCPyV infection. SVGA cells were infected with JCPyV or mock-infected for 1 h, then placed in

the microplate reader for 3 h to monitor changes in Ca^{2+} flux. Results demonstrated that infection with JCPyV stimulated intracellular Ca^{2+} flux significantly more compared to mock, with a significant difference noted at 2.5 to 4 hpi (Fig. 3.1.B).

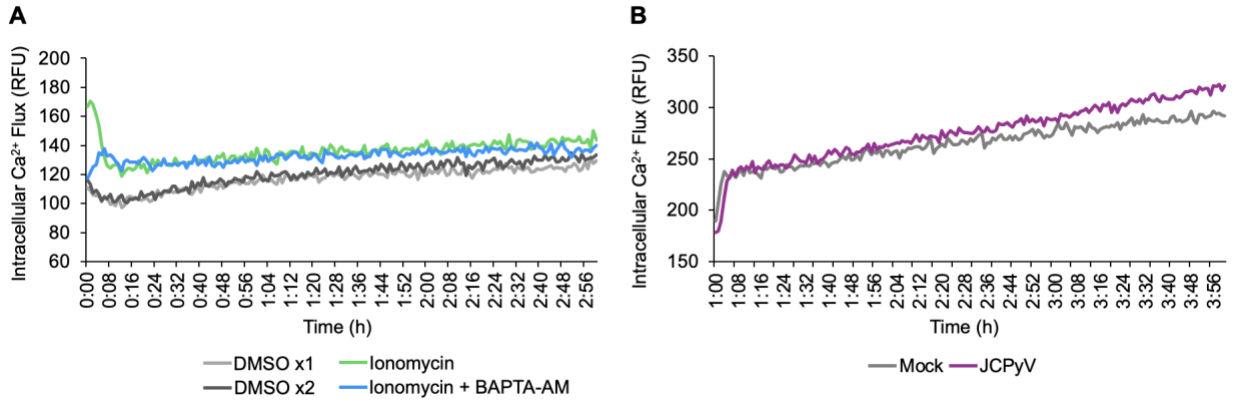

Figure 3.1. JCPyV stimulates intracellular Ca^{2+} flux.
(A) SVGA cells were loaded with Fluo-4 AM [4 µM] at 37°C for 30 min, washed with incomplete MEM, then incubated at 37°C for an additional 30 min. Cells were pre-treated with BAPTA-AM [2.5 µM] at 37°C for 1 h, then ionomycin [5 µM] was added and fluorescence reads began immediately. Reads were taken every minute for 3 h, with 37°C and 5% CO_2 maintained for duration of experiment. (B) SVGA cells were loaded with Fluo-4 AM [4 µM] at 37°C for 30 min, washed with incomplete MEM, then incubated at 37°C for an additional 30 min. Cells were infected with JCPyV (MOI = 5 FFU/cell) or mock-infected at 37°C for 1 h. Fluorescence was then read every minute for 3 h (from 1-4 h post-infection), with 37°C and 5% CO_2 maintained for duration of experiment. Ca^{2+} flux was significantly increased for JCPyV treatment compared to mock ($P < 0.05$). Student's t-test was used to determine statistical significance and graphs represent 3 replicates performed in triplicate.

3.3.2. Chemical inhibition of the IP_3R does not impact JCPyV infectivity

Several Ca^{2+}-related inhibitors have been tested for the capability to impair JCPyV infection, but none that directly target the IP_3R, an important Ca^{2+} channel located on the endoplasmic reticulum (ER) that is responsible for release of ER Ca^{2+} stores into the cytoplasm [323]. Cellular viability assays were first performed to ensure the use of non-cytotoxic concentrations of 2-APB in SVGA cells. To perform these assays, SVGA cells were pre-treated with 2-APB or DMSO volume control for 2 h, mock infected with cell media for 1 h, fed back with cell media for 72 h, and cell viability was assessed using MTS reagent. Results

demonstrated that concentrations up to 200 µM could be used without significant cellular toxicity (Fig. 3.2.A). To test the impact of 2-APB on JCPyV infection, SVGA cells were pre-treated with 2-APB or DMSO volume control for 2 h, infected with JCPyV for 1 h, then fed back with cell media for 72 h and assessed for infection by ICW assay. No significant reduction in JCPyV infection was observed at any of the tested concentrations (Fig. 3.2.B).

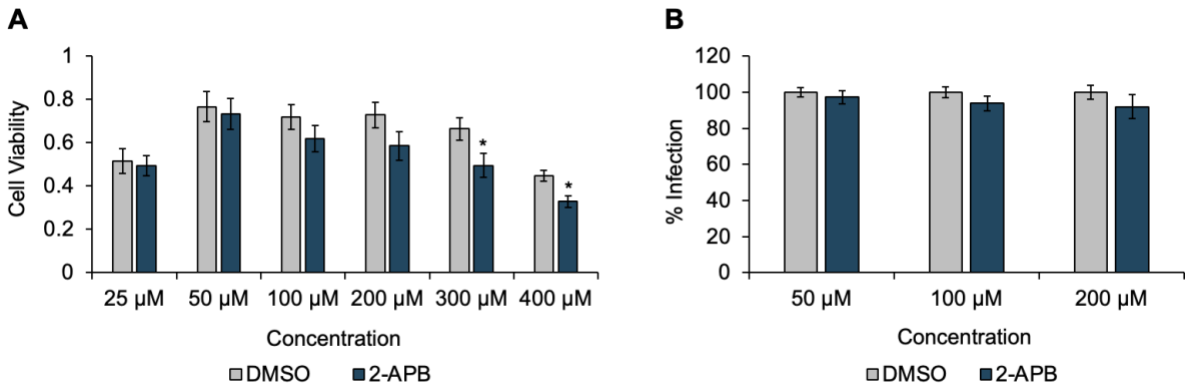

Figure 3.2. IP_3R inhibitor 2-APB does not impact JCPyV infectivity.
(A) SVGA cells were pre-treated with 2-APB or DMSO at 37°C for 2 h, mock-infected with cell media for 1 h, then fed with 100 µl/well cell media and incubated at 37°C for 72 h. MTS reagent was added to all wells, incubated at 37°C for 1 h, and absorbance was measured at 490 nm. (B) SVGA cells were pre-treated with 2-APB or DMSO at 37°C for 2 h, infected with JCPyV (MOI = 2 FFU/cell) in absence of inhibitor at 37°C for 1 h, then fed with 100 µl/well cell media and incubated at 37°C for 72 h. PFA was added for fixation, then cells were stained for VP1 and CellTag and analyzed by ICW using a LI-COR CLx. Determination of % infection was calculated by subtracting background from the 800 nm channel (VP1), then dividing the 800 nm signal from each well by its respective 700 nm signal (CellTag) and normalizing control values to 100%. Graphs represent 3 replicates performed in triplicate. Error bars represent SEM. Student's t-test was used to determine statistical significance. *, $P < 0.05$.

3.3.3. JCPyV infection is not altered by IP_3R2 knockdown

Although JCPyV infection was unaltered upon treatment with 2-APB, a chemical inhibitor of IP_3Rs, some reports demonstrate that this inhibitor inconsistently blocks IP_3R-mediated Ca^{2+} release [324, 325]. A more targeted approach to understanding the role of IP_3Rs in JCPyV infection was warranted, given that Ca^{2+} is important and Ca^{2+} flux occurs upon infection with

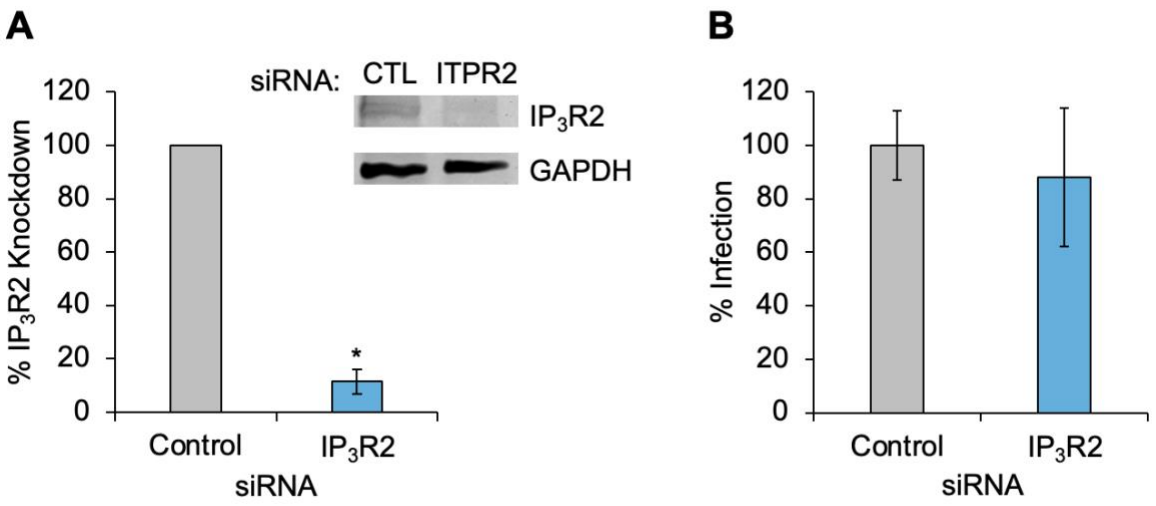

Figure 3.3. JCPyV infection is not influenced by siRNA-mediated knockdown of IP_3R2.
SVGA cells were transfected with siRNA targeting ITPR2 or an irrelevant nontargeting control for 72 h. (A) Cells were harvested and processed for protein knockdown by Western blotting. Data represent the average of triplicate samples for 3 replicates normalized to the housekeeping control GAPDH. (Inset) Representative Western blot image. (B) Cells were infected with JCPyV (MOI = 1 FFU/cell) and fixed at 72 h post-infection. Infections were stained for VP1 and DAPI and were quantified by FFU assay with 5 FOV/well counted. Determination of % infection was calculated by dividing the number of infected cells/the number of DAPI+ cells in each 20X visual field and normalizing to 100%. Error bars represent SEM. Student's t-test was used to determine statistical significance. *, $P < 0.05$.

JCPyV (Fig.3.1.B). To reduce protein production from the IP_3R2 gene, ITPR2, siRNA was utilized. SVGA cells were transfected with ITPR2 or negative control siRNA for 72 h. Cells were then either harvested and processed for evaluation of protein knockdown by Western blot (Fig. 3.3.A) or were infected with JCPyV for another 72 h and assessed for infection (Fig. 3.3.B). Results demonstrated at least an 80% reduction in IP_3R2 protein expression, which was deemed sufficient for infection experiments (Fig. 3.3.A). Infection of SVGA cells with JCPyV was unaltered by knockdown of the IP_3R (Fig. 3.3.B).

3.4. Discussion

JCPyV infection is impacted by several inhibitors of Ca^{2+} channels and Ca^{2+} signaling-related proteins, including TPCs, L-type Ca^{2+} channels, and calmodulin. Herein, we report that

intracellular Ca^{2+} flux is activated upon JCPyV infection, and this increased Ca^{2+} flux occurs around 2.5 hpi and is sustained through 4 hpi. To understand which intracellular stores of Ca^{2+} are utilized for this sustained Ca^{2+} flux, the ER was explored as a potential source, as the ER is the largest intracellular store of Ca^{2+} [326]. Results showed that neither chemical inhibition of the IP_3Rs, nor siRNA knockdown of the IP_3R2 impacted JCPyV infectivity, suggesting that the IP_3Rs may not be the source of calcium stores impacted upon JCPyV infection.

Fluo-4 AM is a cell permeable fluorescent Ca^{2+}-binding dye. Once the AM ester is cleaved, Fluo-4 becomes capable of binding free Ca^{2+} in the cell – no matter the source of the Ca^{2+}. Once bound with Ca^{2+}, Fluo-4 can emit fluorescence, and fluorescence increases as more Ca^{2+} binds. Results shown herein demonstrate increased intracellular Ca^{2+} levels upon infection with JCPyV. When cells were treated with ionomycin, an ionophore, a relatively quick spike in Ca^{2+} levels was demonstrated, which is expected because ionomycin works quickly to mobilize Ca^{2+} into the cell (Fig 3.1.A). However, when cells were infected with JCPyV, a gradual increase rather than a spike in Ca^{2+} levels was observed compared to mock beginning at 2.5 hpi, and the increase in Ca^{2+} levels was sustained through 4 hpi (Fig. 3.1.B). These results could suggest a slower, more gradual influx or release of Ca^{2+} during JCPyV infection or that perhaps a specific event in the viral infectious cycle triggers calcium release. This finding combined with my previous findings that the calmodulin inhibitor, trifluoperazine, inhibits JCPyV during viral entry, suggest that Ca^{2+} involvement during JCPyV infection begins during viral internalization.

The IP_3Rs have been implicated in both RV and HIV infections in different ways. For RV infection, IP_3R knockout cells did not reduce Ca^{2+} signaling in infected cells but eliminated RV-induced intercellular Ca^{2+} waves [327]. For HIV infection, the HIV protein Nef is able to bind

IP_3R1 and to activate plasma membrane Ca^{2+} influx channels and promote T-cell activation, which is important for HIV pathogenesis [328].

The IP_3Rs are the main Ca^{2+}-release channels from the ER, so it was hypothesized that these channels would be activated during JCPyV infection. However, our results by chemical inhibition suggested that IP_3Rs may be dispensable during JCPyV infection. Interestingly, chemical inhibition of IP_3Rs by 2-APB has been reported as inconsistent, with several off-target effects [324, 325]. Therefore, we utilized a more specific siRNA knockdown approach, and while the knockdown of IP_3R2 was robust, the silencing of IP_3R2 did not result in a reduction of infection. We initially targeted IP_3R2 because Ca^{2+} release from this subtype is reported to be more prolonged, potentially due to IP_3 binding with greater affinity to IP_3R2 [329]. However, subtypes IP_3R1 and IP_3R3 have not yet been investigated and their involvement in JCPyV infection cannot be ruled out. All IP_3R subtypes are expressed in the brain, and recently it has been suggested that all subtypes are expressed specifically in astrocytes, warranting further exploration into IP_3R1 and IP_3R3 [330, 331].

Other intracellular Ca^{2+} stores have been implicated in viral infections, so it is possible that ER Ca^{2+} stores are not the main contributor to the increased Ca^{2+} flux during JCPyV infection. Mitochondrial, Golgi, and lysosomal Ca^{2+} stores should also be considered, as well as the possibility that Ca^{2+} influx could be occurring from extracellular sources. Given that TPCs are located on lysosomes, and that TPCs have been implicated in MCPyV, SV40, and JCPyV infections, likely during endolysosomal fusion with the ER, investigation of other intracellular Ca^{2+} stores during JCPyV infection is justified [253, 318].

CHAPTER 4

CONCLUSIONS, DISCUSSION, AND FUTURE DIRECTIONS

My thesis research largely focused on understanding the role of cellular Ca^{2+} signaling during JCPyV infection. Although Ca^{2+} signaling is a well-understood biological signaling pathway, little was known about Ca^{2+} in the context of JCPyV infection. Dependence of JCPyV on Ca^{2+} signaling, especially during early stages of viral infection, became apparent after conducting this research. Reduction of JCPyV infection was observed upon treatment with several inhibitors, including inhibitors of L-type Ca^{2+} channels (nifedipine), NAADP-sensitive TPCs (tetrandrine), and CaM (TFP and W-7). Reduced infection was noted for several cell types, including immortalized kidney (HEK-2C) and brain (SVGA) cells and primary kidney cells (RPTECs). Interestingly, though, some cell-type dependent differences in infection were observed for treatments with nifedipine and tetrandrine in kidney and brain cells. This could have implications for treatment plans if nifedipine or tetrandrine were approved to treat JCPyV infection, as infection in the kidneys was more sensitive to inhibition by nifedipine and tetrandrine. CaM inhibitors remained consistent, with reduction of JCPyV infection for all cell types tested, as well as for other viral infections (SV40, BKPyV, and SARS-CoV-2). Overall, CaM inhibitors may be a more effective treatment than nifedipine or tetrandrine, as CaM inhibitors blocked infection in both brain and kidney cells, which represent the major sites of infection in the host. This research also demonstrated that in addition to Ca^{2+} signaling inhibitors reducing JCPyV infection, the virus stimulates an increase in Ca^{2+} flux within the cell.

JCPyV infection induced an increase in intracellular Ca^{2+} levels at early time points in infection yet the cellular source for this Ca^{2+} flux has not been determined. Analysis of Ca^{2+} flux

revealed an increase from 2.5-4 hpi, which is consistent with viral entry and trafficking. Our results suggest that intracellular Ca^{2+} is likely not increasing due to regulation of IP_3R2 and potentially not through IP_3Rs at all. Thus, other ER Ca^{2+} channels should not be discounted, and other Ca^{2+} sources need to be thoroughly explored, including extracellular Ca^{2+} through L-type Ca^{2+} channels and lysosomal Ca^{2+} through TPCs. Time of addition assays for both tetrandrine (data not shown) and TFP demonstrated marked reduction in infection at early timepoints in JCPyV infection (0-4 hpi) that are consistent with entry and trafficking, and lesser reduction at later timepoints (6-24 hpi) that are consistent with trafficking, uncoating, and transcription. Coupled with results from a JCPyV internalization assay specifically evaluating viral entry during treatment with TFP, conclusions were drawn that TFP was impacting JCPyV infection most significantly during viral entry. Taken together, these results indicate that Ca^{2+} flux occurs during JCPyV internalization, possibly triggering the activation of Ca^{2+} signaling pathways which include L-Type Ca^{2+} channels, CaM, and TPCs that could impact lysosomal Ca^{2+} stores.

Viral manipulation of the ER and lysosomal Ca^{2+} stores have been implicated at the point of viral entry for other viruses [250, 332]. Additionally, TFP and tetrandrine, two drugs that reduced JCPyV infection, have been shown to reduce entry of SARS-CoV-2 and Ebola, respectively [250, 295]. Although one study suggests that SV40 is inhibited by tetrandrine at the point of endolysosomal fusion with the ER, it cannot be ruled out that this inhibition occurs earlier as those time points were not reported [253]. Timecourse assays for tetrandrine showed reduction in JCPyV infection early in infection, suggesting a potential role for lysosomal Ca^{2+} in JCPyV entry. The role of lysosomal Ca^{2+} stores in JCPyV entry and infection should be further

explored through chemical inhibition of lysosomal Ca^{2+} channels or use of a lysosome-targeted Ca^{2+} sensor [333].

CaM is a ubiquitous Ca^{2+} sensor protein and plays innumerable roles within all eukaryotic cells, including regulating many Ca^{2+} channels [334]. Several reports have linked CaM to the IP_3Rs, demonstrating that IP_3Rs rely on CaM and that CaM acts as a regulator of Ca^{2+} release from IP_3Rs [301, 334-336]. Due to interactions of CaM with IP_3Rs, and since other DNA viruses such as HSV and HBV utilize IP_3Rs, these seemed like logical receptors to investigate during JCPyV infection [332, 337, 338]. Our results suggest that IP_3Rs may not actually be necessary for JCPyV infection, but that CaM may be involved in infection in some other way and that the increased Ca^{2+} seen during JCPyV infection may be due to other Ca^{2+} stores or extracellular Ca^{2+} flux into the cell. Since CaM interacts with hundreds of cellular proteins, it may be difficult to pinpoint exactly in which capacity it is involved in JCPyV infection [339].

In several other viral infections, such as HIV, HBV, and rubella, viral proteins bind CaM directly to regulate infection [257-259]. In viral infections by DENV, Ebola, and SARS-CoV-2, the mechanism of CaM involvement remains unknown [260-262]. Of note, CaM has been shown to bind to Ras1, a member of the MAPK/ERK signaling pathway which is activated by JCPyV infection [216, 340]. One theory for how CaM plays a role in JCPyV infection may be through activation of the MAPK/ERK signaling pathway. If JCPyV stimulates Ca^{2+} flux during infection, CaM may become activated by this free Ca^{2+}, leading to binding of CaM to Ras1 and activating the MAPK/ERK pathway. Another possibility is that CaM binds to the $5\text{-}HT_2Rs$ through conserved CaM-binding domains to promote receptor stabilization on the plasma membrane, leading to more internalized virus [298]. Alternatively, β-arrestin is also important for JCPyV entry, and

CaM is a known binding partner of β-arrestin; perhaps this interaction promotes JCPyV infection [144, 341]. Interestingly, in absence of virus, CaM binding to 5-HT_{2C}R is necessary for β-arrestin recruitment by the 5-HT_{2C}R and for β-arrestin-dependent ERK1/2 signaling in HEK 293 cells [298]. Thus, the mechanism of CaM involvement in JCPyV infection may be due to interactions with Ras1, β-arrestin, or both early on in viral infection.

Exactly how CaM is involved in JCPyV infection remains unclear. Further experimentation is necessary to understand if CaM is a binding partner of a JCPyV protein, if CaM is involved in β-arrestin recruitment to the 5-HT_2Rs, if CaM is triggering the MAPK/ERK cascade, or if it is involved by some alternative mechanism. CaM is ubiquitous and is responsible for a wide variety of functions within the cell. One follow-up experiment for investigation of CaM implications and mechanisms during JCPyV infection includes mutation of the CaM-binding domains located in the 5-HT_2Rs and testing whether these mutations affect JCPyV entry and/or CaM binding during JCPyV infection. Previously, it was shown that mutation of the CaM-binding motif on 5-HT_{2C}R inhibited β-arrestin recruitment to the receptor and ERK1/2 signaling upon activation by 5-HT [298]. It is unclear whether the same would occur upon stimulation by JCPyV and whether this would occur for 5-HT_{2A}R and 5-HT_{2B}R as well, but is worth investigating, as JCPyV relies on 5-HT_{2A-C}Rs equally and all contain CaM-binding domains [141, 342].

Finally, results from Chapter 2 suggest TFP and nifedipine as potential candidates for treatment of JCPyV infection or PML. TFP showed broad inhibition of JCPyV infection in all cell types tested, including immortalized brain and kidney cells and primary kidney cells. Early treatment with TFP would likely be most effective since it can reduce infection in kidney cells, and TFP is capable of crossing the blood-brain barrier (BBB) and reduces JCPyV infection in glial

cells [343]. TFP is currently FDA-approved for treatment of schizophrenia [344], but may be repurposed for JCPyV. Interestingly, viral infections of several other viruses are also reduced by TFP including BKPyV, SARS-CoV-2, DENV, measles, EBV, influenza, and arenaviruses [306-309, 311, 312, 318] suggesting that this could serve as a broad-spectrum antiviral treatment. Nifedipine is currently FDA-approved for treatment of hypertension and easily crosses the BBB [345, 346]. Reduction of JCPyV infection by nifedipine was observed only in immortalized and primary kidney cells, pointing to use of this drug as a prophylactic treatment prior to spread of JCPyV from the kidneys to the brain. For example, patients with HIV or patients with MS who are receiving natalizumab are at a higher risk of developing PML [347, 348]. These patient populations could benefit from nifedipine to potentially reduce the risk of JCPyV spread to the brain and development of PML. Our results showed no impact on JCPyV infection in glial cells, so if nifedipine were repurposed for JCPyV infection, treatment would likely need to begin before development of PML.

Overall, the work highlighted herein demonstrates a role for cellular Ca^{2+} signaling during JCPyV infection. Several key pieces of evidence about Ca^{2+} signaling during JCPyV infection were uncovered, though the puzzle remains to be pieced together. Understanding the role of Ca^{2+} signaling in JCPyV infection could uncover several new drug targets for treatment of JCPyV infection and PML and deepen our understanding of Ca^{2+} signaling during viral infection. As there are still no targeted, approved antivirals for treatment of this disease, there is a great need for further research on this topic and in this field. Involvement of Ca^{2+} signaling in viral infections continues to be discovered for many viruses, and these Ca^{2+} pathways could potentially serve as broad antiviral targets. Moreover, repurposing existing drugs for treatment

of viral infections remains an efficient method for antiviral drug discovery and identifying cellular factors that regulate viral infection.

CHAPTER 5

REFERENCES

1. Bahsoun, M.A., et al., *FLAIR MRI biomarkers of the normal appearing brain matter are related to cognition.* Neuroimage Clin, 2022. **34**: p. 102955.

2. Marzocchetti, A., et al., *Rearrangement of the JC virus regulatory region sequence in the bone marrow of a patient with rheumatoid arthritis and progressive multifocal leukoencephalopathy.* J Neurovirol, 2008. **14**(5): p. 455-8.

3. Mayberry, C.L., et al., *Sending mixed signals: polyomavirus entry and trafficking.* Curr Opin Virol, 2021. **47**: p. 95-105.

4. Lustig, A. and A.J. Levine, *One hundred years of virology.* J Virol, 1992. **66**(8): p. 4629-31.

5. *Virus Taxonomy: 2022 Release*. 2022 [cited 2024 17 April]; Available from: https://ictv.global/taxonomy.

6. Jones, R.A.C., *Global Plant Virus Disease Pandemics and Epidemics.* Plants (Basel), 2021. **10**(2).

7. Ristaino, J.B., et al., *The persistent threat of emerging plant disease pandemics to global food security.* Proc Natl Acad Sci U S A, 2021. **118**(23).

8. Silva, S., E. Goosby, and M.J.A. Reid, *Assessing the impact of one million COVID-19 deaths in America: economic and life expectancy losses.* Sci Rep, 2023. **13**(1): p. 3065.

9. Martin, R., et al., *Lessons learnt from COVID-19 to reduce mortality and morbidity in the Global South: addressing global vaccine equity for future pandemics.* BMJ Glob Health, 2024. **9**(1).

10. Trilla, A., G. Trilla, and C. Daer, *The 1918 "Spanish flu" in Spain.* Clin Infect Dis, 2008. **47**(5): p. 668-73.

11. Bhadoria, P., G. Gupta, and A. Agarwal, *Viral Pandemics in the Past Two Decades: An Overview.* J Family Med Prim Care, 2021. **10**(8): p. 2745-2750.

12. Pirofski, L.A. and A. Casadevall, *Q and A: What is a pathogen? A question that begs the point.* BMC Biol, 2012. **10**: p. 6.

13. Gelderblom, H.R., *Structure and Classification of Viruses*, in *Medical Microbiology*, S. Baron, Editor. 1996: Galveston (TX).

14. Helenius, A., *Virus Entry: Looking Back and Moving Forward.* J Mol Biol, 2018. **430**(13): p. 1853-1862.

15. Gao, H., W. Shi, and L.B. Freund, *Mechanics of receptor-mediated endocytosis.* Proc Natl Acad Sci U S A, 2005. **102**(27): p. 9469-74.

16. Burrell, C.J., Howard, C.R., Murphy, F.A., *Virus Replication.* Fenner and White's Medical Virology, 2017: p. 39-55.

17. Rampersad, S.a.T., P., *Replication and Expression Strategies of Viruses.* Viruses, 2018: p. 55-82.

18. Perlmutter, J.D. and M.F. Hagan, *Mechanisms of virus assembly.* Annu Rev Phys Chem, 2015. **66**: p. 217-39.

19. Payne, S., *3 - Virus Interactions with the Cell*. Viruses (Second Edition). 2023: Academic Press.

20. Sanjuan, R., *The Social Life of Viruses.* Annu Rev Virol, 2021. **8**(1): p. 183-199.

21. Louten, J., *Virus Transmission and Epidemiology.* Essential Human Virology, 2016: p. 71-92.

22. Bomsel, M. and A. Alfsen, *Entry of viruses through the epithelial barrier: pathogenic trickery.* Nat Rev Mol Cell Biol, 2003. **4**(1): p. 57-68.

23. Gross, L., *A filterable agent, recovered from Ak leukemic extracts, causing salivary gland carcinomas in C3H mice.* Proc Soc Exp Biol Med, 1953. **83**(2): p. 414-21.

24. Morgan, G.J., *Ludwik Gross, Sarah Stewart, and the 1950s discoveries of Gross murine leukemia virus and polyoma virus.* Stud Hist Philos Biol Biomed Sci, 2014. **48 Pt B**: p. 200-9.

25. Moens, U., et al., *Biology, evolution, and medical importance of polyomaviruses: An update.* Infect Genet Evol, 2017. **54**: p. 18-38.

26. Ciotti, M.P., C.; Peitropaolo, V., *An overview on human polyomaviruses biology and related diseases.* Future Virology, 2019. **14**(7).

27. Klufah, F., et al., *Emerging role of human polyomaviruses 6 and 7 in human cancers.* Infect Agent Cancer, 2021. **16**(1): p. 35.

28. Prado, J.C.M., et al., *Human polyomaviruses and cancer: an overview.* Clinics (Sao Paulo), 2018. **73**(suppl 1): p. e558s.

29. Ferenczy, M.W., et al., *Molecular biology, epidemiology, and pathogenesis of progressive multifocal leukoencephalopathy, the JC virus-induced demyelinating disease of the human brain.* Clin Microbiol Rev, 2012. **25**(3): p. 471-506.

30. Ogris, E., I. Mudrak, and E. Wintersberger, *Polyomavirus large and small T antigens cooperate in induction of the S phase in serum-starved 3T3 mouse fibroblasts.* J Virol, 1992. **66**(1): p. 53-61.

31. Porras, A., S. Gaillard, and K. Rundell, *The simian virus 40 small-t and large-T antigens jointly regulate cell cycle reentry in human fibroblasts.* J Virol, 1999. **73**(4): p. 3102-7.

32. Liddington, R.C., et al., *Structure of simian virus 40 at 3.8-A resolution.* Nature, 1991. **354**(6351): p. 278-84.

33. Sweet, B.H. and M.R. Hilleman, *The vacuolating virus, S.V. 40.* Proc Soc Exp Biol Med, 1960. **105**: p. 420-7.

34. Eddy, B.E., et al., *Identification of the oncogenic substance in rhesus monkey kidney cell culture as simian virus 40.* Virology, 1962. **17**: p. 65-75.

35. Girardi, A.J., et al., *Development of tumors in hamsters inoculated in the neonatal period with vacuolating virus, SV-40.* Proc Soc Exp Biol Med, 1962. **109**: p. 649-60.

36. Butel, J.S., S.S. Tevethia, and J.L. Melnick, *Oncogenicity and cell transformation by papovavirus SV40: the role of the viral genome.* Adv Cancer Res, 1972. **15**: p. 1-55.

37. Butel, J.S. and J.A. Lednicky, *Cell and molecular biology of simian virus 40: implications for human infections and disease.* J Natl Cancer Inst, 1999. **91**(2): p. 119-34.

38. Feng, H., et al., *Clonal integration of a polyomavirus in human Merkel cell carcinoma.* Science, 2008. **319**(5866): p. 1096-100.

39. Pietropaolo, V., C. Prezioso, and U. Moens, *Merkel Cell Polyomavirus and Merkel Cell Carcinoma.* Cancers (Basel), 2020. **12**(7).

40. Shuda, M., et al., *T antigen mutations are a human tumor-specific signature for Merkel cell polyomavirus.* Proc Natl Acad Sci U S A, 2008. **105**(42): p. 16272-7.

41. Lemos, B.D., et al., *Pathologic nodal evaluation improves prognostic accuracy in Merkel cell carcinoma: analysis of 5823 cases as the basis of the first consensus staging system.* J Am Acad Dermatol, 2010. **63**(5): p. 751-61.

42. Becker, J.C., et al., *Merkel cell carcinoma.* Nat Rev Dis Primers, 2017. **3**: p. 17077.

43. Paulson, K.G., et al., *Merkel cell carcinoma: Current US incidence and projected increases based on changing demographics.* J Am Acad Dermatol, 2018. **78**(3): p. 457-463 e2.

44. Minutilli, E. and A. Mule, *Merkel cell polyomavirus and cutaneous Merkel cell carcinoma.* Future Sci OA, 2016. **2**(4): p. FSO155.

45. Kaufman, H.L., et al., *Avelumab in patients with chemotherapy-refractory metastatic Merkel cell carcinoma: a multicentre, single-group, open-label, phase 2 trial.* Lancet Oncol, 2016. **17**(10): p. 1374-1385.

46. Villani, A., et al., *Merkel Cell Carcinoma: Therapeutic Update and Emerging Therapies.* Dermatol Ther (Heidelb), 2019. **9**(2): p. 209-222.

47. Dimitraki, M.G. and G. Sourvinos, *Merkel Cell Polyomavirus (MCPyV) and Cancers: Emergency Bell or False Alarm?* Cancers (Basel), 2022. **14**(22).

48. Kean, J.M., et al., *Seroepidemiology of human polyomaviruses.* PLoS Pathog, 2009. **5**(3): p. e1000363.

49. De Gascun, C.F. and M.J. Carr, *Human polyomavirus reactivation: disease pathogenesis and treatment approaches.* Clin Dev Immunol, 2013. **2013**: p. 373579.

50. Sharma, R., et al., *BK Virus in Kidney Transplant: Current Concepts, Recent Advances, and Future Directions.* Exp Clin Transplant, 2016. **14**(4): p. 377-84.

51. Vigil, D., et al., *BK nephropathy in the native kidneys of patients with organ transplants: Clinical spectrum of BK infection.* World J Transplant, 2016. **6**(3): p. 472-504.

52. Myint, T.M., et al., *Polyoma BK Virus in Kidney Transplant Recipients: Screening, Monitoring, and Management.* Transplantation, 2022. **106**(1): p. e76-e89.

53. Hirsch, H.H., et al., *Polyomavirus-associated nephropathy in renal transplantation: interdisciplinary analyses and recommendations.* Transplantation, 2005. **79**(10): p. 1277-86.

54. Bennett, S.M., N.M. Broekema, and M.J. Imperiale, *BK polyomavirus: emerging pathogen.* Microbes Infect, 2012. **14**(9): p. 672-83.

55. Ramos, E., et al., *Clinical course of polyoma virus nephropathy in 67 renal transplant patients.* J Am Soc Nephrol, 2002. **13**(8): p. 2145-51.

56. Padgett, B.L., et al., *Cultivation of papova-like virus from human brain with progressive multifocal leucoencephalopathy.* Lancet, 1971. **1**(7712): p. 1257-60.

57. Laine, H.K., et al., *Seroprevalence of polyomaviruses BK and JC in Finnish women and their spouses followed-up for three years.* Sci Rep, 2023. **13**(1): p. 879.

58. Pinto, M. and S. Dobson, *BK and JC virus: a review.* J Infect, 2014. **68 Suppl 1**: p. S2-8.

59. Padgett, B.L. and D.L. Walker, *Prevalence of antibodies in human sera against JC virus, an isolate from a case of progressive multifocal leukoencephalopathy.* J Infect Dis, 1973. **127**(4): p. 467-70.

60. Chang, H., et al., *High incidence of JC viruria in JC-seropositive older individuals.* J Neurovirol, 2002. **8**(5): p. 447-51.

61. Berger, J.R., et al., *JC virus detection in bodily fluids: clues to transmission.* Clin Infect Dis, 2006. **43**(1): p. e9-12.

62. White, M.K. and K. Khalili, *Pathogenesis of progressive multifocal leukoencephalopathy--revisited.* J Infect Dis, 2011. **203**(5): p. 578-86.

63. Astrom, K.E., E.L. Mancall, and E.P. Richardson, Jr., *Progressive multifocal leuko-encephalopathy; a hitherto unrecognized complication of chronic lymphatic leukaemia and Hodgkin's disease.* Brain, 1958. **81**(1): p. 93-111.

64. Berger, J.R. and E.O. Major, *Progressive multifocal leukoencephalopathy.* Semin Neurol, 1999. **19**(2): p. 193-200.

65. Kuhn, S., et al., *Oligodendrocytes in Development, Myelin Generation and Beyond.* Cells, 2019. **8**(11).

66. Kiernan, M.C. and R. Kaji, *Physiology and pathophysiology of myelinated nerve fibers.* Handb Clin Neurol, 2013. **115**: p. 43-53.

67. Pavlovic, D., et al., *T cell deficiencies as a common risk factor for drug associated progressive multifocal leukoencephalopathy.* Immunobiology, 2018. **223**(6-7): p. 508-517.

68. Chapagain, M.L. and V.R. Nerurkar, *Human polyomavirus JC (JCV) infection of human B lymphocytes: a possible mechanism for JCV transmigration across the blood-brain barrier.* J Infect Dis, 2010. **202**(2): p. 184-91.

69. Haley, S.A., et al., *Human polyomavirus receptor distribution in brain parenchyma contrasts with receptor distribution in kidney and choroid plexus.* Am J Pathol, 2015. **185**(8): p. 2246-58.

70. O'Hara, B.A., et al., *Susceptibility of Primary Human Choroid Plexus Epithelial Cells and Meningeal Cells to Infection by JC Virus.* J Virol, 2018. **92**(8).

71. Corbridge, S.M., et al., *JC virus infection of meningeal and choroid plexus cells in patients with progressive multifocal leukoencephalopathy.* J Neurovirol, 2019. **25**(4): p. 520-524.

72. White, F.A., 3rd, et al., *JC virus DNA is present in many human brain samples from patients without progressive multifocal leukoencephalopathy.* J Virol, 1992. **66**(10): p. 5726-34.

73. Anand, P., et al., *Progressive multifocal leukoencephalopathy: A 25-year retrospective cohort study.* Neurol Neuroimmunol Neuroinflamm, 2019. **6**(6).

74. Berger, J.R., *Progressive multifocal leukoencephalopathy.* Handb Clin Neurol, 2014. **123**: p. 357-76.

75. Khoury, M.N., et al., *Hyperintense cortical signal on magnetic resonance imaging reflects focal leukocortical encephalitis and seizure risk in progressive multifocal leukoencephalopathy.* Ann Neurol, 2014. **75**(5): p. 659-69.

76. Berger, J.R., *The clinical features of PML.* Cleve Clin J Med, 2011. **78 Suppl 2**: p. S8-12.

77. Kleinschmidt-DeMasters, B.K. and K.L. Tyler, *Progressive multifocal leukoencephalopathy complicating treatment with natalizumab and interferon beta-1a for multiple sclerosis.* N Engl J Med, 2005. **353**(4): p. 369-74.

78. Van Assche, G., et al., *Progressive multifocal leukoencephalopathy after natalizumab therapy for Crohn's disease.* N Engl J Med, 2005. **353**(4): p. 362-8.

79. Goldberg, S.L., et al., *Unusual viral infections (progressive multifocal leukoencephalopathy and cytomegalovirus disease) after high-dose chemotherapy with autologous blood stem cell rescue and peritransplantation rituximab.* Blood, 2002. **99**(4): p. 1486-8.

80. Berger, J.R. and M. Concha, *Progressive multifocal leukoencephalopathy: the evolution of a disease once considered rare.* J Neurovirol, 1995. **1**(1): p. 5-18.

81. Berger, J.R., et al., *Progressive multifocal leukoencephalopathy in patients with HIV infection.* J Neurovirol, 1998. **4**(1): p. 59-68.

82. Holman, R.C., et al., *Progressive multifocal leukoencephalopathy in the United States, 1979-1994: increased mortality associated with HIV infection.* Neuroepidemiology, 1998. **17**(6): p. 303-9.

83. Del Valle, L. and S. Pina-Oviedo, *Human Polyomavirus JCPyV and Its Role in Progressive Multifocal Leukoencephalopathy and Oncogenesis.* Front Oncol, 2019. **9**: p. 711.

84. Schwab, N., et al., *Natalizumab-associated PML: Challenges with incidence, resulting risk, and risk stratification.* Neurology, 2017. **88**(12): p. 1197-1205.

85. Yousry, T.A., et al., *Evaluation of patients treated with natalizumab for progressive multifocal leukoencephalopathy.* N Engl J Med, 2006. **354**(9): p. 924-33.

86. Major, E.O., *Progressive multifocal leukoencephalopathy in patients on immunomodulatory therapies.* Annu Rev Med, 2010. **61**: p. 35-47.

87. Cohen, M., et al., *BEST-MS: A prospective head-to-head comparative study of natalizumab and fingolimod in active relapsing MS.* Mult Scler, 2021. **27**(10): p. 1556-1563.

88. Kaiserman, J., et al., *An Elusive Target: Inhibitors of JC Polyomavirus Infection and Their Development as Therapeutics for the Treatment of Progressive Multifocal Leukoencephalopathy.* Int J Mol Sci, 2023. **24**(10).

89. Pavlovic, D., et al., *Progressive multifocal leukoencephalopathy: current treatment options and future perspectives.* Ther Adv Neurol Disord, 2015. **8**(6): p. 255-73.

90. Khatri, B.O., et al., *Effect of plasma exchange in accelerating natalizumab clearance and restoring leukocyte function.* Neurology, 2009. **72**(5): p. 402-9.

91. Tan, I.L., et al., *Immune reconstitution inflammatory syndrome in natalizumab-associated PML.* Neurology, 2011. **77**(11): p. 1061-7.

92. Dahlhaus, S., et al., *Disease course and outcome of 15 monocentrically treated natalizumab-associated progressive multifocal leukoencephalopathy patients.* J Neurol Neurosurg Psychiatry, 2013. **84**(10): p. 1068-74.

93. Tan, K., et al., *PML-IRIS in patients with HIV infection: clinical manifestations and treatment with steroids.* Neurology, 2009. **72**(17): p. 1458-64.

94. Clifford, D.B., *Progressive multifocal leukoencephalopathy therapy.* J Neurovirol, 2015. **21**(6): p. 632-6.

95. Yatawara, A., et al., *Small-molecule inhibitors of JC polyomavirus infection.* J Pept Sci, 2015. **21**(3): p. 236-42.

96. Kast, R.E., et al., *Treatment schedules for 5-HT2A blocking in progressive multifocal leukoencephalopathy using risperidone or ziprasidone.* Bone Marrow Transplant, 2007. **39**(12): p. 811-2.

97. Pho, M.T., A. Ashok, and W.J. Atwood, *JC virus enters human glial cells by clathrin-dependent receptor-mediated endocytosis.* J Virol, 2000. **74**(5): p. 2288-92.

98. Atwood, W.J., *A combination of low-dose chlorpromazine and neutralizing antibodies inhibits the spread of JC virus (JCV) in a tissue culture model: implications for prophylactic and therapeutic treatment of progressive multifocal leukencephalopathy.* J Neurovirol, 2001. **7**(4): p. 307-10.

99. Elphick, G.F., et al., *The human polyomavirus, JCV, uses serotonin receptors to infect cells.* Science, 2004. **306**(5700): p. 1380-3.

100. Park, J.H., et al., *Dual therapy with cidofovir and mirtazapine for progressive multifocal leukoencephalopathy in a sarcoidosis patient.* Case Rep Neurol, 2011. **3**(3): p. 258-62.

101. Verma, S., et al., *Mirtazapine in progressive multifocal leukoencephalopathy associated with polycythemia vera.* J Infect Dis, 2007. **196**(5): p. 709-11.

102. Cettomai, D. and J.C. McArthur, *Mirtazapine use in human immunodeficiency virus-infected patients with progressive multifocal leukoencephalopathy.* Arch Neurol, 2009. **66**(2): p. 255-8.

103. Maginnis, M.S., C.D. Nelson, and W.J. Atwood, *JC polyomavirus attachment, entry, and trafficking: unlocking the keys to a fatal infection.* J Neurovirol, 2015. **21**(6): p. 601-13.

104. Nelson, C.D., et al., *A retrograde trafficking inhibitor of ricin and Shiga-like toxins inhibits infection of cells by human and monkey polyomaviruses.* mBio, 2013. **4**(6): p. e00729-13.

105. Treasure, T. and C.D.S. Nelson, *Inhibition of JC polyomavirus infectivity by the retrograde transport inhibitor Retro-2.1.* Microbiol Immunol, 2020. **64**(12): p. 783-791.

106. Hou, J. and E.O. Major, *The efficacy of nucleoside analogs against JC virus multiplication in a persistently infected human fetal brain cell line.* J Neurovirol, 1998. **4**(4): p. 451-6.

107. Gosert, R., et al., *CMX001 (1-O-hexadecyloxypropyl-cidofovir) inhibits polyomavirus JC replication in human brain progenitor-derived astrocytes.* Antimicrob Agents Chemother, 2011. **55**(5): p. 2129-36.

108. Jiang, Z.G., et al., *Hexadecyloxypropyl-cidofovir (CMX001) suppresses JC virus replication in human fetal brain SVG cell cultures.* Antimicrob Agents Chemother, 2010. **54**(11): p. 4723-32.

109. Kerr, D.A., et al., *Inhibition of human neurotropic virus (JCV) DNA replication in glial cells by camptothecin.* Virology, 1993. **196**(2): p. 612-8.

110. Heilbronn, R., et al., *Human cytomegalovirus induces JC virus DNA replication in human fibroblasts.* Proc Natl Acad Sci U S A, 1993. **90**(23): p. 11406-10.

111. Josephson, M.A., et al., *Leflunomide in solid organ transplantation and polyoma virus infection.* Adv Exp Med Biol, 2006. **577**: p. 255-65.

112. Demir, E., et al., *Childhood case of progressive multifocal leukoencephalopathy with improved clinical outcome.* J Child Neurol, 2005. **20**(3): p. 241-4.

113. Epker, J.L., et al., *Progressive multifocal leukoencephalopathy, a review and an extended report of five patients with different immune compromised states.* Eur J Intern Med, 2009. **20**(3): p. 261-7.

114. Williams, J.W., et al., *Leflunomide for polyomavirus type BK nephropathy.* N Engl J Med, 2005. **352**(11): p. 1157-8.

115. Berger, J., Pall, L., McArthur, J., Hall, C., Cimoch, P., Evans, B. et al., *A pilot study of recombinant alpha 2a interferon in the treatment of AIDS-related progressive multifocal leukoencephalopathy.* Neurology, 1992. **42 (Suppl.3)**(257).

116. Miller, C.S., et al., *Disease-modifying drugs for multiple sclerosis and JC virus expression.* J Neurovirol, 2012. **18**(5): p. 411-5.

117. Przepiorka, D., et al., *Successful treatment of progressive multifocal leukoencephalopathy with low-dose interleukin-2.* Bone Marrow Transplant, 1997. **20**(11): p. 983-7.

118. Re, D., et al., *Progressive multifocal leukoencephalopathy after autologous bone marrow transplantation and alpha-interferon immunotherapy.* Bone Marrow Transplant, 1999. **23**(3): p. 295-8.

119. Buckanovich, R.J., et al., *Nonmyeloablative allogeneic stem cell transplantation for refractory Hodgkin's lymphoma complicated by interleukin-2 responsive progressive multifocal leukoencephalopathy.* Ann Hematol, 2002. **81**(7): p. 410-3.

120. Kunschner, L. and T.F. Scott, *Sustained recovery of progressive multifocal leukoencephalopathy after treatment with IL-2.* Neurology, 2005. **65**(9): p. 1510.

121. Mackall, C.L., T.J. Fry, and R.E. Gress, *Harnessing the biology of IL-7 for therapeutic application.* Nat Rev Immunol, 2011. **11**(5): p. 330-42.

122. Alstadhaug, K.B., et al., *Treatment of progressive multifocal leukoencephalopathy with interleukin 7.* JAMA Neurol, 2014. **71**(8): p. 1030-5.

123. Gasnault, J., et al., *Efficacy of recombinant human interleukin 7 in a patient with severe lymphopenia-related progressive multifocal leukoencephalopathy.* Open Forum Infect Dis, 2014. **1**(2): p. ofu074.

124. Patel, A., J. Patel, and J. Ikwuagwu, *A case of progressive multifocal leukoencephalopathy and idiopathic CD4+ lymphocytopenia.* J Antimicrob Chemother, 2010. **65**(12): p. 2697-8.

125. Cortese, I., et al., *Pembrolizumab Treatment for Progressive Multifocal Leukoencephalopathy.* N Engl J Med, 2019. **380**(17): p. 1597-1605.

126. Jelcic, I., et al., *Broadly neutralizing human monoclonal JC polyomavirus VP1-specific antibodies as candidate therapeutics for progressive multifocal leukoencephalopathy.* Sci Transl Med, 2015. **7**(306): p. 306ra150.

127. Balduzzi, A., et al., *Polyomavirus JC-targeted T-cell therapy for progressive multiple leukoencephalopathy in a hematopoietic cell transplantation recipient.* Bone Marrow Transplant, 2011. **46**(7): p. 987-92.

128. Boland, C., *JC virus vaccine*. 2012.

129. Martin, R., Sospedra, M., Jelcic, I., Yousef, S., Schippling, S., *Polyoma virus JC peptides and proteins in vaccination and diagnostic applications*. 2011.

130. Jelcic, I., Martin, R., Schippling, S., Sospreda, M., Yousef, S., *Polyoma virus JC peptides and proteins in vaccination and diagnostic applications*. 2013.

131. Sospedra, M., et al., *Treating progressive multifocal leukoencephalopathy with interleukin 7 and vaccination with JC virus capsid protein VP1.* Clin Infect Dis, 2014. **59**(11): p. 1588-92.

132. Neu, U., et al., *Structure-function analysis of the human JC polyomavirus establishes the LSTc pentasaccharide as a functional receptor motif.* Cell Host Microbe, 2010. **8**(4): p. 309-19.

133. Stroh, L.J., et al., *The Greater Affinity of JC Polyomavirus Capsid for alpha2,6-Linked Lactoseries Tetrasaccharide c than for Other Sialylated Glycans Is a Major Determinant of Infectivity.* J Virol, 2015. **89**(12): p. 6364-75.

134. Haley, S.A., B.A. O'Hara, and W.J. Atwood, *Adipocyte Plasma Membrane Protein (APMAP) promotes JC Virus (JCPyV) infection in human glial cells.* Virology, 2020. **548**: p. 17-24.

135. Geoghegan, E.M., et al., *Infectious Entry and Neutralization of Pathogenic JC Polyomaviruses.* Cell Rep, 2017. **21**(5): p. 1169-1179.

136. O'Hara, S.D., T. Stehle, and R. Garcea, *Glycan receptors of the Polyomaviridae: structure, function, and pathogenesis.* Curr Opin Virol, 2014. **7**: p. 73-8.

137. Erickson, K.D., R.L. Garcea, and B. Tsai, *Ganglioside GT1b is a putative host cell receptor for the Merkel cell polyomavirus.* J Virol, 2009. **83**(19): p. 10275-9.

138. Campanero-Rhodes, M.A., et al., *N-glycolyl GM1 ganglioside as a receptor for simian virus 40.* J Virol, 2007. **81**(23): p. 12846-58.

139. Atwood, W.J. and L.C. Norkin, *Class I major histocompatibility proteins as cell surface receptors for simian virus 40.* J Virol, 1989. **63**(10): p. 4474-7.

140. Maginnis, M.S., et al., *Role of N-linked glycosylation of the 5-HT2A receptor in JC virus infection.* J Virol, 2010. **84**(19): p. 9677-84.

141. Assetta, B., et al., *5-HT2 receptors facilitate JC polyomavirus entry.* J Virol, 2013. **87**(24): p. 13490-8.

142. Assetta, B., et al., *Genetic and Functional Dissection of the Role of Individual 5-HT(2) Receptors as Entry Receptors for JC Polyomavirus.* Cell Rep, 2019. **27**(7): p. 1960-1966 e6.

143. Querbes, W., et al., *A JC virus-induced signal is required for infection of glial cells by a clathrin- and eps15-dependent pathway.* J Virol, 2004. **78**(1): p. 250-6.

144. Mayberry, C.L., et al., *JC Polyomavirus Entry by Clathrin-Mediated Endocytosis Is Driven by beta-Arrestin.* J Virol, 2019. **93**(8).

145. Anderson, H.A., Y. Chen, and L.C. Norkin, *Bound simian virus 40 translocates to caveolin-enriched membrane domains, and its entry is inhibited by drugs that selectively disrupt caveolae.* Mol Biol Cell, 1996. **7**(11): p. 1825-34.

146. Richterova, Z., et al., *Caveolae are involved in the trafficking of mouse polyomavirus virions and artificial VP1 pseudocapsids toward cell nuclei.* J Virol, 2001. **75**(22): p. 10880-91.

147. Dugan, A.S., S. Eash, and W.J. Atwood, *Update on BK virus entry and intracellular trafficking.* Transpl Infect Dis, 2006. **8**(2): p. 62-7.

148. Becker, M., et al., *Infectious Entry of Merkel Cell Polyomavirus.* J Virol, 2019. **93**(6).

149. Engel, S., et al., *Role of endosomes in simian virus 40 entry and infection.* J Virol, 2011. **85**(9): p. 4198-211.

150. Zhao, L., et al., *Caveolin- and clathrin-independent entry of BKPyV into primary human proximal tubule epithelial cells.* Virology, 2016. **492**: p. 66-72.

151. Querbes, W., et al., *Invasion of host cells by JC virus identifies a novel role for caveolae in endosomal sorting of noncaveolar ligands.* J Virol, 2006. **80**(19): p. 9402-13.

152. Morris-Love, J., et al., *JC Polyomavirus Uses Extracellular Vesicles To Infect Target Cells.* mBio, 2019. **10**(2).

153. Handala, L., et al., *BK Polyomavirus Hijacks Extracellular Vesicles for En Bloc Transmission.* J Virol, 2020. **94**(6).

154. Jiang, M., et al., *Early events during BK virus entry and disassembly.* J Virol, 2009. **83**(3): p. 1350-8.

155. Ashok, A. and W.J. Atwood, *Contrasting roles of endosomal pH and the cytoskeleton in infection of human glial cells by JC virus and simian virus 40.* J Virol, 2003. **77**(2): p. 1347-56.

156. Hornikova, L., K. Brustikova, and J. Forstova, *Microtubules in Polyomavirus Infection.* Viruses, 2020. **12**(1).

157. Pelkmans, L., et al., *Caveolin-stabilized membrane domains as multifunctional transport and sorting devices in endocytic membrane traffic.* Cell, 2004. **118**(6): p. 767-80.

158. Eash, S., W. Querbes, and W.J. Atwood, *Infection of vero cells by BK virus is dependent on caveolae.* J Virol, 2004. **78**(21): p. 11583-90.

159. Zhao, L. and M.J. Imperiale, *Identification of Rab18 as an Essential Host Factor for BK Polyomavirus Infection Using a Whole-Genome RNA Interference Screen.* mSphere, 2017. **2**(4).

160. Bagchi, P., et al., *Selective EMC subunits act as molecular tethers of intracellular organelles exploited during viral entry.* Nat Commun, 2020. **11**(1): p. 1127.

161. Schelhaas, M., et al., *Simian Virus 40 depends on ER protein folding and quality control factors for entry into host cells.* Cell, 2007. **131**(3): p. 516-29.

162. Magnuson, B., et al., *ERp29 triggers a conformational change in polyomavirus to stimulate membrane binding.* Mol Cell, 2005. **20**(2): p. 289-300.

163. Walczak, C.P. and B. Tsai, *A PDI family network acts distinctly and coordinately with ERp29 to facilitate polyomavirus infection.* J Virol, 2011. **85**(5): p. 2386-96.

164. Inoue, T. and B. Tsai, *A large and intact viral particle penetrates the endoplasmic reticulum membrane to reach the cytosol.* PLoS Pathog, 2011. **7**(5): p. e1002037.

165. Daniels, R., et al., *SV40 VP2 and VP3 insertion into ER membranes is controlled by the capsid protein VP1: implications for DNA translocation out of the ER.* Mol Cell, 2006. **24**(6): p. 955-66.

166. Geiger, R., et al., *BAP31 and BiP are essential for dislocation of SV40 from the endoplasmic reticulum to the cytosol.* Nat Cell Biol, 2011. **13**(11): p. 1305-14.

167. Bagchi, P., T. Inoue, and B. Tsai, *EMC1-dependent stabilization drives membrane penetration of a partially destabilized non-enveloped virus.* Elife, 2016. **5**.

168. Walczak, C.P., et al., *A cytosolic chaperone complexes with dynamic membrane J-proteins and mobilizes a nonenveloped virus out of the endoplasmic reticulum.* PLoS Pathog, 2014. **10**(3): p. e1004007.

169. Goodwin, E.C., et al., *BiP and multiple DNAJ molecular chaperones in the endoplasmic reticulum are required for efficient simian virus 40 infection.* mBio, 2011. **2**(3): p. e00101-11.

170. Nelson, C.D., et al., *The VP1 subunit of JC polyomavirus recapitulates early events in viral trafficking and is a novel tool to study polyomavirus entry.* Virology, 2012. **428**(1): p. 30-40.

171. Dupzyk, A., et al., *SGTA-Dependent Regulation of Hsc70 Promotes Cytosol Entry of Simian Virus 40 from the Endoplasmic Reticulum.* J Virol, 2017. **91**(12).

172. Dupzyk, A. and B. Tsai, *Bag2 Is a Component of a Cytosolic Extraction Machinery That Promotes Membrane Penetration of a Nonenveloped Virus.* J Virol, 2018. **92**(15).

173. Weis, K., *Importins and exportins: how to get in and out of the nucleus.* Trends Biochem Sci, 1998. **23**(5): p. 185-9.

174. Nakanishi, A., et al., *Interaction of the Vp3 nuclear localization signal with the importin alpha 2/beta heterodimer directs nuclear entry of infecting simian virus 40.* J Virol, 2002. **76**(18): p. 9368-77.

175. Nakanishi, A., et al., *Molecular dissection of nuclear entry-competent SV40 during infection.* Virus Res, 2007. **124**(1-2): p. 226-30.

176. Bennett, S.M., et al., *Role of a nuclear localization signal on the minor capsid proteins VP2 and VP3 in BKPyV nuclear entry.* Virology, 2015. **474**: p. 110-6.

177. Qu, Q., et al., *Nuclear entry mechanism of the human polyomavirus JC virus-like particle: role of importins and the nuclear pore complex.* J Biol Chem, 2004. **279**(26): p. 27735-42.

178. Soldatova, I., et al., *Interaction of the Mouse Polyomavirus Capsid Proteins with Importins Is Required for Efficient Import of Viral DNA into the Cell Nucleus.* Viruses, 2018. **10**(4).

179. Giorda, K.M., et al., *The viroporin activity of the minor structural proteins VP2 and VP3 is required for SV40 propagation.* J Biol Chem, 2013. **288**(4): p. 2510-20.

180. Suzuki, T., et al., *Viroporin activity of the JC polyomavirus is regulated by interactions with the adaptor protein complex 3.* Proc Natl Acad Sci U S A, 2013. **110**(46): p. 18668-73.

181. Frisque, R.J., G.L. Bream, and M.T. Cannella, *Human polyomavirus JC virus genome.* J Virol, 1984. **51**(2): p. 458-69.

182. Chen, X.S., T. Stehle, and S.C. Harrison, *Interaction of polyomavirus internal protein VP2 with the major capsid protein VP1 and implications for participation of VP2 in viral entry.* EMBO J, 1998. **17**(12): p. 3233-40.

183. Assetta, B. and W.J. Atwood, *The biology of JC polyomavirus.* Biol Chem, 2017. **398**(8): p. 839-855.

184. Hirsch, H.H., et al., *The human JC polyomavirus (JCPyV): virological background and clinical implications.* APMIS, 2013. **121**(8): p. 685-727.

185. Atkinson, A.L. and W.J. Atwood, *Fifty Years of JC Polyomavirus: A Brief Overview and Remaining Questions.* Viruses, 2020. **12**(9).

186. Ault, G.S. and G.L. Stoner, *Human polyomavirus JC promoter/enhancer rearrangement patterns from progressive multifocal leukoencephalopathy brain are unique derivatives of a single archetypal structure.* J Gen Virol, 1993. **74 (Pt 8)**: p. 1499-507.

187. Padgett, B.L., et al., *Differential neurooncogenicity of strains of JC virus, a human polyoma virus, in newborn Syrian hamsters.* Cancer Res, 1977. **37**(3): p. 718-20.

188. Myers, C., R.J. Frisque, and R.R. Arthur, *Direct isolation and characterization of JC virus from urine samples of renal and bone marrow transplant patients.* J Virol, 1989. **63**(10): p. 4445-9.

189. Wilczek, M.P., et al., *Rearrangement in the Hypervariable Region of JC Polyomavirus Genomes Isolated from Patient Samples and Impact on Transcription Factor-Binding Sites and Disease Outcomes.* Int J Mol Sci, 2022. **23**(10).

190. Liu, C.K., A.P. Hope, and W.J. Atwood, *The human polyomavirus, JCV, does not share receptor specificity with SV40 on human glial cells.* J Neurovirol, 1998. **4**(1): p. 49-58.

191. Chen, B.J. and W.J. Atwood, *Construction of a novel JCV/SV40 hybrid virus (JCSV) reveals a role for the JCV capsid in viral tropism.* Virology, 2002. **300**(2): p. 282-90.

192. Gee, G.V., et al., *Modeling a sialic acid binding pocket in the external loops of JC virus VP1.* J Biol Chem, 2004. **279**(47): p. 49172-6.

193. Shishido-Hara, Y., et al., *Analysis of capsid formation of human polyomavirus JC (Tokyo-1 strain) by a eukaryotic expression system: splicing of late RNAs, translation and nuclear transport of major capsid protein VP1, and capsid assembly.* J Virol, 2000. **74**(4): p. 1840-53.

194. Ou, W.C., et al., *Analysis of minimal sequences on JC virus VP1 required for capsid assembly.* J Neurovirol, 2001. **7**(4): p. 298-301.

195. Saribas, A.S., et al., *Human polyoma JC virus minor capsid proteins, VP2 and VP3, enhance large T antigen binding to the origin of viral DNA replication: evidence for their involvement in regulation of the viral DNA replication.* Virology, 2014. **449**: p. 1-16.

196. Zheng, H.C., H. Xue, and C.Y. Zhang, *The oncogenic roles of JC polyomavirus in cancer.* Front Oncol, 2022. **12**: p. 976577.

197. Saribas, A.S., M.K. White, and M. Safak, *JC virus agnoprotein enhances large T antigen binding to the origin of viral DNA replication: evidence for its involvement in viral DNA replication.* Virology, 2012. **433**(1): p. 12-26.

198. Saribas, A.S., et al., *Emerging From the Unknown: Structural and Functional Features of Agnoprotein of Polyomaviruses.* J Cell Physiol, 2016. **231**(10): p. 2115-27.

199. Sami Saribas, A., et al., *Essential roles of Leu/Ile/Phe-rich domain of JC virus agnoprotein in dimer/oligomer formation, protein stability and splicing of viral transcripts.* Virology, 2013. **443**(1): p. 161-76.

200. Coric, P., et al., *Nuclear magnetic resonance structure revealed that the human polyomavirus JC virus agnoprotein contains an alpha-helix encompassing the Leu/Ile/Phe-rich domain.* J Virol, 2014. **88**(12): p. 6556-75.

201. Okada, Y., et al., *Dissociation of heterochromatin protein 1 from lamin B receptor induced by human polyomavirus agnoprotein: role in nuclear egress of viral particles.* EMBO Rep, 2005. **6**(5): p. 452-7.

202. Suzuki, T., et al., *Identification of FEZ1 as a protein that interacts with JC virus agnoprotein and microtubules: role of agnoprotein-induced dissociation of FEZ1 from microtubules in viral propagation.* J Biol Chem, 2005. **280**(26): p. 24948-56.

203. Suzuki, T., et al., *The human polyoma JC virus agnoprotein acts as a viroporin.* PLoS Pathog, 2010. **6**(3): p. e1000801.

204. Lane, D.P. and L.V. Crawford, *T antigen is bound to a host protein in SV40-transformed cells.* Nature, 1979. **278**(5701): p. 261-3.

205. McCormick, F. and E. Harlow, *Association of a murine 53,000-dalton phosphoprotein with simian virus 40 large-T antigen in transformed cells.* J Virol, 1980. **34**(1): p. 213-24.

206. Nair, A., et al., *Conceptual Evolution of Cell Signaling.* Int J Mol Sci, 2019. **20**(13).

207. Bukoreshtliev, N.V., K. Haase, and A.E. Pelling, *Mechanical cues in cellular signalling and communication.* Cell Tissue Res, 2013. **352**(1): p. 77-94.

208. Brumbaugh, J., B. Di Stefano, and K. Hochedlinger, *Reprogramming: identifying the mechanisms that safeguard cell identity.* Development, 2019. **146**(23).

209. Lounsbury, K., *Signal Transduction and Second Messengers*. Pharmacology Principles and Practice. 2009: Academic Press.

210. Radhakrishnan, K., et al., *Quantitative understanding of cell signaling: the importance of membrane organization.* Curr Opin Biotechnol, 2010. **21**(5): p. 677-82.

211. Avruch, J., *MAP kinase pathways: the first twenty years.* Biochim Biophys Acta, 2007. **1773**(8): p. 1150-60.

212. Keshet, Y. and R. Seger, *The MAP kinase signaling cascades: a system of hundreds of components regulates a diverse array of physiological functions.* Methods Mol Biol, 2010. **661**: p. 3-38.

213. Guo, Y.J., et al., *ERK/MAPK signalling pathway and tumorigenesis.* Exp Ther Med, 2020. **19**(3): p. 1997-2007.

214. Owens, D.M. and S.M. Keyse, *Differential regulation of MAP kinase signalling by dual-specificity protein phosphatases.* Oncogene, 2007. **26**(22): p. 3203-13.

215. Soares-Silva, M., et al., *The Mitogen-Activated Protein Kinase (MAPK) Pathway: Role in Immune Evasion by Trypanosomatids.* Front Microbiol, 2016. **7**: p. 183.

216. DuShane, J.K., et al., *ERK Is a Critical Regulator of JC Polyomavirus Infection.* J Virol, 2018. **92**(7).

217. DuShane, J.K. and M.S. Maginnis, *Human DNA Virus Exploitation of the MAPK-ERK Cascade.* Int J Mol Sci, 2019. **20**(14).

218. Clapham, D.E., *Calcium signaling.* Cell, 2007. **131**(6): p. 1047-58.

219. Bootman, M.D. and G. Bultynck, *Fundamentals of Cellular Calcium Signaling: A Primer.* Cold Spring Harb Perspect Biol, 2020. **12**(1).

220. Bootman, M.D., *Calcium signaling.* Cold Spring Harb Perspect Biol, 2012. **4**(7): p. a011171.

221. Bagur, R. and G. Hajnoczky, *Intracellular Ca(2+) Sensing: Its Role in Calcium Homeostasis and Signaling.* Mol Cell, 2017. **66**(6): p. 780-788.

222. Chandran, A., et al., *Exploration of inositol 1,4,5-trisphosphate (IP(3)) regulated dynamics of N-terminal domain of IP(3) receptor reveals early phase molecular events during receptor activation.* Sci Rep, 2019. **9**(1): p. 2454.

223. Lanner, J.T., et al., *Ryanodine receptors: structure, expression, molecular details, and function in calcium release.* Cold Spring Harb Perspect Biol, 2010. **2**(11): p. a003996.

224. Webb, S.E., J.J. Kelu, and A.L. Miller, *Role of Two-Pore Channels in Embryonic Development and Cellular Differentiation.* Cold Spring Harb Perspect Biol, 2020. **12**(1).

225. Vangeel, L. and T. Voets, *Transient Receptor Potential Channels and Calcium Signaling.* Cold Spring Harb Perspect Biol, 2019. **11**(6).

226. Chami, M., B. Oules, and P. Paterlini-Brechot, *Cytobiological consequences of calcium-signaling alterations induced by human viral proteins.* Biochim Biophys Acta, 2006. **1763**(11): p. 1344-62.

227. Zhou, Y., T.K. Frey, and J.J. Yang, *Viral calciomics: interplays between Ca2+ and virus.* Cell Calcium, 2009. **46**(1): p. 1-17.

228. Saurav, S., et al., *Dysregulation of host cell calcium signaling during viral infections: Emerging paradigm with high clinical relevance.* Mol Aspects Med, 2021. **81**: p. 101004.

229. Dugas, B., et al., *Extracellular but not intracellular calcium mobilization is required for Epstein-Barr virus-containing supernatant-induced B cell activation.* Eur J Immunol, 1989. **19**(10): p. 1867-71.

230. Nugent, K.M. and J.D. Shanley, *Verapamil inhibits influenza A virus replication.* Arch Virol, 1984. **81**(1-2): p. 163-70.

231. Fujioka, Y., et al., *A Sialylated Voltage-Dependent Ca(2+) Channel Binds Hemagglutinin and Mediates Influenza A Virus Entry into Mammalian Cells.* Cell Host Microbe, 2018. **23**(6): p. 809-818 e5.

232. Zocchi, M.R., et al., *HIV-1 Tat inhibits human natural killer cell function by blocking L-type calcium channels.* J Immunol, 1998. **161**(6): p. 2938-43.

233. Wang, S., et al., *Screening of FDA-Approved Drugs for Inhibitors of Japanese Encephalitis Virus Infection.* J Virol, 2017. **91**(21).

234. Lavanya, M., et al., *siRNA screen for genes that affect Junin virus entry uncovers voltage-gated calcium channels as a therapeutic target.* Sci Transl Med, 2013. **5**(204): p. 204ra131.

235. Srikanth, S. and Y. Gwack, *Orai1, STIM1, and their associating partners.* J Physiol, 2012. **590**(17): p. 4169-77.

236. Yao, J.H., et al., *Hepatitis B Virus X Protein Upregulates Intracellular Calcium Signaling by Binding C-terminal of Orail Protein.* Curr Med Sci, 2018. **38**(1): p. 26-34.

237. Diaz, Y., et al., *Dissecting the Ca(2)(+) entry pathways induced by rotavirus infection and NSP4-EGFP expression in Cos-7 cells.* Virus Res, 2012. **167**(2): p. 285-96.

238. Dionicio, C.L., et al., *Dengue virus induced changes in Ca(2+) homeostasis in human hepatic cells that favor the viral replicative cycle.* Virus Res, 2018. **245**: p. 17-28.

239. Han, Z., et al., *Calcium Regulation of Hemorrhagic Fever Virus Budding: Mechanistic Implications for Host-Oriented Therapeutic Intervention.* PLoS Pathog, 2015. **11**(10): p. e1005220.

240. Chen, X., R. Cao, and W. Zhong, *Host Calcium Channels and Pumps in Viral Infections.* Cells, 2019. **9**(1).

241. Chami, M., et al., *Caspase-dependent alterations of Ca2+ signaling in the induction of apoptosis by hepatitis B virus X protein.* J Biol Chem, 2003. **278**(34): p. 31745-55.

242. Diaz, Y., et al., *Expression of nonstructural rotavirus protein NSP4 mimics Ca2+ homeostasis changes induced by rotavirus infection in cultured cells.* J Virol, 2008. **82**(22): p. 11331-43.

243. Luganini, A., et al., *Human cytomegalovirus US21 protein is a viroporin that modulates calcium homeostasis and protects cells against apoptosis.* Proc Natl Acad Sci U S A, 2018. **115**(52): p. E12370-E12377.

244. Dellis, O., et al., *Modulation of B-cell endoplasmic reticulum calcium homeostasis by Epstein-Barr virus latent membrane protein-1.* Mol Cancer, 2009. **8**: p. 59.

245. Ehrlich, L.S., et al., *Activation of the inositol (1,4,5)-triphosphate calcium gate receptor is required for HIV-1 Gag release.* J Virol, 2010. **84**(13): p. 6438-51.

246. Bouchard, M.J., L.H. Wang, and R.J. Schneider, *Calcium signaling by HBx protein in hepatitis B virus DNA replication.* Science, 2001. **294**(5550): p. 2376-8.

247. Piccoli, C., et al., *Hepatitis C virus protein expression causes calcium-mediated mitochondrial bioenergetic dysfunction and nitro-oxidative stress.* Hepatology, 2007. **46**(1): p. 58-65.

248. Kruman, II, A. Nath, and M.P. Mattson, *HIV-1 protein Tat induces apoptosis of hippocampal neurons by a mechanism involving caspase activation, calcium overload, and oxidative stress.* Exp Neurol, 1998. **154**(2): p. 276-88.

249. Nie, J., et al., *Activation of CaMKII via ER-stress mediates coxsackievirus B3-induced cardiomyocyte apoptosis.* Cell Biol Int, 2020. **44**(2): p. 488-498.

250. Sakurai, Y., et al., *Ebola virus. Two-pore channels control Ebola virus host cell entry and are drug targets for disease treatment.* Science, 2015. **347**(6225): p. 995-8.

251. Gunaratne, G.S., et al., *NAADP-dependent Ca(2+) signaling regulates Middle East respiratory syndrome-coronavirus pseudovirus translocation through the endolysosomal system.* Cell Calcium, 2018. **75**: p. 30-41.

252. Ou, X., et al., *Characterization of spike glycoprotein of SARS-CoV-2 on virus entry and its immune cross-reactivity with SARS-CoV.* Nat Commun, 2020. **11**(1): p. 1620.

253. Dobson, S.J., J. Mankouri, and A. Whitehouse, *Identification of potassium and calcium channel inhibitors as modulators of polyomavirus endosomal trafficking.* Antiviral Res, 2020. **179**: p. 104819.

254. Khan, N., et al., *BK channels regulate extracellular Tat-mediated HIV-1 LTR transactivation.* Sci Rep, 2019. **9**(1): p. 12285.

255. Hoffmann, H.H., et al., *Diverse Viruses Require the Calcium Transporter SPCA1 for Maturation and Spread.* Cell Host Microbe, 2017. **22**(4): p. 460-470 e5.

256. Madigan, V.J., et al., *The Golgi Calcium ATPase Pump Plays an Essential Role in Adeno-associated Virus Trafficking and Transduction.* J Virol, 2020. **94**(21).

257. Hayashi, N., et al., *Nef of HIV-1 interacts directly with calcium-bound calmodulin.* Protein Sci, 2002. **11**(3): p. 529-37.

258. Kim, M.J., et al., *Hepatitis B virus X protein enhances liver cancer cell migration by regulating calmodulin-associated actin polymerization.* BMB Rep, 2021. **54**(12): p. 614-619.

259. Zhou, Y., et al., *Calcium-dependent association of calmodulin with the rubella virus nonstructural protease domain.* J Biol Chem, 2010. **285**(12): p. 8855-68.

260. Bautista-Carbajal, P., et al., *The calmodulin antagonist W-7 (N-(6-aminohexyl)-5-chloro-1-naphthalenesulfonamide hydrochloride) inhibits DENV infection in Huh-7 cells.* Virology, 2017. **501**: p. 188-198.

261. Han, Z. and R.N. Harty, *Influence of calcium/calmodulin on budding of Ebola VLPs: implications for the involvement of the Ras/Raf/MEK/ERK pathway.* Virus Genes, 2007. **35**(3): p. 511-20.

262. Sultan, F., K. Ahuja, and R.K. Motiani, *Potential of targeting host cell calcium dynamics to curtail SARS-CoV-2 infection and COVID-19 pathogenesis.* Cell Calcium, 2022. **106**: p. 102637.

263. Ludlow, J.W. and R.A. Consigli, *Localization of calcium on the polyomavirus VP1 capsid protein.* J Virol, 1987. **61**(9): p. 2934-7.

264. Haynes, J.I., 2nd, D. Chang, and R.A. Consigli, *Mutations in the putative calcium-binding domain of polyomavirus VP1 affect capsid assembly.* J Virol, 1993. **67**(5): p. 2486-95.

265. Kuksin, D. and L.C. Norkin, *Disassembly of simian virus 40 during passage through the endoplasmic reticulum and in the cytoplasm.* J Virol, 2012. **86**(3): p. 1555-62.

266. Gee, G.V., et al., *Pseudovirus mimics cell entry and trafficking of the human polyomavirus JCPyV.* Virus Res, 2013. **178**(2): p. 281-6.

267. Polo, C., et al., *Prevalence and patterns of polyomavirus urinary excretion in immunocompetent adults and children.* Clin Microbiol Infect, 2004. **10**(7): p. 640-4.

268. Vanchiere, J.A., et al., *Polyomavirus shedding in the stool of healthy adults.* J Clin Microbiol, 2009. **47**(8): p. 2388-91.

269. Prezioso, C., et al., *JC polyomavirus: a short review of its biology, its association with progressive multifocal leukoencephalopathy, and the diagnostic value of different methods to manifest its activity or presence.* Expert Rev Mol Diagn, 2023. **23**(2): p. 143-157.

270. Joly, M., et al., *Progressive multifocal leukoencephalopathy: epidemiology and spectrum of predisposing conditions.* Brain, 2023. **146**(1): p. 349-358.

271. Nelson, C.D., et al., *Modulation of a pore in the capsid of JC polyomavirus reduces infectivity and prevents exposure of the minor capsid proteins.* J Virol, 2015. **89**(7): p. 3910-21.

272. DeCaprio, J.A. and R.L. Garcea, *A cornucopia of human polyomaviruses.* Nat Rev Microbiol, 2013. **11**(4): p. 264-76.

273. Tsai, B. and M. Qian, *Cellular entry of polyomaviruses.* Curr Top Microbiol Immunol, 2010. **343**: p. 177-94.

274. Clark, P., et al., *Phosphoinositide 3'-Kinase gamma Facilitates Polyomavirus Infection.* Viruses, 2020. **12**(10).

275. Straus, M.R., et al., *Inhibitors of L-Type Calcium Channels Show Therapeutic Potential for Treating SARS-CoV-2 Infections by Preventing Virus Entry and Spread.* ACS Infect Dis, 2021. **7**(10): p. 2807-2815.

276. Perlman, M. and M.D. Resh, *Identification of an intracellular trafficking and assembly pathway for HIV-1 gag.* Traffic, 2006. **7**(6): p. 731-45.

277. Barrows, N.J., et al., *A Screen of FDA-Approved Drugs for Inhibitors of Zika Virus Infection.* Cell Host Microbe, 2016. **20**(2): p. 259-70.

278. Lee, N., et al., *High-throughput drug screening using the Ebola virus transcription- and replication-competent virus-like particle system.* Antiviral Res, 2018. **158**: p. 226-237.

279. Garcia, G., Jr., et al., *Antiviral drug screen identifies DNA-damage response inhibitor as potent blocker of SARS-CoV-2 replication.* Cell Rep, 2021. **35**(1): p. 108940.

280. DuShane, J.K., et al., *High-Throughput Characterization of Viral and Cellular Protein Expression Patterns During JC Polyomavirus Infection.* Front Microbiol, 2019. **10**: p. 783.

281. Major, E.O., et al., *Establishment of a line of human fetal glial cells that supports JC virus multiplication.* Proc Natl Acad Sci U S A, 1985. **82**(4): p. 1257-61.

282. Vacante, D.A., R. Traub, and E.O. Major, *Extension of JC virus host range to monkey cells by insertion of a simian virus 40 enhancer into the JC virus regulatory region.* Virology, 1989. **170**(2): p. 353-61.

283. Harcourt, J., et al., *Severe Acute Respiratory Syndrome Coronavirus 2 from Patient with Coronavirus Disease, United States.* Emerg Infect Dis, 2020. **26**(6): p. 1266-1273.

284. Regan, D.P., et al., *Improved Recovery of Captured Airborne Bacteria and Viruses with Liquid-Coated Air Filters.* ACS Appl Mater Interfaces, 2022. **14**(45): p. 50543-50556.

285. Stanifer, M.L., et al., *Critical Role of Type III Interferon in Controlling SARS-CoV-2 Infection in Human Intestinal Epithelial Cells.* Cell Rep, 2020. **32**(1): p. 107863.

286. Mehmood, K., et al., *Dynamics and Patterning of 5-Hydroxytryptamine 2 Subtype Receptors in JC Polyomavirus Entry.* Viruses, 2022. **14**(12).

287. Mainou, B.A., et al., *Reovirus cell entry requires functional microtubules.* mBio, 2013. **4**(4).

288. Mayberry, C.L., et al., *GRK2 mediates beta-arrestin interactions with 5-HT(2) receptors for JC polyomavirus endocytosis.* J Virol, 2021. **95**(7).

289. Jia, Y., et al., *Nifedipine inhibits angiotensin II-induced cardiac fibrosis via downregulating Nox4-derived ROS generation and suppressing ERK1/2, JNK signaling pathways.* Pharmazie, 2013. **68**(6): p. 435-41.

290. Ma, J.W., et al., *Tetrandrine Exerts a Radiosensitization Effect on Human Glioma through Inhibiting Proliferation by Attenuating ERK Phosphorylation.* Biomol Ther (Seoul), 2017. **25**(2): p. 186-193.

291. Zhao, T., et al., *Nifedipine stimulates proliferation and migration of different breast cancer cells by distinct pathways.* Mol Med Rep, 2017. **16**(2): p. 2259-2263.

292. Vandonselaar, M., et al., *Trifluoperazine-induced conformational change in Ca(2+)-calmodulin.* Nat Struct Biol, 1994. **1**(11): p. 795-801.

293. Osawa, M., et al., *Solution structure of calmodulin-W-7 complex: the basis of diversity in molecular recognition.* J Mol Biol, 1998. **276**(1): p. 165-76.

294. Lambert, D.W., et al., *Calmodulin interacts with angiotensin-converting enzyme-2 (ACE2) and inhibits shedding of its ectodomain.* FEBS Lett, 2008. **582**(2): p. 385-90.

295. Yuan, W., et al., *Screening for inhibitors against SARS-CoV-2 and its variants.* Biosaf Health, 2022. **4**(3): p. 186-192.

296. Dittmar, M., et al., *Drug repurposing screens reveal cell-type-specific entry pathways and FDA-approved drugs active against SARS-Cov-2.* Cell Rep, 2021. **35**(1): p. 108959.

297. Turner, J.H. and J.R. Raymond, *Interaction of calmodulin with the serotonin 5-hydroxytryptamine2A receptor. A putative regulator of G protein coupling and receptor phosphorylation by protein kinase C.* J Biol Chem, 2005. **280**(35): p. 30741-50.

298. Labasque, M., et al., *Physical interaction of calmodulin with the 5-hydroxytryptamine2C receptor C-terminus is essential for G protein-independent, arrestin-dependent receptor signaling.* Mol Biol Cell, 2008. **19**(11): p. 4640-50.

299. Manley, K., et al., *NFAT4 is required for JC virus infection of glial cells.* J Virol, 2006. **80**(24): p. 12079-85.

300. Jackson, C.B., et al., *Mechanisms of SARS-CoV-2 entry into cells.* Nat Rev Mol Cell Biol, 2022. **23**(1): p. 3-20.

301. Kang, S., et al., *Trifluoperazine, a Well-Known Antipsychotic, Inhibits Glioblastoma Invasion by Binding to Calmodulin and Disinhibiting Calcium Release Channel IP3R.* Mol Cancer Ther, 2017. **16**(1): p. 217-227.

302. Lemaitre, M., et al., *Protective activity of tetracycline analogs against the cytopathic effect of the human immunodeficiency viruses in CEM cells.* Res Virol, 1990. **141**(1): p. 5-16.

303. Murugan, K., et al., *Fighting arboviral diseases: low toxicity on mammalian cells, dengue growth inhibition (in vitro), and mosquitocidal activity of Centroceras clavulatum-synthesized silver nanoparticles.* Parasitol Res, 2016. **115**(2): p. 651-62.

304. Wang, Y., et al., *Remdesivir in adults with severe COVID-19: a randomised, double-blind, placebo-controlled, multicentre trial.* Lancet, 2020. **395**(10236): p. 1569-1578.

305. Cao, J., J.C. Forrest, and X. Zhang, *A screen of the NIH Clinical Collection small molecule library identifies potential anti-coronavirus drugs.* Antiviral Res, 2015. **114**: p. 1-10.

306. Bohn, W., et al., *Inhibition of measles virus budding by phenothiazines.* Virology, 1983. **130**(1): p. 44-55.

307. Nemerow, G.R. and N.R. Cooper, *Infection of B lymphocytes by a human herpesvirus, Epstein-Barr virus, is blocked by calmodulin antagonists.* Proc Natl Acad Sci U S A, 1984. **81**(15): p. 4955-9.

308. Ochiai, H., M. Kurokawa, and S. Niwayama, *Influence of trifluoperazine on the late stage of influenza virus infection in MDCK cells.* Antiviral Res, 1991. **15**(2): p. 149-60.

309. Candurra, N.A., L. Maskin, and E.B. Damonte, *Inhibition of arenavirus multiplication in vitro by phenotiazines.* Antiviral Res, 1996. **31**(3): p. 149-58.

310. Chockalingam, K., et al., *A cell protection screen reveals potent inhibitors of multiple stages of the hepatitis C virus life cycle.* Proc Natl Acad Sci U S A, 2010. **107**(8): p. 3764-9.

311. Xiao, X., et al., *Identification of Potent and Safe Antiviral Therapeutic Candidates Against SARS-CoV-2.* Front Immunol, 2020. **11**: p. 586572.

312. Piccini, L.E., V. Castilla, and E.B. Damonte, *Inhibition of dengue virus infection by trifluoperazine.* Arch Virol, 2022. **167**(11): p. 2203-2212.

313. Wilczek, M.P., et al., *PI3K/AKT/mTOR Signaling Pathway Is Required for JCPyV Infection in Primary Astrocytes.* Cells, 2021. **10**(11).

314. Koonin, E.V., V.V. Dolja, and M. Krupovic, *The logic of virus evolution.* Cell Host Microbe, 2022. **30**(7): p. 917-929.

315. Lam, A.K. and A. Galione, *The endoplasmic reticulum and junctional membrane communication during calcium signaling.* Biochim Biophys Acta, 2013. **1833**(11): p. 2542-59.

316. Kania, E., et al., *IP(3) Receptor-Mediated Calcium Signaling and Its Role in Autophagy in Cancer.* Front Oncol, 2017. **7**: p. 140.

317. Mikoshiba, K., *Role of IP3 receptor signaling in cell functions and diseases.* Adv Biol Regul, 2015. **57**: p. 217-27.

318. Bond, A.C.S., et al., *High-throughput drug screen identifies calcium and calmodulin inhibitors that reduce JCPyV infection.* Antiviral Res, 2024. **222**: p. 105817.

319. Gee, K.R., et al., *Chemical and physiological characterization of fluo-4 Ca(2+)-indicator dyes.* Cell Calcium, 2000. **27**(2): p. 97-106.

320. Bigdelou, P. and A.M. Farnoud, *Induction of Eryptosis in Red Blood Cells Using a Calcium Ionophore.* J Vis Exp, 2020(155).

321. Sharma, S.K., et al., *Measuring Cellular Ion Transport by Magnetoencephalography.* ACS Omega, 2020. **5**(8): p. 4024-4031.

322. Liu, F.S., et al., *Ca(2+) Regulates Autophagy Through CaMKKbeta/AMPK/mTOR Signaling Pathway in Mechanical Spinal cord Injury: An in vitro Study.* Neurochem Res, 2023. **48**(2): p. 447-457.

323. Hamada, K. and K. Mikoshiba, *IP(3) Receptor Plasticity Underlying Diverse Functions.* Annu Rev Physiol, 2020. **82**: p. 151-176.

324. Bootman, M.D., et al., *2-aminoethoxydiphenyl borate (2-APB) is a reliable blocker of store-operated Ca2+ entry but an inconsistent inhibitor of InsP3-induced Ca2+ release.* FASEB J, 2002. **16**(10): p. 1145-50.

325. Iwasaki, H., et al., *2-Aminoethoxydiphenyl borate (2-APB) inhibits capacitative calcium entry independently of the function of inositol 1,4,5-trisphosphate receptors.* Recept Channels, 2001. **7**(6): p. 429-39.

326. Raffaello, A., et al., *Calcium at the Center of Cell Signaling: Interplay between Endoplasmic Reticulum, Mitochondria, and Lysosomes.* Trends Biochem Sci, 2016. **41**(12): p. 1035-1049.

327. Perry, J.L., et al., *Host IP(3)R channels are dispensable for rotavirus Ca(2+) signaling but critical for intercellular Ca(2+) waves that prime uninfected cells for rapid virus spread.* mBio, 2024. **15**(1): p. e0214523.

328. Manninen, A. and K. Saksela, *HIV-1 Nef interacts with inositol trisphosphate receptor to activate calcium signaling in T cells.* J Exp Med, 2002. **195**(8): p. 1023-32.

329. Mataragka, S. and C.W. Taylor, *All three IP(3) receptor subtypes generate Ca(2+) puffs, the universal building blocks of IP(3)-evoked Ca(2+) signals.* J Cell Sci, 2018. **131**(16).

330. Sherwood, M.W., et al., *Astrocytic IP(3) Rs: Contribution to Ca(2+) signalling and hippocampal LTP.* Glia, 2017. **65**(3): p. 502-513.

331. Sherwood, M.W., et al., *Astrocytic IP(3)Rs: Beyond IP(3)R2.* Front Cell Neurosci, 2021. **15**: p. 695817.

332. Cheshenko, N., et al., *Multiple receptor interactions trigger release of membrane and intracellular calcium stores critical for herpes simplex virus entry.* Mol Biol Cell, 2007. **18**(8): p. 3119-30.

333. McCue, H.V., et al., *Generation and characterization of a lysosomally targeted, genetically encoded Ca(2+)-sensor.* Biochem J, 2013. **449**(2): p. 449-57.

334. Kasri, N.N., et al., *Endogenously bound calmodulin is essential for the function of the inositol 1,4,5-trisphosphate receptor.* J Biol Chem, 2006. **281**(13): p. 8332-8.

335. Taylor, C.W. and A.J. Laude, *IP3 receptors and their regulation by calmodulin and cytosolic Ca2+.* Cell Calcium, 2002. **32**(5-6): p. 321-34.

336. Sun, Y. and C.W. Taylor, *A calmodulin antagonist reveals a calmodulin-independent interdomain interaction essential for activation of inositol 1,4,5-trisphosphate receptors.* Biochem J, 2008. **416**(2): p. 243-53.

337. Cheshenko, N., et al., *Herpes simplex virus triggers activation of calcium-signaling pathways.* J Cell Biol, 2003. **163**(2): p. 283-93.

338. Yang, B. and M.J. Bouchard, *The hepatitis B virus X protein elevates cytosolic calcium signals by modulating mitochondrial calcium uptake.* J Virol, 2012. **86**(1): p. 313-27.

339. Villalobo, A., M. Gonzalez-Munoz, and M.W. Berchtold, *Proteins with calmodulin-like domains: structures and functional roles.* Cell Mol Life Sci, 2019. **76**(12): p. 2299-2328.

340. Parvathaneni, S., Z. Li, and D.B. Sacks, *Calmodulin influences MAPK signaling by binding KSR1.* J Biol Chem, 2021. **296**: p. 100577.

341. Wu, N., et al., *Arrestin binding to calmodulin: a direct interaction between two ubiquitous signaling proteins.* J Mol Biol, 2006. **364**(5): p. 955-63.

342. Turner, J.N., et al., *Calmodulin Is a 5-HT Receptor-Interacting and Regulatory Protein*, in *Serotonin Receptors in Neurobiology*, A. Chattopadhyay, Editor. 2007: Boca Raton (FL).

343. Zhang, X., et al., *Trifluoperazine prolongs the survival of experimental brain metastases by STAT3-dependent lysosomal membrane permeabilization.* Am J Cancer Res, 2020. **10**(2): p. 545-563.

344. Jeong, J.Y., et al., *Trifluoperazine and Its Analog Suppressed the Tumorigenicity of Non-Small Cell Lung Cancer Cell; Applicability of Antipsychotic Drugs to Lung Cancer Treatment.* Biomedicines, 2022. **10**(5).

345. Khan, K.M., J.B. Patel, and T.J. Schaefer, *Nifedipine*, in *StatPearls*. 2024: Treasure Island (FL).

346. Hirasawa, M. and Q.J. Pittman, *Nifedipine facilitates neurotransmitter release independently of calcium channels.* Proc Natl Acad Sci U S A, 2003. **100**(10): p. 6139-44.

347. Prezioso, C., et al., *Which is the best PML risk stratification strategy in natalizumab-treated patients affected by multiple sclerosis?* Mult Scler Relat Disord, 2020. **41**: p. 102008.

348. Graf, L.M., et al., *Clinical Presentation and Disease Course of 37 Consecutive Cases of Progressive Multifocal Leukoencephalopathy (PML) at a German Tertiary-Care Hospital: A Retrospective Observational Study.* Front Neurol, 2021. **12**: p. 632535.

CHAPTER 6

BIOGRAPHY OF THE AUTHOR

Avery Bond was born in Augusta, Maine on April 11th, 1997. She was raised in Jefferson, Maine and graduated from high school at Erskine Academy in 2015. She attended the University of New England and graduated in 2019 with a Bachelor of Science degree in Medical Biology. Directly after her undergraduate studies, she joined the University of Maine and department of Molecular and Biomedical Sciences to pursue a graduate degree in Microbiology. Avery is a candidate for Doctor of Philosophy in Microbiology from the University of Maine in August 2024.